

ANALYSIS AND DESIGN OF A LAMINAR FLOW  
AEROSOL REACTOR FOR THE  
PRODUCTION OF ZnSe  
POWDER

By

DELMAR RAY MORRISON III

Bachelor of Arts

Knox College

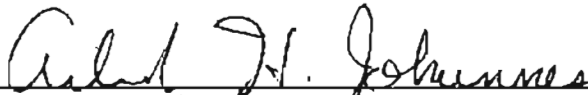
Galesburg, Illinois

1997

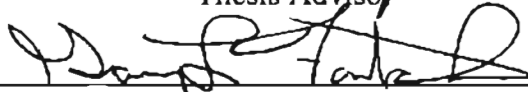
Submitted to the Faculty of the  
Graduate College of the  
Oklahoma State University  
in partial fulfillment of  
the requirements for  
the Degree of  
MASTER OF SCIENCE  
December, 1998

ANALYSIS AND DESIGN OF A LAMINAR FLOW  
AEROSOL REACTOR FOR THE  
PRODUCTION OF ZnSe  
POWDER

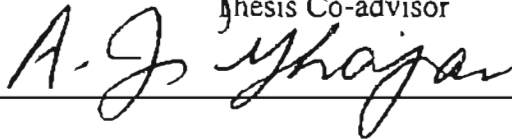
Thesis Approved:

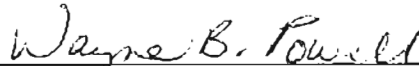


Thesis Advisor



Thesis Co-advisor





Dean of the Graduate College

## ACKNOWLEDGEMENTS

I wish to sincerely thank my graduate advisor, “A. J.” Johannes for his support through the transition from chemist to chemical engineer. Without his guidance, my tenure at OSU would most certainly have been more tortuous. I also wish to thank Dr. Gary L. Foutch, Dr. Afshin Ghajar, and Tom Potts for their advisement and technical assistance in completing this research. The financial assistance provided jointly through Oklahoma State University and Eagle-Picher, Inc. as OCAST funding is greatly appreciated.

I would also like to express thanks to Brent Foster and Jake Nikolic for their assistance in both experimentation and theory. My sincere thanks also go to Chris Shay for his undying devotion to seeing things a different way from me. I feel as though I have been greatly rewarded by our hours of “discussion” pertaining to research, thesis, and civilization in general. I only hope he can have learned as much from me as I from him. Special gratitude and appreciation are extended to my parents Del and Judy Morrison for their undying support. I would also like to thank the most valuable person in my life, Julie McFadden, for her intellectual, emotional, and AutoCAD support.

## TABLE OF CONTENTS

Chapter	Page
INTRODUCTION.....	1
Aerosol Flow Reactor.....	2
Objective.....	5
LITERATURE REVIEW.....	6
II-VI Processes.....	6
Reactor Design.....	10
POSSIBLE REACTOR CONFIGURATIONS.....	15
Current Process Description.....	17
Process Analysis.....	20
Experimental Study.....	23
Data Set.....	27
Reactor Performance.....	28
Reactant Mass Transfer.....	34
Molar Flow Rate.....	34
Energy Balance.....	37
Boiler Efficiency.....	39
Temperature Profiles.....	40
Boiling Effects.....	46
Modeling.....	50
Dimensional Analysis.....	51
FLUENT/UNS Flow Model.....	53
Kinetic Study Using FLUENT/UNS Model.....	56
Conclusions from Process Analysis.....	61
Potential New Configurations.....	63
Goals for Redesign.....	63
Review of Possible Reactor Schemes.....	64
Design Basis.....	73
PROTOTYPE REACTOR DESIGN.....	75
Overview.....	75
Boilers.....	79
Body.....	81
Neck.....	81
Argon Supply Tubes.....	82

Monitoring and Control.....	83
Heaters.....	84
Nozzles.....	87
Reactor Body.....	88
Product Collection Tube.....	88
Product Tube Insertion/Removal.....	92
Reactor Tube.....	93
Condenser.....	94
Production Comparison.....	96
CONCLUSIONS AND RECOMMENDATIONS.....	98
REFERENCES.....	101
APPENDICIES.....	107
APPENDIX A. THERMODYNAMIC, TRANSPORT, AND PHYSICAL PROPERTIES.....	108
Physical Properties.....	109
Thermodynamic Properties.....	114
Transport Properties.....	122
APPENDIX B. MASS FLOW ESTIMATES AND OTHER DERIVED VALUES.....	130
APPENDIX C. DESCRIPTION OF FLUENT/UNS MODEL.....	137
General Set-up.....	140
Input Species Properties.....	144
FLUENT/UNS Kinetic Study Data.....	147
APPENDIX D. NOZZLE DESIGN THROUGH CFD SIMULATION....	149
Minimum Mole Flow/Maximum Nozzle Throat.....	150
Maximum Mole Flow/Minimum Nozzle Throat.....	151
Nozzle Position and Orientation.....	156
Discussion.....	157
APPENDIX E. PROTOTYPE REACTOR CALCULATIONS.....	161
Prototype Design Calculations.....	161
Production Comparison.....	164
General Protocol for Reactor Operation.....	168
APPENDIX F. CURRENT EP PROTOCOL AND REACTOR DIMENSIONS.....	171

## LIST OF TABLES

Table		Page
III-1	Enthalpy and Heat Capacity for Vapor Species.....	39
III-2	Average Temperature (Kelvin) Estimates for Each Set of Runs A, B, C, and Overall. ....	45
III-3	Normalized Process Variables and Reactant Mole Flow Rates.....	62
A-1	Species Molecular Weights.....	109
A-2	Physical Properties – Miscellaneous.....	109
A-4	Physical Properties – Phase Transition Temperatures.....	110
A-5	Physical Properties – Density.....	111
A-6	Physical Properties – Surface Tension.....	112
A-7	Physical Properties – Vapor Pressure.....	113
A-8	Enthalpy Values for ZnSe Formation.....	115
A-9	Thermodynamic Properties – Equilibrium Constants.....	116
A-10	Thermodynamic Properties – Heat Capacity.....	117
A-11	Thermodynamic Properties – Enthalpy.....	118-119
A-12	Thermodynamic Properties – Gibbs Free Energy of Formation.....	120
A-13	Thermodynamic Properties – Entropy.....	121
A-14	Lennard-Jones Parameters for Gaseous Species.....	122
A-15	Gas Viscosity and Thermal Conductivity Estimates at Selected Temperatures.....	124

A-16	Lennard-Jones Parameters for Binary Gas Mixtures.....	126
A-17	Gas Diffusion Coefficient Estimates at Selected Temperatures.....	126
A-18	Liquid Thermal Conductivity.....	127
A-19	Liquid Viscosity Data for Zinc.....	128
A-20	Liquid Viscosity Data for Selenium.....	129
B-1	Mass Transfer Estimates.....	131-132
B-2	Boiler And Vaporization Duties.....	133
B-3	System Temperatures.....	134
B-4	Dimensionless Numbers And Heat Transfer Coefficients.....	135
B-5	Critical Heat Flux.....	136
C-1	FLUENT/UNS Species Properties.....	144
C-2	FLUENT/UNS Input Ideal Gas Density.....	145
C-3	FLUENT/UNS Input Gas Viscosity.....	145
C-4	FLUENT/UNS Input Gas Thermal Conductivity.....	146
C-5	FLUENT/UNS Input Mass Diffusivity.....	146
C-6	Reactant Stream Inputs for Kinetic Estimates and k Values.....	147
C-7	FLUENT/UNS Inputs for Reactant Streams in Parametric Study of Flow Effects on ZnSe Yield.....	148
D-1	Speed of Sound in Pure Species Gases at 1000 K.....	155
D-2	Initial Experimental Levels for CFD Model.....	157
D-3	Turbulent Jet Angles.....	158
D-4	Estimated Mixture Viscosities and Densities at 1248 K and 1 atm.....	159
D-5	Estimated Nozzle Reynolds Number for Experimental CFD at 1248 K and 1 atm. ....	160

E-1	Run Timeline Comparison.....	165
E-2	Estimated Cost Savings on Prototype Reactor.....	167



## LIST OF FIGURES

Figure		Page
III-1	Drawing of the current EP reactor system.....	17
III-2	Power and temperature readings for the zinc boiler during run BA97209. ....	30
III-3	Typical terminal settling velocity as a function of particle diameter for particles within the Stoke's regime in argon at 1250 K and 1 atm..	34
III-4	Normalized molar flow rate of reactants plotted against normalized molar flow rate of argon. A, B, and C refer to run classification.....	36
III-5	Normalized average vaporization duty plotted as a function of normalized average boiler duty. ....	37
III-6	Schematic of heat transfer into boiling liquid metal. ....	41
III-7	Typical boiling curve for water at 1 atm (Incropera and DeWitt, 1996). ....	46
III-8	Apparent boiling heat flux versus $T_e$ for liquid zinc.....	49
III-9	Apparent boiling heat flux versus $T_e$ for liquid selenium.....	49
III-10	Arhenius plot of FLUENT/UNS-fit k values to estimate pre- exponential and activation energy.....	59
III-11	3D plot of reactant mole flow rate effects on yield.....	60
III-12	Possible schemes for redesign of EP system.....	71-72
IV-1	Schematic of prototype LFAR system.....	78
IV-2	Cross-section of prototype boiler.....	80
IV-3	Cross-section of boiler and transport tube furnace.....	86

IV-4	Enlarged view of prototype reactor faceplate.....	88
IV-5	Cross-section of reactor tube with product tube inserted.....	91
IV-6	Radial cross-section of reactor tube.....	93
IV-7	Axial cross-section of prototype condenser.....	95
A-1	Enthalpy diagram for the ZnSe formation process.....	115
C-1	Foster geometry for EP reactor.....	138
C-2	Laminar velocity profile in FLUENT/UNS output.....	139
F-1	Drawing of EP reactor tube.....	172
F-2	Selenium transfer arm.....	173
F-3	Zinc transfer arm.....	174
F-4	Selenium boiler.....	175
F-5	Zinc boiler.....	176

## NOMENCLATURE

### *Roman Symbols*

$a$	Speed of sound, m/sec
$A$	Area, $m^2$
$A_c$	Cross-sectional area, $m^2$
$C$	Stoke's constant $\sim 1$ , dimensionless
$C_i$	Concentration of species $i$ , $mol/m^3$
$C_p$	Constant pressure heat capacity, J/mol-K
$\hat{C}_p$	Constant pressure heat capacity, J/kg-K
$C_\mu$	Empirical constant for FLUENT/UNS, 0.0845
$\mathcal{D}$	Average diffusivity, $m^2/sec$
$D$	Diameter, m
$D_p$	Particle diameter, m
$E_A$	Activation energy, kJ/mol
$E_l$	Lattice Energy, kJ/mol
$f$	Run service factor, dimensionless
$g$	Gravity, $9.81 m/sec^2$
$Gr$	Grashof number, dimensionless
$h$	Heat transfer coefficient, $W/m^2-K$

$h$	Height of column of liquid, m
$\Delta H$	Change in enthalpy, J/mol
$\Delta H_{rxn}$	Heat of reaction, J/mol
$k$	Turbulent kinetic energy, W
$k$	Thermal conductivity, W/m-K
$k$	Rate constant, $\text{sec}^{-1}$
$k_0$	Pre-exponential for Arrhenius rate law, $\text{sec}^{-1}$
$L$	Length, m
$L_c$	Entrance length for fully developed laminar flow, m
$M_i$	Molecular weight of species $i$ , kg/kmol
MFR	Mole flow rate, mol/sec
$N_A$	Avogadro's number, $6.023 \times 10^{23}$ molecules/mol
$N$	Mole flux, $\text{mol/m}^2\text{-sec}$
$\dot{N}$	Mole flow rate, mol/sec
$Nu$	Nusselt number, dimensionless
$\overline{Nu}$	Effective Nusselt number, dimensionless
$p$	Pressure for FLUENT/UNS equations, Pa
$P$	Pressure, Pa
$Pe$	Peclet number, dimensionless
$P_m$	Vapor pressure at melting point, atm
$Pr$	Prandtl number, dimensionless

$q$	Heat flux, $W/m^2$
$\dot{Q}$	Heat transfer rate, W
$r$	Radius, m
$\bar{r}$	Dimensionless reactor tube radius
$R$	Reactor tube radius, m
$R$	Ideal gas constant, $8.314 \text{ J-Pa/mol-m}^3\text{-K}$
$R_A$	Rate of disappearance of component A, $\text{mol/m}^3\text{-sec}$
$Re$	Reynolds number, dimensionless
$R_i$	Rate of formation of species i, $\text{mol/m}^3\text{-sec}$
$s$	Arc length, m
Se	Selenium
$Se_2$	Selenium gas
$T$	Temperature, K
$T_b$	Normal boiling point temperature, K
$T_c$	Excess temperature, $T_{iw} - T_{sat}$ , K
$T_{iw}$	Boiler inner wall temperature, K
$T_L$	Liquid temperature, K
$T_m$	Melting point temperature, K
$T_s$	Sublimation temperature, K
$T_{sat}$	Liquid saturation (boiling) temperature, K
$u$	Velocity, m/sec

$\bar{u}$	Dimensionless velocity
$u_0$	Nozzle exit velocity, m/sec
$u_{0,\min}$	Minimum nucleation velocity, m/sec
$u_t$	Particle terminal settling velocity, m/sec
$V$	Volume, $m^3$
$X_i$	Mass fraction of component $i$
$\bar{z}$	Dimensionless reactor length
Zn	Zinc

*Greek Symbols*

$\alpha$	Thermal diffusivity, $m^2/sec$
$\alpha_k$	Inverse effective Prandtl number for $k$ , dimensionless
$\alpha_\varepsilon$	Inverse effective Prandtl number for $\varepsilon$ , dimensionless
$\alpha_0$	FLUENT/UNS constant = 1.0, $m^2/sec$
$\alpha_T$	Thermal diffusivity, $m^2/sec$
$\beta$	Volume expansion coefficient, $K^{-1}$
$\varepsilon$	Rate of dissipation of turbulent kinetic energy, W
$\varepsilon$	Characteristic energy of interaction for kinetic theory, erg
$\gamma$	Ratio of specific heats, $C_p/C_v$ , dimensionless
$\eta$	Efficiency, %
$\kappa$	Boltzmann's constant, $1.30 \times 10^{-16}$ erg/K
$\mu$	Fluid viscosity, kg/m-sec

$\mu_{\text{eff}}$	Effective viscosity calculated in FLUENT/UNS, kg/m-sec
$\mu_{\text{mol}}$	Molecular viscosity supplied to FLUENT/UNS, kg/m-sec
$\nu$	Kinematic viscosity, m <sup>2</sup> /sec
$\Theta$	Angle, radians
$\rho$	Density, kg/m <sup>3</sup>
$\sigma$	Surface tension, kg/m
$\sigma_i$	Collision diameter of species i for kinetic theory, Å
$\sigma_i$	Molecular diameter of species i for collision theory, m
$\tau$	Reactor residence time, sec
$\bar{\tau}$	Average residence time, sec
$\Omega_{\mu}, \Omega_k$	Collision diffusion integral, dimensionless

*Subscripts and Superscripts*

<sup>o</sup>	standard state
$\infty$	bulk, i.e. bulk temperature
—	average
b	boiling
BP	boiling point
crit	critical
f	formation
g	gas phase
G	gas phase

hor	horizontal
iw	inner wall
i or j	component i or j
l	liquid phase
L	length
L	liquid phase
m	melting
min	minimum
M	metal
ow	outer wall
ONB	onset of nucleation boiling
qz	quartz
s	solid phase
sub	sublimation
Vap	vaporization
vert	vertical



## CHAPTER I

### INTRODUCTION

The compounds zinc selenide (ZnSe), zinc sulfide (ZnS), cadmium selenide (CdSe), and cadmium sulfide (CdS) among others are known as Group II-VI compounds due to the parent elements' location on the periodic table. Group II-VI compounds are collectively known as semiconductor materials. The electronic and optical properties possessed by these species promote ongoing research into new applications. Eagle Picher, Inc. (EP) specializes in producing large single crystals, wafers, and polycrystalline powders at a purity up to 6 nines (99.9999%). Production demands for these materials fluctuate from year to year while the demand for higher purity increases. Increased purity translates to increased lifetime in most applications. Two methods are available for obtaining high purity materials: either synthesize the materials in high purity or add a purification step to their manufacture.

Group II-VI compounds are commonly produced via three techniques: metalorganic vapor phase, wet chemical, and chemical vapor reaction (or aerosol) methods. Metalorganic vapor phase methods such as MOCVD (metalorganic chemical vapor deposition) or MOVPE (metalorganic vapor phase epitaxy) are two common industrial processes. These processes deposit a thin, microscopic layer of II-VI semiconductor species on wafers or other substrates. This method, though well studied, does not conventionally produce bulk amounts of material. Wet chemical methods

produce extremely large batches of II-VI powders through an aqueous precipitation method. This least-expensive method also produces less pure product. Wet chemical methods yield unwanted byproducts which offer a separation and purification challenge. But chemical vapor reaction methods, in this case aerosol processes, produce pure polycrystalline II-VI powders through the high-temperature homogeneous reaction of elemental II-VI components. The purity of the final product is limited only by purity of starting materials and handling methods, since solid products can be removed from the gas stream without any postprocessing steps (Pratsinis and Vemury, 1996).

### Aerosol Flow Reactor

The vapor phase reactor utilized by EP is properly termed an “aerosol flow reactor.” An aerosol process is characterized by formation of small particles in a gas stream. Aerosols are common to everyday society. Everything from a cough to photochemical smog involves particles suspended in the atmosphere. An aerosol flow reactor utilizes the properties of a reacting or condensing system to yield a bulk powder. The EP process utilizes gas-to-particle coagulation/nucleation by an undetermined mechanism to produce Group II-VI microcrystalline powders. This method of synthesis offers several processing advantages. Powder product separates completely from the unreacted feed and carrier gas stream. Currently, EP is investigating the effect of elemental starting material purity on powder product purity.

Aerosol flow reactor design involves the consideration of particle formation rate and collection. Three rates can control overall particle formation kinetics: chemical reaction, reactant mixing, and particle growth (Kodas et al., 1987). At reactor

conditions, exact chemical reaction kinetics are unknown, but common practice dictates that the limiting rate is either mixing or particle growth. Reactor inlet nozzle design controls the rate of mixing. With a high mixing rate (large turbulence), particle growth dominates, while the inverse is also true (Kodas et al., 1987). Along with kinetic considerations, Sadakata et al.(1996) include gas residence time in the reactor to account for particle collection. Usable particle collection determines the apparent extent of reaction because particles collected outside the reactor are waste.

The field of aerosol-flow reactor design has developed recently. Aerosol flow reactors are beginning to replace existing synthesis methods for powders and thick films in the microelectronics industry due to the benefits described above (Pratsinis and Vemury, 1996). Aerosol flow reactor design involves the usual design equations for pressure, concentration, residence time, and energy as a function of position within the reactor. In addition to these tools, another important tool that can be incorporated into the design process for a new reactor is CFD (computational fluid dynamics). Several software packages are on the market, which perform CFD analysis to improve reactor design. For high temperature reactors, such as the II-VI synthesis reactors, CFD models offer a low cost method to evaluate complex flow schemes and mixing patterns (Ranade, 1997). One of the more powerful tools is the FLUENT family of CFD packages. These CFD packages have not yet gained large scale publication in the field of aerosol flow reactor design despite their advantages. Implementation of these reactor design techniques will be discussed later.

EP approached Oklahoma State University to use these reactor design techniques to assist them in characterizing, improving, and increasing yields in their existing aerosol

process. The EP aerosol flow process was designed circa 1950's. Very little information on the original design is available, since constant modifications were made to the process in the ensuing years. The system was designed to operate on a laboratory scale without industrial scale production in mind. The current reactor design and operating conditions are a descendent of those initial operating conditions. Through the life of the process, operating conditions such as carrier flow rate, reactant loading, boiler and reactor temperature have been adjusted by "feel" to yield as much II-VI product as possible. The process has evolved into an art form— or as one of the members of the research group terms it, "an out of control process"— because repeatability between run outcomes is almost impossible. Due to the out of control nature, waste levels of 40 to 100% are common to the current system. This waste is composed of uncollected product powders and unreacted, high purity elemental Groups II and VI starting materials. These wastes are collected in a condenser and cannot be further used in the process. The wasted starting materials comprise the largest process expense . Reuse of these waste materials to produce sellable product was investigated early in the study, but reactor redesign proved to be the prudent measure for process improvement.

Initially EP was the end user for all of their II-VI powders. The powders were used only as feedstock for their large single-crystal growth business. These single crystals are produced at cutting-edge purity. The market for these crystals covers the spectrum of optical electronics, everything from LED's to infrared transmission windows. Recently, some of these markets have decreased, so EP is exploring the II-VI powder market. The powder market appears to be growing slowly for EP. The strength of this market will decide the destination for this and three other theses.

## Objectives

1. Characterize the current reactor design of new system
2. Design a new reactor that meets these requirements:
  - A. Incorporates aerosol flow reactor design principles
  - B. Still a horizontal layout
  - C. Reduced waste
  - D. Greater process control
  - E. Reduced turnaround time
  - F. Increased capacity by a factor 2 to 3
  - G. Increased efficiency

These goals can be achieved through traditional chemical engineering techniques and practice. Initially hands on knowledge of the process was gained, then these techniques were used to design a prototype reactor from those observations and literature research into existing aerosol flow reactor systems.

## CHAPTER II

### LITERATURE REVIEW

A general background on the current uses and manufacturing techniques that involve ZnSe will be covered initially during this section. This II-VI process section aims to inform the reader about current reservoirs of knowledge regarding II-VI compounds and uses. The second section introduces the reader to the aspects of aerosol reactors while the third details relevant reactor design issues.

#### II-VI Processes

As mentioned in the introduction, Group II-VI compounds are noted in the literature often. A great deal of research has gone into using ZnSe for end use in high efficiency blue-light emitting devices (LED's) and room temperature lasers (Grein et al., 1997). Current research topics for ZnSe are thin film growth, single crystal growth, and vaporization studies. Accordingly, the previous two topics are transport-related subjects (research centers around modeling and explaining heat and mass transfer) while the latter topic is based in thermodynamic analysis. No research has been done on the reaction kinetics of the direct vapor phase synthesis from the elemental species, but some work has been done on related synthesis routes. As with any chemical reactor, all four of these topics offer valuable insight for design of a new II-VI synthesis process. Currently two general methods are used to produce thin films; chemical vapor deposition (CVD)

methods and molecular beam epitaxy (MBE) are prevalent. Physical vapor transport (PVT) and chemical vapor transport (CVT) methods are studied in detail for single crystal growth. None of these methods describe the current EP II-VI synthesis, but some harbor analogous traits while others offer possible end uses for high purity II-VI powders. Therefore, a brief discussion of each technique is necessary.

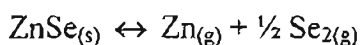
CVD methods usually employ the metalorganic precursors alkyl metals and chalcogen (Group VIA elements) hydrides. These processes now become known as metalorganic CVD or MOCVD processes. MOCVD reactors usually consist of a cool walled reactor with a heated substrate surface to which thin film growth is localized. The gas phase precursors are used to grow multilayer heterostructures on these substrates (Veuhoff, 1995). The resulting compound semiconductor material is used in the fabrication of both infrared and green-blue light emitting devices depending on the exact alloy makeup. These CVD processes have been around since 1960 (Veuhoff, 1995). Though well used, these processes are still not well understood. Surface deposition is limited by transport rates as well as surface deposition reaction rates (Durst et al., 1995). Several authors have undertaken modeling efforts to characterize MOCVD processes. Operating temperatures vary from 350 to 500 °C. Varying the substrate temperature tends to affect the Langmuir-Hinshelwood reaction mechanism by affecting the activation energy for the surface reactions while changing gas precursor concentrations affects the mass transport to the surface. Irvine and Bajaj (1994) discuss the relative importance of these factors and derive a growth rate expression that correlates well to experimental data. Study of the MOCVD literature provides no direct assistance to the study of EP's current II-VI synthesis process, but the related field of MBE has some similar traits.

MBE, like the EP process, can be performed using pure elemental components. These elemental components are heated in Knudsen effusion ovens in an ultra high vacuum environment (Yao and Shigeru, 1981). The resultant molecular or atomic beams are projected onto a heated crystalline substrate. Substrate temperatures are comparable to MOCVD temperatures. Upon this heated substrate, the deposition reaction occurs. The ultra high vacuum applied is usually between  $10^{-10}$  to  $10^{-11}$  torr. Multilayer heterostructures are grown atomic layer by atomic layer allowing exact control over composition, doping, and layer interfaces (Alavi, 1995). Not only elemental materials are used, metalorganics and even pure powders can be used as source material. MBE is therefore a possible end user of EP-produced high purity II-VI powders. Yoshikawa et al. (1989) discovered that growth rate for cracked metalorganic precursors (essentially molecular Zn and Se vapors) decreased steadily with increasing temperature. He explained this by comparing the observed phenomena to that explained by Yao et al. (1977) for the decrease of sticking coefficients with increasing temperature. These sticking coefficients determine the probability of a Zn atom “sticking” to a Se atom on the substrate surface and vice versa. The sticking ability was correlated directly to the growth rate of the layer. This sticking ability may have direct ramifications in the EP reactor. Since the reactor is at such high temperature ( $\sim 1000$  °C), growth reactions may actually proceed slower than anticipated. Without suitable empirical techniques, though, this information offers only conjecture as to the actual particle growth rate, though it might offer a possible explanation for low amounts of wall deposition on the quartz inner walls. Bulk phase particle growth rates will be discussed further in the Reactor Design section.

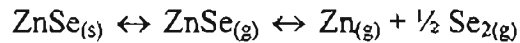


Much more useful information for synthesis of II-VI compounds has come from the single crystal growth literature. These single crystals are used as substrates for optical windows and thin film deposition processes. Goldfinger and Jeunehomme (1963) are the pioneers in the vaporization studies of II-VI compounds. Their early thermodynamic property equations and values are still cited in most contemporary vaporization and crystal growth literature. Methods for vaporization rate study of II-VI incorporate a Knudsen effusion oven to vaporize the solid ZnSe source material. To determine the composition of the gas phase as well as the mass transfer rate, optical density (absorbance) was used by Brebrick and Liu (1996), mass spectrometry by Goldfinger and Jeunehomme (1963), and thermogravimetric measurements by Bardi and Trionfetti (1990) all in conjunction with a Knudsen effusion cell. To better understand ZnSe crystal growth, these authors have used these vaporization techniques to determine equilibrium constants, vapor compositions, vaporization kinetics, and the resulting thermodynamic properties, heat capacity, enthalpy, entropy, and Gibbs energy. As part of this thesis, a compilation has been made of all the acquired empirical properties for Zn, Se, and ZnSe solids, liquids, and vapors. These properties are listed in Appendix A. It is not the intention of this thesis to gauge the reliability of the individual sources; it is therefore assumed that the most recent property correlations are most valid in subsequent analysis.

Initially, vaporization studies implied that ZnSe sublimation occurred through a decomposition type mechanism.



But recent studies by Schönherr et al. (1998) suggest that the sublimation process does involve the ZnSe gas intermediate.



Thermodynamic equilibrium correlations for the above sublimation have been tabulated in Appendix A, but a kinetic expression for the formation reaction does not exist in the literature. Indeed, very little data has been gathered on the vapor phase formation reaction. Libicky (1967) discusses synthesis of ZnSe from the molten elements. His bench-top experiment produces only 50 g of material and does not offer a kinetic expression, though. Hahn et al. (1997) published kinetic data for the corresponding metalorganic synthesis technique. To gain theoretical estimates for an Arrhenius type rate constant, Levenspiel (1972) describes a transition state theory method to estimate the activation energy and a collision theory method to estimate the pre-exponential. Transition state theory describes an arbitrary relationship between the activation energy and the change in energy between the reactants and the activated complex. This transition state energy can approximately be described as the activation energy for the reaction.

## Reactor Design

Since redesign of the entire reactor system is required in this system, the various components of the reactor must be discussed. References for design of the reactant boilers, reactant mixing, reactor body, and reactor modeling will be covered. Typical reactor design assumes control of reactant inlet streams but is not the case for the system described in this thesis. To develop an empirical correlation between the heat and mass

transfer in the EP boilers, a thorough knowledge of the boiling process is required. The analogous modes of heat and mass transfer in boiling processes are discussed by Hsu and Graham (1976), Incropera and DeWitt (1996), and Tong and Tang (1997). Tong and Tang (1997) discuss the similarities between heat transfer mechanisms for both ordinary and low Prandtl number fluids. Due to low Prandtl numbers for liquid metals, boiling heat transfer coefficients can be estimated using convective heat transfer correlations. A review of the latest empirical convective heat transfer correlations is located in Kays and Crawford (1993). A combination of these methods results in a comprehensive approach for analyzing heat and mass transfer in boiling metal systems.

Performance of every flow reactor is based on the mixing condition of reactants. For diffusion-controlled reactors, premixed feed offers the highest reactor conversion (Nauman, 1987). If feed streams cannot be premixed, suitable mixing techniques must be developed. Design of subsonic nozzles for introduction of reactant inlet streams to the reactor is of optimum importance for dictating reactor performance. Abramovich (1963) describes the theory of turbulent jets upon which nozzle design is based. Kleinstreuer (1997) further defines turbulent jets by placing Reynolds number bounds on the turbulent jet behavior. Turbulent jets form for round nozzles for Reynolds number greater than 30 based on nozzle diameter. Tilton (1997) describes the regions of flow within a turbulent free jet. Establishment of flow requires a length of approximately six nozzle diameters, while the established flow region can have a length up to one hundred nozzle diameters. Rushton (1980) provides a correlation for the spread angle of a turbulent jet based on the fluid's kinematic viscosity. Even though the nozzle Reynolds number may be turbulent, the reactor may be highly laminar. Different Reynolds numbers apply to the flow within

the reactor because they are based on tube diameter. Typically, Reynolds numbers of the order of one signal laminar flow for reactor situations. Reynolds numbers less than 0.1 can be termed creeping flow (Bird et al., 1960). Nauman (1987) discusses the modeling of convective diffusion within reactors. The dimensional relevance of radial and axial diffusion within flow systems is described. The temperature dependence of the flow characteristics within the laminar flow region is also discussed. Computational fluid dynamics (CFD) software packages such as FLUENT/UNS perform complicated fluid dynamics analyses such as these with ease. For systems with high temperature or otherwise a high degree of hazard or difficulty in direct observation, CFD models offer the best and sometimes only tool available for studying fluid dynamics (Ranade, 1997). Current CFD software packages do not easily model the influence of particles on the flow within a reactor, nor the gas-to-particle conversion. Alternate methods of modeling must be used in most cases.

The EP synthesis reactor is best described as an aerosol reactor since product powder is supplied by gas-to-particle conversion. Initial study of aerosols was focused on atmospheric phenomena with industrial applications of aerosol reactors only being developed lately. Hidy (1984) provides a comprehensive source detailing every aspect of atmospheric, large volume air mass, and combustion of aerosols, but curiously does not discuss industrial aerosol reactors. Regardless, aerosol particle formation theory, gas kinetic theory, and the required probabilistic methods are described in detail. The more recent application of aerosol technology lies in the development of aerosol flow reactors. Currently, carbon black, fumed silica, pigmentary titania, metal oxides, and other particles are produced in industrial scale aerosol flow reactors. These volume

commodities are produced by the millions of tons yearly (Pratsinis and Vemury, 1996). In this same article, Pratsinis and Vemury present a review of gas-to-particle conversion and various synthesis routes. Aerosol processes are preferred over wet methods for producing fine particles because of the lack of liquid byproducts and the ease of separating product particles from the reactant stream.

Pratsinis (1988) offers a probabilistic model to simulate simultaneous nucleation, coagulation, and condensation in a constant rate aerosol reactor. This model is suitable to apply to well-characterized aerosol systems. The term “coagulation” refers to particle growth by agglomeration of molecules or particles (Hidy, 1984), “nucleation” refers to particle growth by heterogeneous reaction on molecular clusters (Kodas et al., 1987), and “condensation” refers to formation of liquid droplets from the saturated vapor phase. These terms describe the dominant mechanism in particle formation, and the Kelvin equation is used to determine the dominance of nucleation versus coagulation (Xiong and Pratsinis, 1991). Theoretical investigations of aerosol formation and growth for coagulation-driven turbulent systems are described by Xiong and Pratsinis (1991). For nucleation-driven reactors, a systematic aerosol reactor design approach is proposed by Sadakata et al. (1996). Sadakata et al. base their design on five performance indices: reaction conversion, particle production yield, average particle size, particle size distribution, and particle purity. The last four indices are not typically used to describe homogeneous reactors and are specific to aerosol reactors. Parameters considered include characteristic times (gas residence time, particle production time, diffusion time, mixing time, and coagulation time), mixing type (premixed or diffusion mixing), flow type (laminar or turbulent), and reactor type (batch, plug flow, or complete mixing).

Kodas et al. (1987) describe mathematical modeling techniques to simulate aerosol formation for the cases of premixed reactants and mixing of multiple lamellae within the reactor. The similarity between all of these modeling techniques is the need for aerosol formation properties such as the particle formation mechanism, chemical reaction kinetics, particle behavior, and particle size distributions. In general, as Reynolds number is increased, particle size becomes smaller (nanoscale) with the size distribution approaching a monodisperse size distribution for turbulent Reynolds numbers. Typically, monodisperse size distribution is desired for particles such as those mentioned in the previous paragraph. Little direct research has been done on creeping flow aerosol reactors for large (microscale) particle formation.

Though no direct research has been done on creeping flow aerosol reactors that produce II-VI semiconductor powders, the literature contains many fruitful sources for application to this problem. This literature review has attempted to locate all of the relevant tools and properties needed to both analyze and design such a reactor.

## CHAPTER III

### POSSIBLE REACTOR CONFIGURATIONS

EP, using a laminar flow ( $Re < 1$ ) aerosol reactor, has historically performed production of polycrystalline II-VI powders. Optimum process parameters such as carrier flow rate or reactor temperature have eluded the technicians at EP for years. Uncontrolled, unmonitored, and unknown inter-run variations have wreaked havoc on process yields and equipment lifetimes. This homegrown EP process can truly be called an art since it initially requires a steep learning curve to learn how to operate the process effectively then yet another roll of the dice to produce moderate yields. During the year prior to the OCAST study (July 1996 to June 18, 1997), ZnSe production was attempted 48 times with a conservatively estimated average molar yield of 40% based on zinc. Eleven runs were aborted while only twelve runs performed satisfactorily with 60-70% yield. From conversations with EP, this period appears to follow historical trends for II-VI yields. Utilization of elemental raw materials is the main design factor. From the Aldrich Catalog Handbook of Fine Chemicals (Sigma, 1998), the cost for elemental, 99.999% pure selenium shot is \$135/100 g, and 99.9999% pure zinc shot is \$162/100 g. EP lost at least 60% of the value of these materials during that period which amounts to 14.4 kg of zinc waste at \$23,330 and 20.2 kg of selenium waste at \$27,216 in material costs alone. Also, EP incurs further cost for hazardous waste removal since the II-VI

waste is useless in EP's process. Hazardous waste disposal charges for these metals currently runs approximately \$1760/kg waste (\$800/lb) which amounted to approximately \$60,900 for the year prior to the study period. Based on these estimates, EP lost over \$100,000 on this process alone to produce ZnSe; therefore, the necessity of process redesign and optimization is paramount.

EP's reactor is based on physical vapor transport (PVT) of vapor reactant species into a mixing chamber where they can combine to form a solid, microcrystalline product. The ZnSe synthesis method was studied in detail by the OCAST team. The method of synthesizing other II-VI compounds should vary predictably from the investigated one. Process parameters such as reactant loading, carrier flow, boiler and reactor temperatures are among some of the major parameters. ZnSe was chosen due to reactants' and product's perceived low toxicity as well as the cost associated with performing several experimental runs. Not only did runs suffer a large chance of failure, but also the scope of the experimental study produced 5.2 kilograms of surplus microcrystalline ZnSe powder in the short span of six weeks. Therefore, the process parameters investigated and developed in the study deal exclusively with ZnSe. Two runs were performed to synthesize CdSe for comparison with ZnSe.

ZnSe product is removed from the reactor as a yellow powder. This powder can have varying tints. These tints were associated with the presence of excess elemental reactant. A red tint was believed to be due to excess Se since the monoclinic form of Se is red. Similarly, green or gray tint was believed to be due to excess Zn. The available analytical techniques of X-ray diffraction and scanning electron microscopy (SEM) with EDAX could not detect differences in powder composition to correlate to differences in



powder color; therefore, the naked eye was commonly used to subjectively assign powder qualities. EP desired a Se rich powder to put into their crystal growth process. The ZnSe product appeared to be a powder to the naked eye, but upon microscopic investigation this powder was actually composed of blocks and needles of hexagonal crystals of 1 to 20  $\mu\text{m}$  in length. In contrast, CdSe formed visible, black crystal needles.

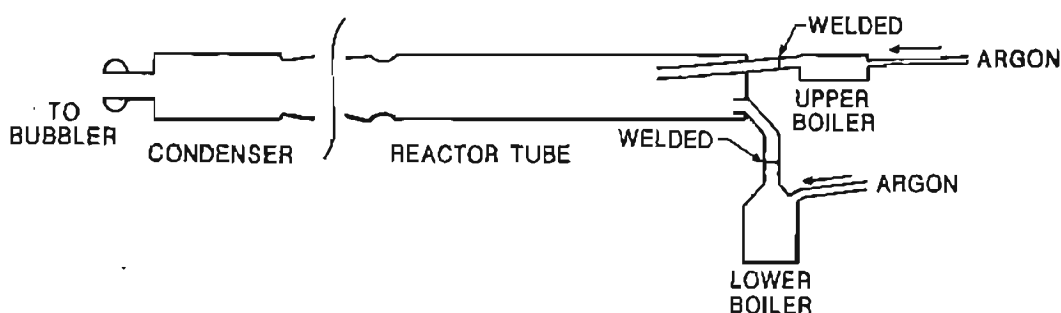


Figure III-1. Drawing of the current EP reactor system (Ghajar et al., 1996).

### Current Process Description

The EP process for II-VI powder synthesis contains four major quartz pieces and three tube furnaces. A diagram copied from the OCAST funding proposal (Ghajar et al., 1996) is displayed in Figure III-1. The synthesis is centered around a horizontal, tubular reactor. This laminar flow reactor serves as a mixing, particle growth, and powder collection chamber. This tubular reactor is inserted into a large tube furnace to act as both a heating source and a heat sink for the reactor. Temperature controllers for the system are mounted on the furnace support table. Each of the two reactants, metal and chalcogen, are introduced to the reactor through offset inlet tubes. Prior to each run, the boilers must be welded to the reactor tube. The reactant species are vaporized in the

boilers independently enclosed in tube furnaces. The front end of the system is insulated with fiberfrax strips. Argon is used as a carrier gas to help transport the vaporized reactant species into the reactor. A water-cooled, quartz condenser is used to collect unreacted vapors when they exit the reactor chamber. The condenser attaches to the reactor with a ground glass joint. This condenser is enclosed in a sheet metal box attached to the rear end of the furnace. The condenser is consistently choked with collected raw materials at run's conclusion.

Performing a synthesis run consists of several steps described below. EP's detailed protocol for operation of the reactor is referenced in Appendix F. Initially a clean reactor tube is inserted into the furnace and centered using quartz shims on the front and rear. Suitable amounts of raw materials are weighed into the respective boilers. Typical runs on the 95 mm inside diameter (ID) reactor tube are loaded with 500 g (7.65 moles) of zinc and 700 g (8.87 moles) of selenium. The bottom (selenium) boiler is then placed in its heater unit and raised into a position where the boiler neck contacts the bottom neck of the reactor. These two pieces are then welded together using an oxygen/hydrogen torch. The top boiler is positioned to meet its inlet neck using a tripod stand and welded. Argon carrier flow is established at this point by attaching the argon supply to each boiler. Precise argon mass flows are unnecessary while the system is purged. Next, the condenser is attached to the rear ground glass quartz connector on the reactor and sealed using a silicon-based stop-cock grease. The bubbler is attached to the condenser along with the cold water supply. Finally, any exposed quartz on the boilers (Se neck, top of Se boiler, and rear of Zn heater) are packed with fiberfrax insulation. The rear end of the furnace is packed with insulation to lower heat loss into the condenser

box. The system is purged overnight with argon to remove any air before commencing the synthesis run. Thermocouples are inserted in to the two reactant boilers and temperature ramps and hold points are set for them. The reactor furnace temperature controllers are set. Argon flow is set to run levels. After the system has purged, the furnace power is activated and the furnace is allowed to warm up for a few hours before the boiler units are activated. The boilers are ramped up to a hold point below the final set point. Initially, this hold point was maintained at the boiling temperature for each component, but after the study it was maintained 10 degrees below the boiling point. This allowed the operator to effectively control the start of mass transfer from the boilers. Seemingly minor factors like the latter were discovered which affect the process performance. These will be discussed in the Process Analysis section. After the final run temperatures are set, the reactor is allowed to run interrupted for several hours, usually 4-6 hours, before shutdown. It is common procedure to visibly check that all the liquids have vaporized before shutting the system down. The reactor is allowed to run until all the reactants are boiled away since leftover zinc shatters the quartz boiler upon cooling and leftover selenium is difficult to remove from the boilers.

After the tube is allowed to cool to a safe handling temperature, usually overnight, it is removed from the reactor. The powdered product is then scraped from the reactor. A “good” vs. “bad” visual characterization is performed at this time to discard “bad” powder. The reactor cleaning process is then begun. The reactor with boilers still attached has to be carried to another wing of the building where the boilers can be sawn off. The three pieces are then returned to the synthesis area where cleaning begins. A 3:1 hydrochloric (HCl) to nitric (HNO<sub>3</sub>) acid mixture is used to clean the reactor tube.

This usually requires about a liter of acid to work effectively. About 250 mL of  $\text{HNO}_3$  is used to clean each of the boilers. The condenser collects a sizable amount of waste material that is scraped into a solid hazardous waste drum. The partially spent aqua regia acid is then used to clean the condenser. This treatment is not done for every run, only when the condenser is especially fouled with pure metals. Initially, the reactor was also cleaned with a hydrofluoric (HF) acid solution, but this was discontinued later on since this acid is strong enough to weaken the joints in the apparatus. After rinsing the apparatus with deionized water, it is thoroughly dried and ready for another run.

### Process Analysis

Process analysis was conducted in two stages. The initial stage began by mastering the techniques used to conduct synthesis runs. This initial stage of process discovery allowed the group to build up its collective skill level in preparation of experimental process analysis. During this stage, operating parameters were ranked according to perceived importance, preliminary sketches of possible design configurations/modifications were made, and characterization of intrinsic flaws within the process was begun. These flaws came in the form of mechanical and procedural inconsistencies inherent in the current reactor design. These inconsistencies could only be addressed through process redesign. The preliminary sketches for alternative process concepts will be discussed in the later reactor configurations section. Statistical process control methods were applied in the second stage to determine the actual importance of the earlier characterized operating parameters. From this study came suggestions for optimum operating conditions for the current design which would maximize powder

yields for ZnSe. In the absence of funding for building a newly designed reactor, the optimization of the current process became paramount.

Discovery of process nuances continued through the duration of the OCAST study. Each experimental run seemed to yield new insight by uncovering uncontrolled process variables. EP had an out of control, hence unpredictable, process to produce II-VI semiconductor powders. The reactor scheme was as follows:

1. Elemental reactants were vaporized in boilers on the front end of the system.
2. These vapor reactants were transported with the help of an argon inert gas stream to the reactor chamber.
3. The reactant vapor streams mixed in a low Re number, laminar flow reactor.
4. Gas-to-particle conversion was carried out through either a nucleation or coagulation driven process.
5. Solid ZnSe particles settled out of the reacting vapor stream.
6. Excess vapor reactants condensed in a water-cooled condenser at the back of the system.

The system was small scale; at optimum it yielded 40-60% conversion of zinc at a maximum capacity of 0.8 kg. Not included in this conversion is the rate of run failure. Currently one out of five runs can be classified as a failure or aborted due to either plugging or excessive structural formation. Selenium was included in excess under the assumption that Se-rich conditions favored high conversion of zinc and therefore increased capacity, but conversely it also increased the risk of run failure.

As stated in the introduction, the single largest cost for this reactor was the high-purity elemental reactants. To address the issue of reactant cost, reactant utilization must be addressed. To date, the only way to decrease reactant cost for the system is to use less pure raw materials, a step with uncertain effects on product quality. Hence, raw material costs cannot decrease so raw material utilization must increase. This means improving yield and using stoichiometric amounts of reactants for each run. Safety was the largest concern that arose out of the current system analysis. As mentioned earlier, the process involves vaporization of metals and near metals, namely zinc, selenium, cadmium, and sulfur. The current system operates in an approximately 12 ft. by 15 ft. enclosure. Air is circulated through the enclosure by drawing it through a fume hood at the rear of the reactor. It was status quo for fumes from the run to escape the enclosure either through the enclosure itself or by escaping through the hood and scrubber system. The reactor system also requires frequent cleaning. Cleaning involves copious amounts of  $\text{HNO}_3$  and  $\text{HCl}$ . A new design needs to account for fugitive metal vapor emissions as well as decrease operator exposure to these vapors and metal-contaminated acid solutions.

Since the reactor and boilers have to be mechanically joined together before each run by welding the quartz joints, the reactor system becomes a single unit. This is the only way to maintain a sealed system and exclude air. Inclusion of air produces unwanted oxides that are difficult to separate from the product powders. After each run, the system must be cut apart into its constitutive pieces before cleaning. This excessive handling and maintenance leads to not only frequent breakage but also a relaxation of tolerances on the reactor pieces. If the pieces do survive numerous runs, apertures are often altered uncontrollably through repeated welding. This allows inconsistent flow

patterns to develop within the boilers, transfer tubes, and the reactor. Alignment of the pieces prior to welding is also inconsistent due to the inconsistent geometry of the pieces. Overall, a large portion of the process inconsistency is believed to come from the physical alterations which occur within the pieces during their maintenance lifetime. A new design should address the perceived effects of reactor maintenance on process performance.

Redesign of the reactor system as a whole is in order to increase safety as well as increase yield. Before redesign can begin, the current design must be evaluated for two reasons. The first reason for thorough evaluation is to improve performance, thereby profit, on the current system by establishing optimum operating parameters. This optimization is detailed in the thesis of Shay (1998). The second reason for evaluation is to gain the process knowledge that will be vital in scale-up and redesign such as boiler performance, temperature effects, inert effects, reactor flow patterns, and condenser performance.

### Experimental Study

A  $2^3$  fractional factorial experimental study was performed on the current system to develop a set of optimum operating parameters. Process variables investigated were argon flow rates, boiler and reactor temperature settings, reactor tube, boiler temperature ramp time, amount of excess selenium, and reactor cool down time. The only valuable response variable was molar percent yield based on zinc. Further discussion of the study is contained in the thesis of Shay (1998). Implementation of the conclusions produced clearly unanticipated performance. Yield of this “optimized” run was 35%. At this

point, other variables were identified which were not rigorously accounted for in the original study. The free standing boilers and their heaters were inadequately insulated to maintain consistent heat transfer characteristics. Also, the procedure used in raising the boiler temperatures to steady state conditions for the runs was not reproducible. The boilers were temperature controlled as opposed to constant heat flux. The boiler temperature ramp was controllably varied from one hour (low level) to two hours (positive level) as a variable in the study. During this ramp, the temperature was raised to a “hold point” which was the boiling point for the liquid metal. This “hold point” was maintained for approximately 5 to 15 minutes, the final boiler temperatures were programmed, and the boilers were maintained at this temperature for the duration of the run. This procedure was the single largest inconsistency within the study since it probably led to nucleation on the nozzles. Before the solution applied to this procedural flaw is discussed, the perceived impact on reactor performance should be addressed.

As mentioned earlier, the only relevant reactor output was yield. High yield runs (>70%) had one common thread; powder was distributed as a loosely-packed bed on the floor of the reactor tube. Low yield runs also had one commonality; a significant proportion of the product powder was deposited as part of a densely-packed, tube-like structure. These tube structures proved to be the bane of the process since they were an extension of the upper inlet tube which sometimes traversed a large fraction of the reactor length. The most extreme of the cases involved a plug at the upper inlet nozzle. This plug was actually a tube whose diameter decreased quickly enough as it grew to close the inlet. These structures were seldom observed at the lower (selenium) inlet probably due to the bouancy of the reactant gas streams.



The main impact of these structures on the reactor yield came by the effective decrease in reactor volume that they induced. As the zinc inlet “grew” toward the reactor exit, mixing, reacting, and settling volumes were decreased even though the characteristic mixing, reacting, and settling times for the reactor remained constant. The tube was not often thin walled, it usually spread to contain a majority of the product powder. The formation of these tubes appeared to be unpredictable and deceptive. In some runs, multiple structures successively formed and fell from the reactor ceiling. In others, the structure adhered to the quartz ceiling and only succumbed with scraping. The tube structures formed as a direct consequence of inconsistent boiling initiation and subsequent mass transfer of reactants. Since the approach to and beyond the boiling point for these liquids was not rigorously controlled, reactant vapor introduction to the reactor was not controlled. In practice (plugged runs) it was noted that an extreme excess of  $\text{Se}_2$  vapor in the reactor would lead to plugging of the zinc nozzle. This condition arose due to either “early” boiling in Se, loss of argon flow through the Zn boiler, or failure to reach boiling in the Zn boiler. Plugged Zn nozzles were the extreme manifestation of this control problem. Less extreme results produced tube structures. The powder deposition pattern could be tied directly to performance. Four regions of powder deposition thus performance were identified: I) zinc inlet plug, II) extensive structural formation, III) a transition region with minor structures, and IV) a bed of loosely-packed powder.

To address the procedural inconsistency in the initiation of boiling and the resulting mass transfer, extra thermocouples were installed for the final confirmation run, BA98009, to monitor boiler and transfer tube temperature outside the heater. (Note that

individual powder synthesis runs performed by EP will be referred to by their product lot numbers. For example a ZnSe product lot is given the first two letters "BA," all runs performed in 1997 begin with "97," and a run performed on January 1 will end with "001." The resulting lot number is BA97001.) Boilers were heated to 10 degrees below the boiling point and maintained at that temperature until the exterior thermocouples reflected a steady internal temperature for the vapor stream and quartz pieces. After equilibration, the final temperature settings were programmed. Boilers reached final temperatures without overshooting. Consequently, the run yielded 70%. This was a good yield but not optimum since two earlier production runs exceeded this value. So attempts at optimization should continue for the current system. But without a better understanding of the performance characteristics of the system, this optimization cannot proceed.

The experimental study concluded that performance, yield, of the reactor system was a function of both excess selenium and boiling temperature with low excess selenium and low boiling temperature preferred. It was hypothesized that optimum reactor performance could be obtained by simultaneous introduction of stoichiometric amounts of reactants to the reactor at a minimum flow rate. This minimum flow rate should be high enough that product cannot nucleate on inlet nozzles yet low enough that reactant molecules have the highest residence time possible within the reactor. To address this hypothesis, the body of data gained from production and experimental runs was examined to determine the impact of mass flow on reactor performance. This data was further used to estimate the relative effects of heat and carrier gas input on the

vaporization process in the boilers. Control over the mass transfer from liquid to gas in boilers and gas reactants to reactor will be the basis for a new reactor design.

### Data Set

Of the approximately twenty runs performed during the OCAST study, seven provided enough data to make mass transfer estimates. Three were production runs (BA97155, BA97161, and BA97142) and four were experimental runs (BA98009, BA97217, BA97209, and BA97204). Yields for these runs varied from 34.8% to 87.6%, and all are tabulated in Appendix B, Table B-1. The 87.6% run (BA97155) was the highest yield ZnSe run on record! Of these runs, tube structures were observed in three of the experimental runs (excluding the final confirmation run BA98009), and a short (~6 inch) tube was noted in BA97142. No record was made of tube structures in BA97155 or BA97161. Yields were, respectively, 87.6% and 73.7% so it was assumed that no tubes formed. The observed deposition patterns for these runs fell nicely into regions II, III, and IV mentioned earlier. The corresponding regions of yield were region II (35-46%), region III (59%), and region IV (70-88%). Approximate ranges of yield could hence be assigned to the powder deposition regions: I) plugging, 0%, II) major structures, 0-45%, III) transition, 45-69%, and IV) loose bed, 69-100%. The 100% maximum yield is also approximate. No good estimate of the theoretical maximum yield has been made yet, but it will certainly be less than this.

These seven runs that make up the mass transfer data set can be categorized according to run conditions. The production runs are category A: Zn boiler was 1226 K, Se boiler was 994 K, and Zn and Se argon flows were  $1.8 \times 10^{-4}$  mol/sec. The parameters

for this category were established by the reactor operator through trial and error and provided the highest yields. The experimental runs, in contrast, were not all aimed at achieving high yields. Two of the runs were factorial levels in the study (BA97204 and BA97209), but the other two (BA97217 and BA98009) were confirmation runs which should have produced a high yield of ZnSe. The latter three runs (BA97209 and BA97009) were classified as category B: Zn boiler was 1223 K, Se boiler was 991 K, and Zn and Se argon flows were 2.0 and  $2.1 \times 10^{-4}$  mol/sec. The final run (BA97204) fell into category C by itself: Zn boiler was 1229 K, Se boiler was 997 K, and Zn and Se argon flows were 1.3 and  $1.4 \times 10^{-4}$  mol/sec. These categories can be simply compared; A has medium temperatures and high carrier flow, B has low temperatures and high carrier flow, and C has high temperatures and low carrier flow. To ease discussion, the intertwined subjects of mass and heat transfer analysis have been separated in the following sections.

### Reactor Performance

Mass transfer was postulated to control yield i.e. reactor performance. The following section describes the technique used to garner mass transfer estimates from pre-existing experimental observations. These estimates were the first obtained in such a manner. Indeed, they were the first mass transfer estimates by any method other than visual inspection. Mechanical interference by removing insulation and/or heaters had unknown effects on the steady state boiling process. After the mass transfer estimating procedure is described, the results of a FLUENT isothermal CFD model with empirical kinetics and similar flow rates is discussed. The correlation between mass flow of

reactants and yield is described from the results of that parametric study. Further discussion is given to the individual runs in the previous experimental data set of mass transfer estimates. The correlation between yield and the concepts of minimum nucleation velocity and stoichiometric flow are identified. Finally, a qualitative comparison is made between reactant mass flows and the yield for the data set on both an individual run and a lumped run basis.

Mass flow estimates were obtained by examining the run observations to estimate total mass flow time. In some cases, a visual inspection of the boiler yielded an approximate time for complete vaporization of the liquid. In the remainder of the cases, the recorded boiler power input and temperature readings were used to estimate vaporization rates. During the runs, readings were periodically taken for each boiler. The boilers were maintained at a steady state temperature throughout the run by using a thermocouple which measured the outside wall temperature of the individual boilers. Run temperature settings average 1226 K for the zinc boiler and 994 K for the selenium boiler. Temperature data is tabulated in Table B-3. The vaporization process was estimated to conclude at large deviations from the steady state readings as shown in Figure III-2. A low, an average, and a high time estimate were made from these readings. The time estimates were then used to estimate average mass flow rates for the reactants. Mass flow time estimates are included along with the resulting average mole flow rates in Table B-1.

Using this technique offered good initial estimates for the mass transfer rate. In all seven runs, the average deviation between the low and high time estimates was 0.47 hours for the Zn estimates which is 12% of the overall average run

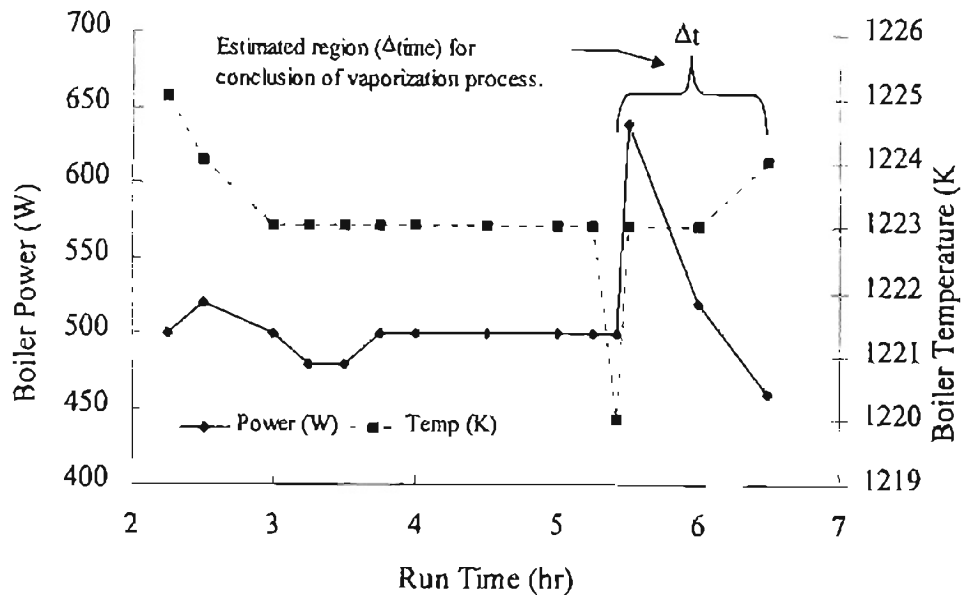


Figure III-2. Power and temperature readings for the zinc boiler during run BA97209.

time of 4.0 hours. The selenium estimates did not maintain such small deviations. The average deviation for selenium time estimates was 1.07 hours which was 34% of the overall average run time of 3.2 hours. This large deviation came from two runs (BA98009 with 2.0 hours and BA97204 with 2.75 hours deviation). The approximate validity of these mass transfer estimates was checked using standard heat transfer calculations that will be described in the following sections. The BA98009 low time estimate correlated to a spurious temperature. Using the low time estimate, a mass flow of  $2.4 \times 10^{-3}$  mol/sec for selenium was estimated. This low time estimate of one hour proved to be too liberal since it corresponded to a liquid  $T_c$  of  $58^\circ$ . The liquid  $T_c$  is defined as the difference between the superheated wall and the liquid's saturation temperature ( $T_c = T_{iw} - T_{sat}$ ). This value was approximately four times the average of all other selenium estimates so it was discarded as being too aggressive. Once the estimates

were adjusted accordingly for selenium mass flow, the average deviation in transfer times was 0.79 hours, which was 24% of the new average run time of 3.33 hours.

The surprising fact dealing with these time estimates is not the uncertainty, but relative difference between the two average flow rates. These estimates dictate that the selenium supply ran out when only three fourths of the zinc had been used. If this were assumed perfectly representative, then the stoichiometric maximum possible yield for these runs would be about 70%. The observed average was 58.8%, which was 22% lower than the maximum. This 22% difference is composed of the uncertainty in the mass flow measurement technique and the theoretical kinetic maximum yield for this laminar reactor scheme. The results of a parametric study performed on an isothermal empirical-kinetics FLUENT/UNS CFD model predicted that yield approaches a maximum for stoichiometric reactant flows. As the magnitude of these flows was decreased within the range  $9 \times 10^{-4}$  to  $3 \times 10^{-4}$  mol/sec, yield steadily increased. If stoichiometry was shifted toward excess selenium, the yield dropped little while a large valley accompanied a shift toward excess zinc. The theoretical maximum yield was predicted by the CFD model using the overall average flow rates ( $5.4 \times 10^{-4}$  for Zn and  $3.8 \times 10^{-4}$  for  $\text{Se}_2$ ). This maximum yield was 71.1%. This value was slightly larger than the stoichiometrically predicted yield due to the laminar flow characteristics of the reactor model. The FLUENT/UNS model is discussed in detail in the following section.

Upon further inspection of the mass flow estimates, some other trends were identified which helped to refine the conclusions of the factorial experimental study. The average yield for each class of run A, B, and C were respectively 73.3%, 48.7%, and 45.5%. The latter two were unacceptably low. To simplify comparison all flow rates

will be rounded to the nearest 1/10,000, expressed in units of  $10^{-4}$  mol/sec, and include inert flow rate. The average molar flow rates through the selenium nozzle were ordered B (11) > A (9) > C (7). According to the conclusions of the factorial study, the yield should be in the reverse order (C>A>B) with lowest selenium flow rate producing the highest yield, but this was clearly not the case. Two possible reasons were postulated for this contradiction:

- a) class C only has one run in the data set, and its results could be in error, or
- b) the yield is not entirely based on the total inflow of selenium.

The governing hypothesis of the system stated earlier indicates that for ideal performance mass flow should be stoichiometric, and inlet nozzle velocity should exceed a minimum nucleation velocity. From the results of the mass flow comparison and the location of product tube formation, this minimum nucleation velocity must be based on the Zn nozzle conditions not the selenium. Since structures formed at the upper (Zn) nozzle, flow should determine the region of powder deposition while the relative amounts of Zn and Se should determine yield within that region. The more important variable in determining final yield should be Zn flow while the Zn to Se ratio should determine maximum yield possible. Indeed, the average Zn mole flows from the data supported this conclusion. The classes ordered according to Zn flow are A (8) > B (7) > C (5) which qualitatively matches the trend in yields of A > B > C. The ratio of Zn to Se flows was A (0.9) > B (0.5) while C (0.7) was intermediate. These ratios combined with the earlier conclusion that low Se flow produced a higher yield are not consistent with the observed yield distribution. This inconsistency led to the conclusion that a minimum inlet velocity must be achieved to prevent product nucleation on the nozzle. Complex structure



formation must determine the outcome of the run. Therefore, the concept of regions for powder deposition patterns was supported.

From this data set, a criterion for minimum nucleation velocity,  $u_{o,min}$ , was developed for the zinc nozzle. In a future system, this criterion can be applied to either reactant nozzle. Based on molar flow estimates, the nozzle velocities for the 18-mm diameter reactant nozzles in the current system are listed in Table B-1. For the three runs, which lay in region II,  $u_o$  ranged from 0.2 to 0.3 m/sec. The transition region III was approximately 0.3 m/sec, and the region IV velocities were slightly higher. But within the accuracy of the time estimates, the mass flows for the different regions were indistinguishable. Taking this insensitivity into account, an approximate criterion was assigned for  $u_{o,min}$  on all subsequent designs. The value of  $u_{o,min}$  was arbitrarily set to 0.5 m/sec that was slightly larger but still the same magnitude as the flows observed.

Another common observation among all experimental and production runs was the lack of ZnSe powder collected in the condenser. Even for low yield runs in region II of powder deposition, little ZnSe product settled in the condenser. This phenomena was a direct result of the change in fluid density caused by the reaction. As molecules of reactant were removed from the vapor phase in the gas-to-particle conversion, the overall fluid velocity decreased. For example, in BA97155 the initial average fluid velocity was 0.02 m/sec while the final velocity was estimated to be 0.008 m/sec – a 50% decrease. The terminal settling velocity can be calculated in the Stoke's regime using the following equation (Cooper and Alley, 1994).

$$u_t = \frac{C\rho D_p^2}{18\mu} \quad (\text{III-1})$$

The constant  $C$  is assumed equal to 1 at reactor conditions. A typical plot is shown in Figure III-3 for the relation between  $u_t$  and  $D_p$  in pure argon at reactor temperatures. The typical particle size distribution for the EP reactor lies within the 1 to 20  $\mu\text{m}$  range. As the particles increase in size, their  $u_t$  approaches the  $u$  for the gas phase within the reactor. This means that near the end of the reactor particles drop more sharply than at the front. This behavior explains the appearance of “even” beds of powder which do not travel into the condenser.

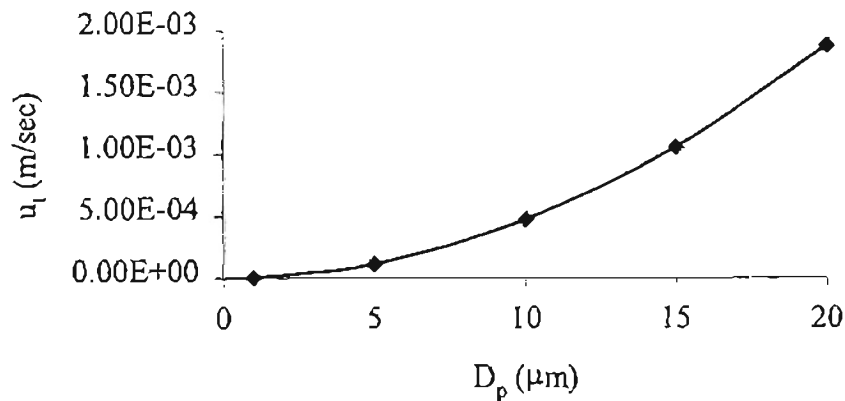


Figure III-3. Typical terminal settling velocity as a function of particle diameter for particles within the Stoke's regime in argon at 1250 K and 1 atm.

### Reactant Mass Transfer

#### Molar Flow Rate

The importance of mass flow of reactants has been shown, but what controls the mass transfer of reactants from the liquid to vapor phase? Boiler performance can be gauged by argon carrier gas flow rate and heat input since they couple to determine the mass flow of reactants. In the following section, those relationships will be explored.

Initially, the effects of argon carrier flow will be compared to mass flow estimates. Then the effects of boiler duty (heat input) will be compared to mass flow estimates. Based on a boiler energy balance, the efficiency of the boiling process will be investigated, and possible reasons for the observed trends will be discussed. The boiling process and the resulting mass transfer will be further discussed through the development of temperature profiles for the boiling system.

Three different levels were used for inert carrier flow into the boilers. For ease of analysis, all argon flows will be expressed in units of  $10^{-4}$  mol/sec rounded to the nearest thousandth. The zinc inlet argon flows were ordered B (2.0) > A (1.8) > C (1.3), and the selenium argon supply was ordered similarly B (2.0) > A (1.8) > C (1.4). As mentioned earlier, the corresponding reactant flows were ordered A > B > C for zinc and B > A > C for selenium. Flows were normalized and the trends are graphically displayed below in Figure III-4. The similarities between the selenium and its argon carrier flow rate may be based on the geometry of the boiler system, and likewise the zinc dissimilarity may be based on the boiler geometry. The mass transfer of selenium from the boiler to the vapor phase then to the reactor appeared to be tied to the argon carrier gas flow rate. The most likely explanation for this difference could be tied to past EP observations of a selenium reflux within the lower boiler. The neck and supply tube were not heated, and temperature measurements for run BA98009 ranged from 500 to 650°C during mass transfer. This same trend must have existed in each run; therefore, selenium could condense on the cooler, unheated surface causing reflux. Hence, higher inert flow rates would allow less of the selenium vapor to diffuse through the boundary layer to the cool wall. Since the entire zinc boiler and supply tube were heated, no such reflux could

occur. Therefore, no coupling was observed between argon carrier flow and zinc mass flow.

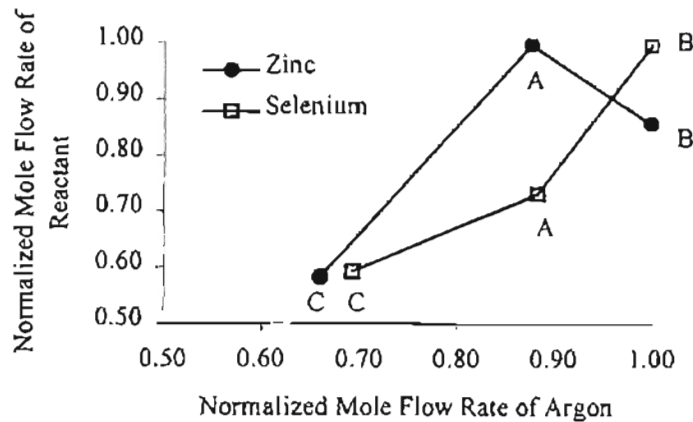


Figure III-4. Normalized molar flow rate of reactants plotted against normalized molar flow rate of argon. A, B, and C refer to run classification.

The second component in the control of mass transfer was the heat input. The boiler duty should directly control the vaporization rate of the reactants. The average boiler duties were found by averaging the recorded entries to determine low, midpoint, and high boiler duty estimates. Reactant mass flow rates were compared to the power inputs. For the zinc boiler, the average boiler duty trend, A (532 W) > B (527 W) > C (480 W), matches the mole flow rate trend, A > B > C. In contrast, the trend for average selenium boiler duty, A (704 W) > B (616 W) > C (588 W), does not match the mole flow rate trend, B > A > C. Individual run values are located in Table B-2. These duties are normalized and compared to the normalized mass flow rates below in Figure III-5. Just as the selenium mass transfer was shown to be coupled to the argon flow rate, so now the zinc flow rate is coupled to the heat input. This result further supports the effects of reflux within the selenium boiler.

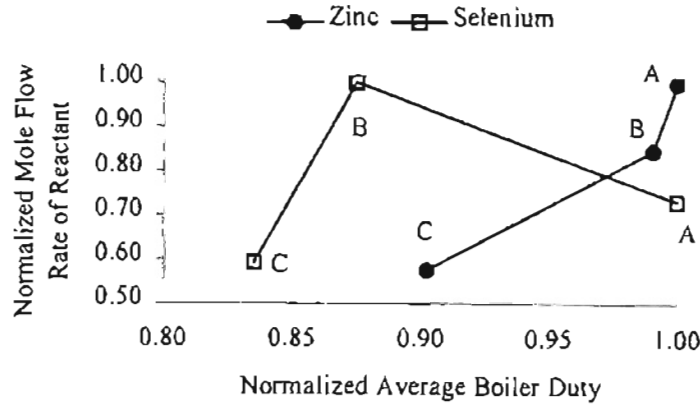


Figure III-5. Normalized average vaporization duty plotted as a function of normalized average boiler duty.

### Energy Balance

The energy balance using the boiler as a control volume is shown in equation (III-2). Equation (III-2) was applied to each of the boilers to determine average boiler efficiencies. Efficiency values reflected any systematic errors within the data set.

$$\dot{Q}_{Ar,In} + \dot{Q}_{Boiler} = \dot{Q}_{M\ Vapor} + \dot{Q}_{Ar,Out} + \dot{Q}_{Loss} \quad (III-2)$$

The uncertainty for each measurement was most likely caused by the inconsistent practices of insulating the boilers and the temperature ramp, and uncertainties can be lumped into the  $\dot{Q}_{Loss}$  term. From the boiler duty, mass flow estimates, and argon flow, the first four terms in equation (III-2) could be determined. The heat input supplied by argon was assumed equal to the product of the reference enthalpy for argon and the mole flow rate for argon as shown in equation (III-3):

$$\dot{Q}_{Ar,In} = \dot{N}_{Ar,In} \Delta H^{\circ} \quad (III-3)$$

The method for obtaining boiler duties was previously described. To obtain the heat loss

from the control volume due to outflow of argon, equation (III-3) was modified to reflect the heat absorbed to raise the argon temperature:

$$\dot{Q}_{Ar.Out} = \dot{N}_{Ar.In} (\Delta H^\circ + \int_{T_1}^{T_2} C_p dT) \quad (III-3a)$$

For the actual systems,  $T_1$  was assumed to be 300 K, and  $T_2$  was assumed to be the bulk liquid temperature of the molten metal. Estimation of the bulk liquid temperature will be described in detail in later paragraphs. Magnitudes of argon duty were small compared to the metal vapor duty. Values are located in Table B-2, and the values ranged from 1 to 5 W. The third term in the energy balance corresponds to heat input to vaporize the metal and raise the vapor temperature to the bulk liquid temperature. This was obtained using equation (III-4):

$$\dot{Q}_{M.Vapor} = \dot{N}_M (\Delta H_{Vap}^{BP} + \int_{T_{BP}}^{T_L} C_p dT) \quad (III-4)$$

where  $M$  = metal, BP signifies “normal boiling point”, and  $T_L$  = bulk liquid temperature. To simplify calculations, the heat capacity term in equation (III-4) was neglected since values were commonly less than 1% of the vaporization portion of the duty. The relevant enthalpies and heat capacities are annotated in Table III-1.

Table III-1

## Enthalpy and Heat Capacity for Vapor Species

	$\Delta H^\circ$ (J/mol)	$\Delta H_{\text{vap}}^{\text{BP}}$ (kJ/mol)	$C_p$ (J/mol-K)
Zn <sub>(g)</sub>	-	114.7 <sup>2</sup>	20.77 <sup>4</sup>
Se <sub>2(g)</sub>	-	121.9 <sup>3</sup>	44.56-2.654x10 <sup>-3</sup> (T) <sup>4</sup>
Ar <sub>(g)</sub>	6227.9 <sup>1</sup>	-	20.8 <sup>1</sup>

<sup>1</sup> T = 300 K, Stewart and Jacobsen, 1989

<sup>2</sup> Morgan, 1985

<sup>3</sup> Kudryavtsev, 1974

<sup>4</sup> Barin et al., 1977

Boiler Efficiency

Analysis of the efficiencies reflects the impact of boiler insulation – both the procedure for insulating and the mechanical design for the heaters. The zinc and selenium heaters are in two different orientations so efficiencies should be discussed separately for each. The horizontal zinc heater is plugged at one end by being pushed against the reactor furnace with a sheet of insulation sandwiched in between. At the other end, a sheet of insulation was placed over the tube opening to ensure that the ends of the heating elements were not exposed. This arrangement provided consistent heating of the entire boiler and transfer tube to the reactor. The resulting efficiency values range from 9 to 14% for the seven runs in the data set with a sample standard deviation of 1.9%. In contrast, the selenium boiler neck and reactant transfer tube protruded from the heater and thus were unheated. This section of the system was manually packed with loose insulation. Heat loss in this area directly affected the mass transfer and reactor yield. Indeed, one of the process modifications mentioned in the Background involved maintaining a steady temperature gradient within this section before boiling was initiated.

The sample standard deviation among boiler efficiency values for the selenium heater varies 4.1% from 10 to 20%. These efficiency values can be averaged to yield a general correlation for an operator to apply to the current system to estimate reactant flow rates. These standard deviations correspond to a 20% error for zinc and a 30-40% error for selenium when used to estimate mass flow rates. These are high values, but not unreasonable for use in the current system since no estimation technique is currently employed.

### Temperature Profiles

Even though the heat required to raise the gas temperature to the bulk liquid temperature was small compared to the heat required to vaporize the metal, an important reason existed for estimating temperature profiles within the boilers. The temperatures should directly reflect the boiling rate within the system. The bulk liquid temperature ( $T_L$ ) not only impacts vapor temperature but also should affect the rate of mass transfer through boiling. The superheated temperature of the inner wall ( $T_{iw}$ ) affects the rate of boiling within the boiler. The next several paragraphs will discuss computational methods before temperature effects can be discussed in detail. A schematic of the boiling system with notation used in the following heat transfer calculations is shown in Figure III-6.



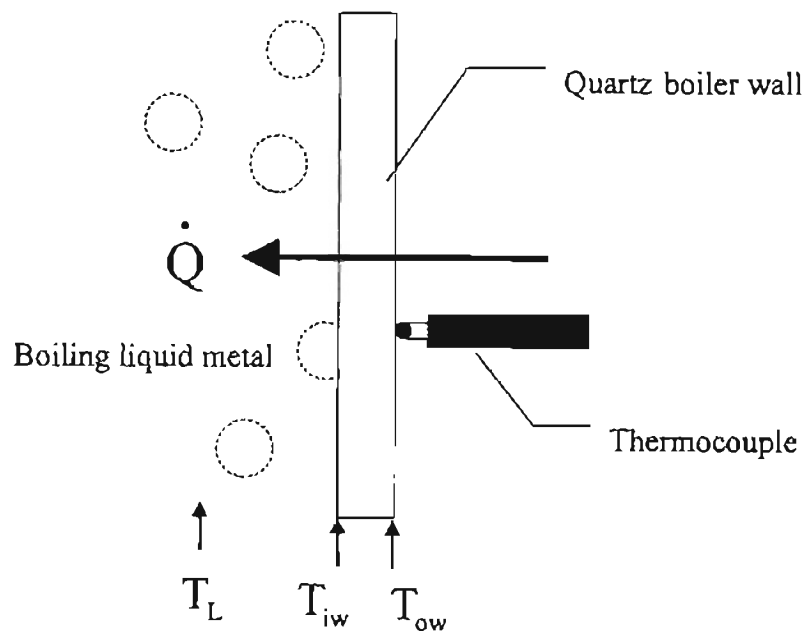


Figure III-6. Schematic of heat transfer into boiling liquid metal.

Both boilers are ordinary cylinders, so Fourier's Law of Conduction and Newton's Law of Cooling are modified for cylinders to calculate system temperatures. Radiation effects were neglected. The following assumptions were made in application of these general laws to the data: steady state heat transfer, heat enters the liquid solely through the wetted surface of the quartz on the walls of the cylinder, and zero heat flux through the ends. Since the boilers had different orientations, horizontal for zinc and vertical for selenium, slightly different forms of the equations were used. Initially,  $T_{iw}$  values were found for the selenium boiler using equation (III-5).

$$\dot{Q}_{Se \text{ vap}} = \frac{2\pi L k_{qz} (T_{ow} - T_{iw})}{\ln\left(\frac{r_{ow}}{r_{iw}}\right)} \quad (\text{III-5})$$

For each run, the liquid height ( $L$ ) was calculated using the density function for liquid selenium  $\rho_{L,Se} \text{ (kg/m}^3\text{)} = 3750 - 0.75 \cdot (T - 493 \text{ K})$  (Lide, 1998), at the boiler outer

wall temperature for the initial loading of selenium. Likewise, an average value of 2.3 W/m-K at 950 K was used for the thermal conductivity of quartz ( $k_{qz}$ ) (Heraeus, 1986). The inner ( $r_{iw}$ ) and outer ( $r_{ow}$ ) radii for the selenium boiler were 0.0375 and 0.040 m respectively. Individual run values for the variables are located in Tables B-1 for L, B-2 for  $\dot{Q}_{Se\ v_{ap}}$ , and B-3 for  $T_{ow}$  and  $T_{iw}$ . In Table III-2 below, the average  $T_{iw}$  are displayed for each set of runs A, B, C, and overall. For the zinc boiler, a slightly modified form of equation (III-5) was used. Since the boiler was horizontal, liquid pooled on the bottom; therefore, wetted area i.e. contact area ( $A_c$ ) was not a uniform function of radius. Using the density for zinc, from  $\rho_{L,Zn}$  ( $kg/m^3$ ) = 6576 - 0.98\*(T - 692 K) (Lide, 1998), the initial volume of molten zinc was determined for each run. This volume was divided by the boiler length, 0.178 m, to determine the initial cross sectional area for the liquid. The following geometry relations were used to calculate the arc length (s) of the wetted segment of the boiler circumference based on the area (A) and the angle ( $\Theta$ ) of the segment.

$$A = \frac{1}{2} r^2 (\Theta - \sin \Theta) \quad (III-6a)$$

$$s = r\Theta \quad (III-6b)$$

The product of the arc length and boiler length (sL) was defined as  $A_c$  for heat transfer into the molten zinc. Fourier's Law was modified to equation (III-7) for the zinc boiler to account for both the cylindrical geometry and the nonuniform contact area.

$$\dot{Q}_{Zn\ v_{ap}} = \frac{A_c k_{qz} (T_{ow} - T_{iw})}{r_{iw} \ln\left(\frac{r_{ow}}{r_{iw}}\right)} \quad (III-7)$$

An average value of 2.7 W/m-K at 1223 K was used for  $k_{qz}$  (Heraeus, 1986), and  $r_{iw}$  and  $r_{ow}$  for the zinc boiler were 0.0225 and 0.050 m respectively. Values of the variables in

equation (III-6) for individual runs are located Tables B-1 for L, B-2 for  $\dot{Q}_{Zn\ vapor}$ , and B-3 for  $T_{ow}$  and  $T_{iw}$ . Table III-2 lists the average  $T_{iw}$  and  $T_{ow}$  for each set of runs A, B, C, and overall.

Estimation of the bulk liquid temperature ( $T_L$ ) for the data set was not as simple as using the law of conduction. For Newton's law of cooling, a value for a heat transfer coefficient ( $h_L$ ) was required. The coefficients are system specific and usually determined empirically. No such coefficients were available for the liquid selenium-quartz or liquid zinc-quartz systems so suitable empirical correlations had to be used. In ordinary liquids, boiling heat transfer is much larger (at least 100% larger) than convective heat transfer (Hsu and Graham, 1976), but in liquid metals greater similarity exists between the convective and boiling coefficients due to low Prandtl numbers (Tong and Tang, 1997). Therefore, free convection correlations were suitable for estimating  $h_L$ . Free convection correlations typically take the form  $Nu = Nu(Gr, Pr)$  where  $Nu$  is the dimensionless Nusselt number in equation (III-8),  $Pr$  is the Prandtl number in equation (III-9), and  $Gr$  is the Grashof number in equation (III-10).

$$\text{Nusselt Number:} \quad Nu_L = \frac{h L}{k} \quad (III-8)$$

$$\text{Prandtl Number:} \quad Pr = \frac{\nu}{\alpha} = \frac{\mu C_p}{k} \quad (III-9)$$

$$\text{Grashof Number:} \quad Gr_L = \frac{g\beta}{\nu^2} (T_0 - T_\infty) L^3, \quad \beta = -\frac{1}{\rho} \left( \frac{\partial \rho}{\partial T} \right)_p \quad (III-10)$$

The characteristic dimension,  $L$ , for equations (III-8) and (III-10) was taken as the cylinder diameter ( $D_{iw} = 0.045$  m) for the zinc boiler and the liquid height for selenium. The  $Nu$  number gauges the effects of convection versus conduction, the  $Gr$  number gives

the ratio of buoyant to viscous forces, and Pr number gives the ratio of kinematic viscosity to thermal diffusivity. The values for individual runs, the average group values, and the overall averages for these dimensionless numbers are located in Table B-4. Liquid metals typically have  $Pr < 0.1$ , and since  $Pr_{zn} = 1 \times 10^{-4}$  and  $Pr_{sc} = 4 \times 10^{-2}$ , they exhibit metallic heat transfer characteristics.

For the vertical selenium boiler, the 1975 correlation of Churchill and Chu for fluids with any Pr,  $Gr < 10^{12}$ , isothermal, vertical semi infinite plate heat source was used (Kays and Crawford, 1993).

$$Nu = \frac{0.15(Gr Pr)^{1/3}}{[1 + (0.492/Pr)^{9/16}]^{16/27}} \quad (III-11)$$

The resulting Nu number was modified to reflect curvature effects using the method recommended by Kays and Crawford (1993) in equation (III-12).

$$\overline{Nu} = \frac{2}{\ln(1 + 2/Nu)} \quad (III-12)$$

For the horizontal zinc boiler, the 1976 correlation of Kuehn and Goldstein for  $GrPr > 10^9$ , turbulent boundary layer, isothermal, and horizontal cylinder was used (Kays and Crawford, 1993).

$$Nu = 0.1(Gr Pr)^{1/3} \quad (III-13)$$

To correct for the observed values of  $Gr < 10^9/Pr$ , equation (III-13) was used again. The resulting values for  $h_L$  were used in Newton's Law of Cooling to estimate  $T_L$  for each run based on initial liquid volumes.

$$\dot{Q}_{M \text{ vap}} = h_L A_c (T_{iw} - T_L) \quad (III-14)$$

Since the physical properties used to calculate the dimensionless numbers are

functions of  $T_L$ , iteration was used to determine final values of  $h_L$  and  $T_L$ . Initial values for  $T_L$  were set at the boiling points for each component. Solutions typically converged within five iterations. The final values of the dimensionless numbers and  $h_L$  values are located in Table B-3, and the final temperature values are located in Table B-4. Average temperature values are displayed below in Table III-2.

Table III-2

Average Temperature (Kelvin) Estimates for Each Set of Runs A, B, C, and Overall.

	Zinc			Selenium		
	$T_{ow}$	$T_{iw}$	$T_L$	$T_{ow}$	$T_{iw}$	$T_L$
A	1226	1220	1220	994	986	975
B	1223	1217	1217	997	980	981
C	1229	1225	1225	997	990	981
Overall	1226	1221	1221	994	986	974

At the elevated temperature levels displayed in Table III-2, the normally insulating nature of quartz becomes relatively inconsequential. An average gradient of only 5 K occurs in the zinc boiler wall while only 8 K through the selenium boiler wall. The greater thermal conductivity and greater metallic nature of zinc are displayed in the  $T_L$  values. No temperature gradient exists between the inner wall and the bulk liquid for zinc while a 12 K gradient exists for the selenium. Consequently, the molten zinc temperature should equilibrate quicker than the selenium for a given temperature ramp. For the zinc boiler, the resistance to heat transfer supplied by the quartz is definitely controlling, but in the selenium both the resistances supplied by the quartz and the selenium itself are roughly equal. Upon reviewing these temperature estimates, an unexplained behavior was noticed. In general, as the mass flow rate of reactant

increased, the excess temperature of the boilers did not follow suit. Intuitively, as the temperature is increased the mass transfer should also increase, but it did not. Before investigating this curious phenomenon, a brief description of the boiling process is required.

### Boiling Effects

Boiling is a complex process. Several authors (Hsu and Graham, Tong and Tang, Incropera and DeWitt, etc.) have offered summaries of the current theories about the mechanism of heat and mass transfer within a boiling system. The boiling heat flux and subsequent mass flux are a function excess temperature ( $T_c = T_{iw} - T_{sat}$ ). Early on, the physical manifestation of boiling was observed to happen within discrete regions. Figure III-7 shows the shape for a typical boiling curve with the regions labeled.

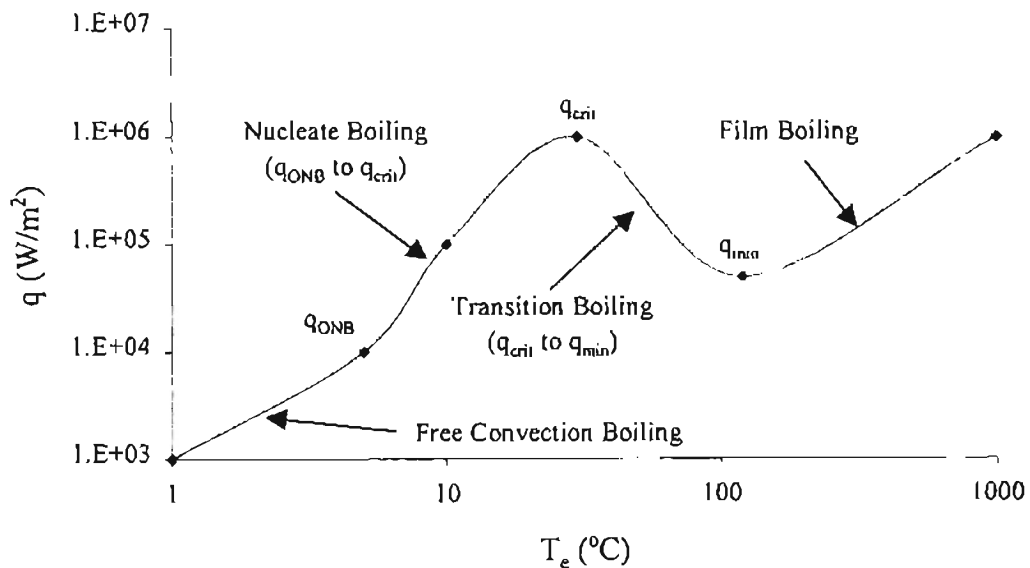


Figure III-7. Typical boiling curve for water at 1 atm (Incropera and DeWitt, 1996).

According to Incropera and DeWitt (1996), for low  $T_e$ ,  $\sim 5^\circ\text{C}$  for water, boiling manifests itself as convective mixing near the heat source within the liquid. The point for onset of nucleation boiling is labeled  $q_{\text{ONB}}$  in Figure III-7. For  $T_e$  from 5 to  $30^\circ\text{C}$  for water, “nucleate boiling” occurs. Nucleate boiling is characterized by small bubbles forming at defects on the heater surface appropriately termed nucleation sites. For  $T_e$  from 30 to  $120^\circ\text{C}$ , unstable patches of vapor form during “transition boiling.” This region extends from the critical heat flux to the minimum heat flux or Leidenfrost point. Within this region, heat transfer decreases with increasing  $T_e$  until the Leidenfrost point due to the insulating value of the growing vapor layer. Above  $120^\circ\text{C}$  for water, “film boiling” occurs. Film boiling forms a consistent layer of vapor between the bulk liquid and the heat source, and heat transfer again increases with increasing  $T_e$ . Since mass transfer and heat transfer mechanisms are analogous, the mass flux should follow similar trends to heat flux in Figure III-7 as a function of  $T_e$ . From the data of Bonilla et al. 1965 and Marto and Rohsenow 1966 displayed in Tong and Tang (1997), the  $T_e$  increases for boiling alkali metals as surface defects (bubble nucleation sites) are removed. Correspondingly, for a constant value of  $T_e$ , the heat flux increases with increasing density of surface defects.

Though no boiling curves could be found for the EP liquid metals, a qualitative comparison can be made to the standard boiling curve for water using this knowledge. For water, heat transfer during boiling (hence mass transfer) is at least 100% larger than free convection alone (Hsu and Graham, 1976). As mentioned earlier, the magnitude of boiling liquid metal heat transfer is much closer to convective heat transfer (Tong and Tang, 1997). From this knowledge, it can be inferred that lower  $T_e$  values will

correspond to the large heat flux values seen on the water boiling curve (see Figure III-7). The EP boilers were initially assumed to operate on the positive slope side of the boiling curve in the nucleate boiling region; therefore,  $T_e$  should increase with heat flux until it reaches the maximum heat flux value. This important reference point,  $q_{crit}$ , was calculated for each boiler for each run using equations (III-15) and (III-16) supplied by Tong and Tang (1997).

$$\text{Horizontal: } q_{crit,hor} = 0.13(\rho_G)^{1/2} \Delta H_{vap} [\sigma_G (\rho_L - \rho_G)]^{1/4} \quad (\text{III-15})$$

$$\text{Vertical: } q_{crit,vert} = 0.098(\rho_G)^{1/2} \Delta H_{vap} [\sigma_G (\rho_L - \rho_G)]^{1/4} \quad (\text{III-16})$$

Critical heat flux values are located in Table B-5 for the time average mass flow rate for each run. All critical heat flux estimates are on the order of  $10^6$  W/m<sup>2</sup>. For run BA97155, equation (III-15) was used to estimate a  $q_{crit}$  value of  $4.0 \times 10^6$  W. This value is about 5 orders of magnitude larger than the estimated metal vapor duty of 63 W! From this comparison, which holds true for all runs, the boiling metals should fall within the nucleate boiling region of the boiling curve. Therefore, mass transfer should increase with increasing  $T_e$  within the data set.

As alluded to earlier, the mass transfer rates for the metal vapors generally decrease with increasing  $T_e$  across the data set. In Figures III-8 and III-9, the values for apparent heat flux into the metal vapor are plotted against calculated  $T_e$  for the individual runs and as group averages. The apparent boiling heat flux is calculated using the earlier-defined  $A_e$ . It can be clearly seen that some unknown factor couples the behavior within each set of runs A, B, and C. Straight-line fits have been applied to the runs in groups A and B with good accuracy. From the curves connecting the average values for each group, the steadily decreasing nature of mass transfer versus increasing  $T_e$  can be



observed. Systematic error can be ruled out as a possible route for this behavior since the third point of group B for selenium and the first point for group B in zinc correspond to data taken approximately 5 months later. These points still follow the trend closely established by the two other data points for group B.

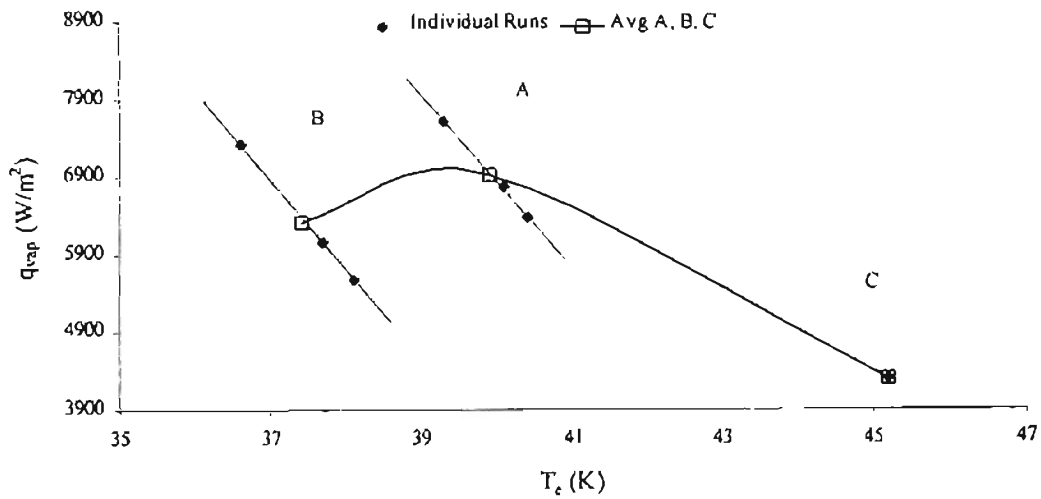


Figure III-8. Apparent boiling heat flux versus  $T_c$  for liquid zinc.

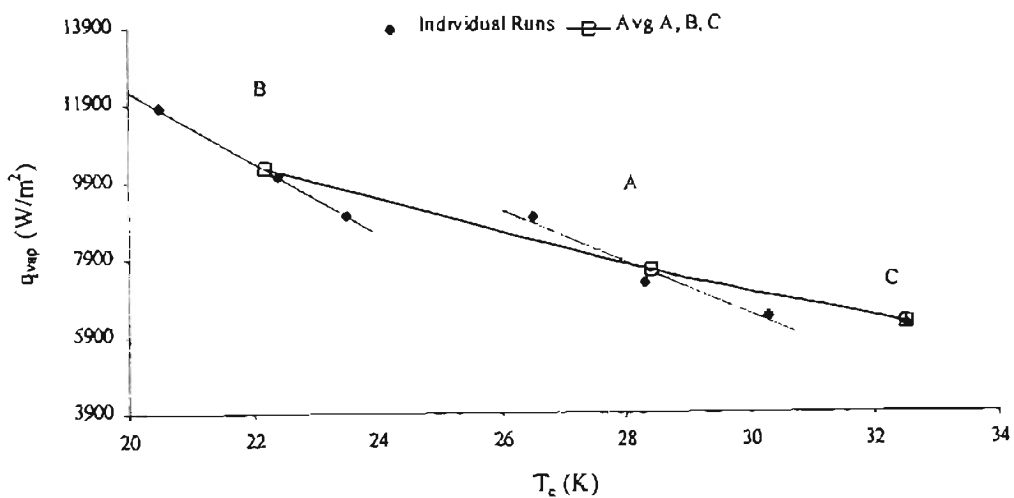


Figure III-9. Apparent boiling heat flux versus  $T_c$  for liquid selenium.

The only conceivable solution to the dilemma of decreasing mass transfer with increasing  $T_e$  implies that the boiling process occurs within the transition boiling region described previously. The boiling curve has a negative slope this region as shown in Figure III-7. But the calculated values for  $q_{crit}$  are orders of magnitude larger than those observed empirically. To reconcile heat flux with the assumption that boiling occurs within the transition region, the boiling heat transfer area,  $A_b$ , must be much smaller than the liquid contact area,  $A_c$ . The heat transfer rate,  $\dot{Q}_{M\ v_{ap}}$ , calculated earlier agrees with the boiler energy balance so the actual heat transfer area, hence the number of surface defects, must be much smaller. The quartz boilers begin their lives by being annealed so they should have very few surface defects when properly maintained. Therefore, the boiling must actually occur through an unsteady process of transition boiling or “bumping” with short periods of inactivity followed by spurts of vapor formation. Further study must be performed, ideally with visual inspection of the boiling process, on the EP boilers before these ideas can be confirmed.

### Modeling

Given the sum of process knowledge accumulated regarding the EP process, including the lack of reaction and particle formation kinetics, several steps were taken toward modeling the system. The first step in modeling the system was to apply traditional dimensional analysis techniques to determine flow characteristics for the reactor. Then further modeling was performed using the commercial FLUENT/UNS computational fluid dynamics (CFD) package. Without additional programming, the FLUENT/UNS software could not account for particle formation and growth in the fluid

system, so simplifying assumptions had to be made. Based on the outputs gained from the CFD model, earlier reactor performance conclusions were evaluated. This verification of reactor performance based on the model was further used to explain possible particle dynamics within the reactor.

### Dimensional analysis

Dimensional analysis can be applied to the EP system to determine bulk flow characteristics. The Reynolds number (Re) can be used to describe the flow as either laminar or turbulent. Based on the overall estimates of flow in Table B-2, initial fluid velocity would be 0.021 m/sec and exit velocity assuming the average conversion of 55.8% based on zinc would be 0.014 m/sec. This yields a Re number,

$$Re = \frac{\rho u D}{\mu} \quad (\text{III-17})$$

of 24 at the entrance and 16 at the exit. An average value of 20 for the Reynolds number means that the reactor operates in the laminar flow regime. The entrance length for the velocity profile to fully develop can be calculated according to equation III-18 (Young et al., 1997).

$$L_e = 0.06 D Re \quad (\text{III-18})$$

The selenium velocity profile should be fully developed by the time it reaches the zinc nozzle since the  $L_{e,Se}$  is about 6 cm (the approximate length of the zinc nozzle). The overall  $L_e$  is about 13 cm from the zinc nozzle. Therefore, for the 1 m long reactor tube, the velocity should have a fully developed parabolic profile within about 20 cm.

The reactant mixing mechanism is either convective or diffusion controlled. The Peclet number represents the ratio of convective to diffusive transport for an isothermal system.

$$Pe = \frac{\mathcal{D}\bar{\tau}}{R^2} \quad (\text{III-19})$$

The average diffusivity is  $\mathcal{D}$ , average residence time is  $\bar{\tau}$ , and  $R$  is reactor tube radius.

Using an average  $\mathcal{D}$  value of  $1.4 \times 10^{-4} \text{ m}^2/\text{sec}$  and the average  $\bar{\tau}$  based on entrance velocity of 48 sec, the  $Pe$  number is 0.27. From the method of Merrill and Hamrin (Nauman, 1987), if  $1/Pe$  is greater than  $3 \times 10^{-3}$ , the reactor mixing is diffusion controlled. Since the average inverse  $Pe$  for the EP reactor is 3.7 which is  $\gg 3 \times 10^{-3}$ , mixing can be considered to be highly diffusion controlled. Nauman (1987) further provides the component material balance and energy balance in dimensionless form for laminar reactors.

$$\text{Component: } \frac{u_z(r)}{\bar{u}} \frac{\partial C_i}{\partial \bar{z}} = \left( \frac{\mathcal{D}_{AB}\bar{\tau}}{R^2} \right) \left[ \underbrace{\frac{1}{\bar{r}} \frac{\partial C_i}{\partial \bar{r}} + \frac{\partial^2 C_i}{\partial \bar{r}^2}}_{\text{Radial Diff.}} + \underbrace{\left( \frac{R}{L} \right)^2 \frac{\partial^2 C_i}{\partial \bar{z}^2}}_{\text{Axial Diff.}} \right] \quad (\text{III-20})$$

$$\text{Energy: } \frac{u_z(r)}{\bar{u}} \frac{\partial T}{\partial \bar{z}} = \left( \frac{\alpha_T \bar{\tau}}{R^2} \right) \left[ \frac{1}{\bar{r}} \frac{\partial T}{\partial \bar{r}} + \frac{\partial^2 T}{\partial \bar{r}^2} \right] - \frac{\Delta H_{rxn} R_A \bar{\tau}}{\rho C_p} \quad (\text{III-21})$$

For the EP reactor,  $(R/L)^2 = 2 \times 10^{-3}$  which is less than  $10^{-2}$ ; therefore, the axial diffusion term in equation III-20 can be neglected (Nauman, 1987). From these two equations, it can be seen that temperature variation can have a significant effect on diffusion within the reactor; therefore, these two equations must be solved simultaneously. Also, something must be known about the velocity profile for the system. Since the flow is two-phase, gas-solid, the fluid is not going to behave like a Newtonian fluid. Based on

this knowledge, a more involved numerical approach can be performed to model the flow conditions within the reactor more precisely. But based on the minimal knowledge of the actual conditions within the reactor, this approach cannot presently be attempted.

#### FLUENT/UNS Flow Model

With a few reasonable assumptions a comprehensive flow model was developed using the FLUENT/UNS CFD software package. Since the Re number is so low for the system and the equilibrium favors solid ZnSe so highly, a cognizant flow model was developed based on the single-phase behavior. Several techniques were attempted to model actual aerosol system behavior. The real difficulty in modeling the system lies in accounting for particle formation. A discrete phase model was investigated, a surface reaction term was added, and a momentum source term was added, all attempting to account for solid particle effects within the system. None of these techniques were successful either due to unfeasibility or operator ignorance. The model was therefore limited to a gas phase mechanism. The general assumption was made that  $ZnSe_{(g)}$  represents  $ZnSe_{(s)}$ , particles of which would settle in the actual system. From the low amounts of blow-through product recorded during experimental observations, this appears to be a good assumption based on the gas-solid equilibrium.

The ZnSe synthesis reactor currently operates like a black box. From operator observations, complex flow phenomena appear to dictate reactor output. Application of CFD therefore yielded insight into the reactor performance. A two dimensional, FLUENT CFD model was applied in the thesis of Foster (in progress) which incorporates the aspects of radiation heat transfer, additional kinetics, and the annular air gap. For this

thesis, a 2D isothermal (no radiation) CFD model based on the current system geometry was developed to correlate both flow effects on complex powder deposition patterns and empirical reaction kinetics based on a simple reaction mechanism for the EP reactor. Development of the chemical reaction model will be discussed in the following section, and further details on the model are described in Appendix C.

As described earlier in the reactor performance section, powder deposition commonly occurs as complex tube structures within the reactor. To this end, the overall laminar nature of the reactor cannot be assumed. At the entrance, nozzle diameter dictates initial turbulence or disruption of flow which can be evaluated based on nozzle  $Re_D$ . A full description of nozzle behavior is given in Appendix D. Earlier in the reactor performance section, an estimate was made for  $u_0$ , minimum nucleation velocity, for these tube structures to form on the zinc nozzle. Application of the flow model aimed to verify this concept based on the seven exemplary runs used earlier. Application also aimed to qualitatively represent the convective rolls as described by Shay (1998) and their effect on formation. Even though the model is 2D with no radiation effects, enough back mixing was evident to develop a plugging correlation. To effectively predict this non-laminar behavior, the built-in RNG  $k$ - $\epsilon$  viscous flow model was used in FLUENT/UNS.

The Renormalization-Group (RNG)-based  $k$ - $\epsilon$  model is a member of the standard  $k$ - $\epsilon$  turbulence models whose major strength lies in the analytically derived constants. The RNG  $k$ - $\epsilon$  model is a multiple gradient model that describes the average behavior of groups of molecules within the system. The major component of this averaging technique is the computation of an effective viscosity which provides an accurate

description of the variation of turbulent transport with the effective Reynolds number (Fluent, 1996).

$$\mu_{\text{eff}} = \mu_{\text{mol}} \left[ 1 + \sqrt{\frac{C_{\mu}}{\mu_{\text{mol}}} \frac{k}{\sqrt{\varepsilon}}} \right]^2 \quad (\text{III-21})$$

This model is capable of describing low Reynolds number flows with only small regions of turbulence like the entrance region of the EP reactor. The most important part of the RNG  $k$ - $\varepsilon$  model for application to the EP reactor is how it deals with the momentum equations. The default turbulence settings were used to develop the model based on the transport equations derived from RNG theory (Fluent, 1996). The momentum balance was used to determine local velocity profiles.

$$\frac{\partial}{\partial t} (\rho u_i) + \frac{\partial}{\partial x_j} (\rho u_i u_j) = \frac{\partial}{\partial x_j} \left[ \mu_{\text{eff}} \left( \frac{\partial u_i}{\partial x_j} + \frac{\partial u_j}{\partial x_i} \right) \right] - \frac{\partial p}{\partial x_i} \quad (\text{III-22})$$

The RNG transport equations for  $k$  and  $\varepsilon$  are

$$\frac{\partial}{\partial t} (\rho k) + \frac{\partial}{\partial x_i} (\rho u_i k) = \frac{\partial}{\partial x_i} \left( \alpha_k \mu_{\text{eff}} \frac{\partial k}{\partial x_i} \right) + \mu_i S^2 - \rho \varepsilon \quad (\text{III-23})$$

and

$$\frac{\partial}{\partial t} (\rho \varepsilon) + \frac{\partial}{\partial x_i} (\rho u_i \varepsilon) = \frac{\partial}{\partial x_i} \left( \alpha_{\varepsilon} \mu_{\text{eff}} \frac{\partial \varepsilon}{\partial x_i} \right) + C_{1\varepsilon} \frac{\varepsilon}{k} \mu_i S^2 - C_{2\varepsilon} \rho \frac{\varepsilon^2}{k} - R \quad (\text{III-24})$$

where  $\alpha_k$  and  $\alpha_{\varepsilon}$  are the inverse effective Prandtl numbers for  $k$  and  $\varepsilon$ . They are computed according to the following analytically derived equation

$$\left| \frac{\alpha - 1.3929}{\alpha_0 - 1.3929} \right|^{0.6321} \left| \frac{\alpha + 2.3929}{\alpha_0 + 2.3929} \right|^{0.3679} = \frac{\mu_{\text{mol}}}{\mu_{\text{eff}}} \quad (\text{III-24})$$

where  $\alpha_0 = 1.0$ . The constants  $S$ ,  $R$ ,  $C_{1\varepsilon}$ , and  $C_{2\varepsilon}$  are all analytically derived using the

RNG theory. All of these values were set to default values for the model.

From visual inspection of the velocity vectors, this model appeared to predict the nozzle exit turbulence. Future recommendations for the model development should include some sort of objective analysis of this entrance phenomena to predict complex structure formation based on Re or exit velocity. Also, comparison of the conclusions for prediction of entrance phenomena should be compared to the 3D model of Nikolic (in progress).

#### Kinetic Study using FLUENT/UNS Model

This FLUENT/UNS model was used to estimate empirical kinetics for the reactor based on the existing reactor observations. To correlate empirical reaction kinetics to EP reactor, the Arrhenius rate constant and activation energy were estimated. Then a parametric study based on varying reactant flow rates was performed. This study yielded important clues about the operations of the EP reactor in support of the previous factorial study. ZnSe powder is formed from the homogeneous reaction of elemental zinc and molecular selenium vapors within the EP reactor. Reaction rate data are not available in the literature for this reaction. Nor is the existing EP reactor system configured to perform a kinetic study to determine a reaction mechanism, rate constants, or reaction orders. The only data contained in the literature deals with the thermodynamics of ZnSe. From the equilibrium studies done by Schönherr et al. (1998), it can be seen that the  $\text{ZnSe}_{(g)}$  species is very thermodynamically unstable. Therefore, the  $\text{ZnSe}_{(g)}$  species will be thought of as unstable intermediate. Several possible mechanisms can be devised to represent this reaction, but analysis was based on a two step mechanism.





Reaction (III-26a) lends itself easily to CFD modeling in FLUENT/UNS, but the basic FLUENT/UNS software cannot presently deal with the gas-to-particle conversion of reaction (III-26b). Even though FLUENT/UNS cannot represent the entire mechanism, some assumptions can be made to obtain a useful model. Since the gas product species is so unstable, its concentration was directly correlated to the observed concentration of solid product. The heat of formation for the solid species was determined by Brebrick and Liu (1996) to be  $-178 \text{ kJ/mol}$ ; therefore, the overall reaction and particle formation mechanism is exothermic. The exothermic nature of the reaction was also evident during temperature profile studies done on the reactor. The exterior reactor temperature peaked in the order of  $10\text{-}20^\circ\text{C}$  above the steady-state temperature. Therefore, this exothermic nature was neglected in the model by assuming isothermal conditions for kinetic correlations. Shay (1998) performed a similar study using empirically fit second order kinetics and diffusion coefficients for a nonisothermal reactor model. Kinetic theory was used to estimate species properties for the model. Property estimation methods are detailed in Appendix A, and the species properties for the model are tabulated in Appendix C. Since no kinetic data were available, the simplest Arrhenius rate form was used to describe the kinetics.

$$R_{\text{ZnSe}} = kC_{\text{Zn}}^1 C_{\text{Se}_2}^0 = k_0 e^{(-E_A/RT)} C_{\text{Zn}}^1 C_{\text{Se}_2}^0 \quad (\text{III-27})$$

This kinetic equation was used as part of the CFD model to empirically fit a pre-exponential ( $k_0$ ) and an activation energy ( $E_A$ ) to three exemplary runs from the data set. Three runs were used in the correlation (BA97155, BA97161, and BA98009) since they

displayed ideal powder deposition. Initial estimates for  $k_0$  and  $E_A$  were obtained from theoretical methods. Transition state theory equates the activation energy for equation (III-27) to the energy required to produce an activated complex (intermediate) which was assumed to be the gas phase product molecule ( $ZnSe_{(g)}$ ) (Levenspiel, 1972). The difference between the heat of formation for  $ZnSe_{(s)}$  (-178 kJ/mol) and the heat of sublimation (370 kJ/mol) was estimated to be the energy of the activated complex. This yielded an initial estimate of 192 kJ/mol as the activation energy for equation (III-27). Collision theory was used to estimate an initial value for the pre-exponential according to equation (III-28) given by Levenspiel (1972).

$$k_0 = \left( \frac{\sigma_{Zn} + \sigma_{Se_2}}{2} \right)^2 \frac{N_A}{10^3} \sqrt{8\pi kT \left( \frac{1}{M_{Zn}} + \frac{1}{M_{Se_2}} \right)} \quad (III-28)$$

Molecular diameters for the elements were estimated to be  $1.3 \times 10^{-8}$  cm for Zn and  $2.3 \times 10^{-8}$  cm for  $Se_2$ . This yielded an initial estimate of  $4.72 \times 10^{10} \text{ sec}^{-1}$  for  $k_0$ .

Transition state theory estimates typically predict values close to those observed while the collision state theory typically serve as a ceiling for values of the pre-exponential (Levenspiel, 1972).

The low, average, and high mass flow estimates for each run were used based on these kinetics. Through trial and error,  $k_0$  values were fit while keeping  $E_A$  constant. The model's average outlet molar yield was fit to the observed experimental yield by adjusting  $k_0$ . This fit was performed for the three sets of estimates for each run. The first two runs, BA97155 and BA97161 were both run at 1273 K while the third was run at 1248 K. A suitable  $k_0$  value could not be obtained for low time estimate for BA97155. The yield reached a maximum value which was less than the observed yield so no  $k_0$

value was obtained for this run estimate. The  $k$  value was calculated using the Arrhenius formula in Equation (III-27). The resulting data points are tabulated in Table C-6 and plotted in Figure III-10. The five data points on the left correspond to the low, average, and high time estimate  $k$  values for the two runs performed at 1273 K while the three on the left correspond to the run at 1248 K. The natural logarithms of the resulting eight  $k$  values were plotted against inverse temperature. A straight line fit to these points yielded an empirical slope  $= -E_A/R$  providing an estimate for activation energy and intercept  $= \ln k_0$  providing an estimate of the pre-exponential (Levenspiel, 1972). The plot is shown in Figure III-10 below. The empirically fit  $E_A$  was 151 kJ/mol and  $k_0$  was  $5.59 \times 10^4 \text{ sec}^{-1}$ . These values were used in subsequent FLUENT/UNS simulations.

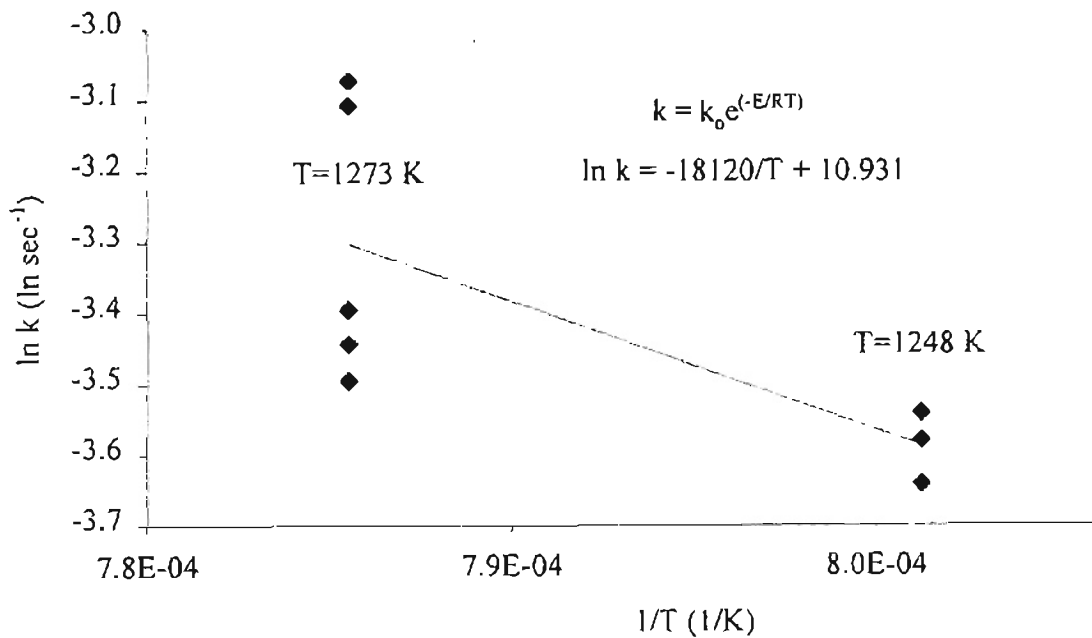


Figure III-10. Arrhenius plot of FLUENT/UNS-fit  $k$  values to estimate pre-exponential and activation energy.

After empirical kinetics were established, reactant flow rates were varied to produce an effect on yield. In this way, the model was used to predict the behavior of stoichiometric, nonstoichiometric, low, and high flows. Temperature was set at 1248 K in agreement with the results of the previous factorial SPC study. The average overall flow rates from Table B-1 were used as guides to setting flow levels. Argon flow was maintained constant at  $2.0 \times 10^{-4}$  mol/sec for each stream. Levels were varied from 3.0 to  $9.0 \times 10^{-4}$  mol/sec for Zn and 1.5 to  $4.5 \times 10^{-4}$  mol/sec for  $\text{Se}_2$ . The resulting yields varied from 50 to 83 %. The data is located in Table C-7 and an interpolated 3D mesh plot is given in Figure III-11.

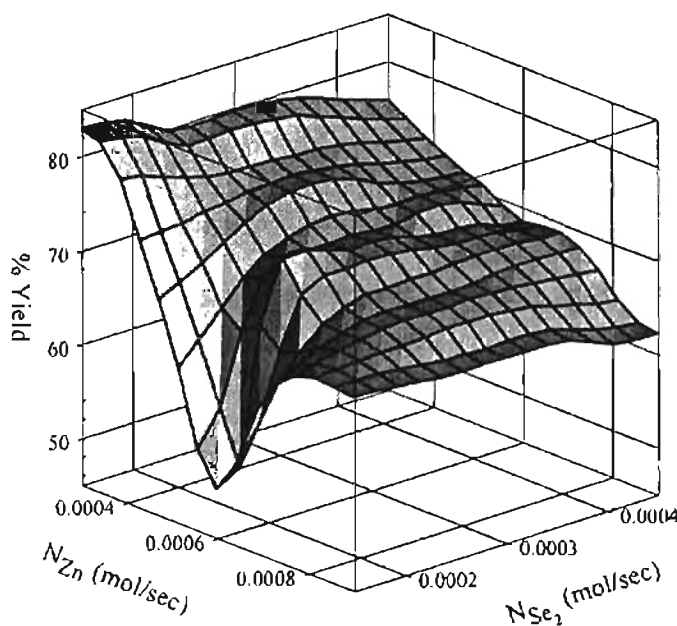


Figure III-11. 3D plot of reactant mole flow rate effects on yield.

The model supports the earlier postulate that stoichiometric, low flows produce the highest yield. If a line of equal stoichiometry is drawn on the plot, yield drops slowly for excess selenium but drops into a large valley for excess zinc. The plot might be

smoothed somewhat by using a laminar flow model, but the initial reactant mixing would not be as representative. The yield surface might also be smoothed by using a higher order rate expression. These conclusions serve as a good basis for performing coupled studies of the EP reactor using the physical reactor to refine the CFD model and vice versa.

### Conclusions from Process Analysis

In summary, the previous analysis supported the conclusions of an earlier 2<sup>3</sup> fractional factorial study which is described in detail by Shay (1998). A more detailed analysis was performed on a data set comprised of both experimental and production runs. Reactor performance was classified into three distinct regions based on product powder deposition characteristics. These regions were further correlated to observed yield indicating dependence upon product deposition characteristics. These regions were further correlated to observed yield indicating dependence upon formation mechanism. Complex structure formation was also postulated to be a function of nozzle exit velocity. Further clarification of this phenomena can be performed using either the FLUENT/UNS model developed in this thesis or those of Shay (1998), Foster (in progress), or Nikolic (in progress). The FLUENT/UNS model described within this thesis correlated isothermal kinetics to empirical data and demonstrated the diffusion-controlled nature of the EP reactor.

The mass flow rate of reactants appeared to be a complicated function of boiler geometry, insulation quality, argon flow rate, and heat input. Only argon flows and boiler heat inputs were obtained directly from the observation data, while all other

process variables were estimated from these. Table III-3 gathers all the relevant process variables for comparison to molar flow rate. All values have been normalized for qualitative comparison. The process variables are ordered according to decreasing molar flow rate. For the zinc vapor estimates, only the energy-related terms follow the decreasing mass transfer trend. For the selenium vapor estimates, only the carrier gas flow rate trend matches the decreasing mass transfer trend. A possible explanation for this behavior is based on reflux within the selenium boiler. The inconsistency of decreasing mass flow rate trend with increasing  $T_e$  is unexplained, but a possible explanation is based on “bumping” within the boiling liquid. Further experimentation is required to refine these conclusions about the mechanism of mass transfer within the system.

Table III-3

Normalized Process Variables and Reactant Mole Flow Rates.

		MFR ( $\frac{\text{mol}}{\text{sec}}$ / $\frac{\text{mol}}{\text{sec}}$ )	Argon FR ( $\frac{\text{mol}}{\text{sec}}$ / $\frac{\text{mol}}{\text{sec}}$ )	$\dot{Q}_{M \text{ vap}}$ (W/W)	$\eta$ (%/%)	$T_e$ (K/K)
Zn	A	1	0.90	1	1	0.89
	B	0.83	1	0.99	0.92	0.82
	C	0.67	0.65	0.90	0.69	1
Se <sub>2</sub>	B	1	1	0.88	1	0.67
	A	0.78	0.90	1	0.63	0.85
	C	0.67	0.70	0.84	0.63	1

## Potential New Configurations

### Goals for Redesign

Based on the process knowledge gained from both operation of the current EP system and performing detailed experimental investigation upon it, the goals for redesign of the EP reactor can be established. Initially, the only goals presented by EP for the redesign were to increase yield and capacity. To increase yield consistently, the reactor should be adapted to perform predictably, something which it does not do currently. From the process analysis, boilers must be redesigned to provide controllable mass transfer. From process operations, the release of fugitive metal vapors needs to be addressed as well. This recurring release of vapors may best be addressed through downstream effluent vapor handling within the production facility. Still other weak points in the current reactor design were engendered by the maintenance and operating procedures. The redesign goals can therefore be summed up.

- 1) Provide predictable performance.
- 2) Increase yield.
- 3) Increase capacity.
- 4) Increase safety.
- 5) Decrease maintenance.

## Review of Possible Reactor Schemes

At the outset of research, powder production was to be scaled up 100 to 1000 times. Midway through the research, estimates of future production requirements were lowered to a required increase by only a factor of two. This large variation in production goals was beneficial because it allowed a wide variety of reactor schemes to be investigated for application to this process. These schemes included the aspects of flow, mixing, and reactor geometries. Schemes ranged from novel to practical and large scale continuous to small semi-batch. Before the final design basis for the new system is discussed in the final section of this chapter, the following section will detail the possible reaction schemes mentioned above. Though most of these schemes are not useful in the current scale-up, they offer future alternative routes for II-VI powder synthesis. This utility to future design work merits description of the various schemes within this thesis. The following section provides sketches for these schemes and a brief discussion of the merits of each. To provide a means for comparison in Figure III-12, the schemes have been classified according to the following means:

- i. Practical vs. novel
- ii. Low vs. high maintenance
- iii. Laminar vs. turbulent flow
- iv. Continuous vs. modified batch reactor
- v. Development cost: low cost means that the existing data and analysis could be effectively applied to this scheme, high means that further study through planned experimentation or complex models is necessary.



Schemes are organized into eight groups according to utility within the design methodology. The groups are flow schemes, flow type, nozzle schemes, mixing schemes, anti-plugging schemes, reactor orientation, and novel reactor schemes. With enough time and money, any of these schemes could be applied to a new reactor, but due to real world constraints these schemes must be filtered. Implementation of these schemes is therefore discussed with the current reactor as a basis for comparison. As it turns out, the design basis offered in the last section of this chapter draws on a single concept from each of the groups except the last one. The redesign goals dictated the design basis such that the schemes were treated as being mutually exclusive within each group.

Flow Schemes: The three traditional flow schemes of countercurrent, crosscurrent, and cocurrent orientation of reactant streams are displayed as schemes (a), (b), and (c) in Figure III-12. The degree of convective mixing decreases from (a) to (c) because the streams are forced to intermingle more in a countercurrent than cocurrent arrangement. Likewise, the degree of diffusive mixing increases from (a) to (c) as the convective term decreases. Based on observations of powder formation patterns and plugging in the current EP system, the practicality appears to decrease from (c) to (a). Countercurrent and crosscurrent nozzles would be seem to be more likely to plug within a new reactor design. Indeed, no references were found in the literature for reactors of this sort in any orientation other than cocurrent flow. The flow schemes (a) and (b) were therefore considered impractical in a tubular flow reactor for aerosol production. Scheme (c) can be classified as a practical and widely used flow model. This flow scheme can also satisfy all of the possibilities i through v listed above.

Flow Type: Two flow types were considered – laminar flow (d) and turbulent flow (e). As described earlier, the current system operates in the laminar flow region with diffusion-controlled mixing. For the given reactor length, this type of flow and mixing are required to enable reasonably high conversions and powder collection within the reactor. Within this flow regime, aerosol particles tend to form a broad particle distribution with the capability of forming large particle diameters. In contrast, turbulent flow increases mixing enough that particle growth is hindered because reactants are used faster than particles can grow. Therefore narrow particle size distributions are produced for turbulent reactors (Wu, J. et al., 1987; Wu, M. et al., 1993; and Pratsinis and Vemury, 1996).

Nozzles: Three main nozzle schemes were identified as possible candidates for a new design. Two general concepts are embodied. Either nozzles are considered as separate entities with anywhere from two to several nozzles, or the different reactant nozzles can be combined into a single nozzle. Both concepts are widely used (Kodas et al., 1987 and Pratsinis and Vemury, 1996). The current reactor employs dual nozzles (f) with a single reactant stream entering through each. Another possible scheme involves several inlet nozzles (g) to supply the reactant streams. The third possible scheme involves annular or concentric nozzles (h). All three types have been described in the literature for both laminar diffusion-controlled reactors and turbulent dispersion-controlled reactors. However, it is currently not feasible to operate the EP system in the turbulent regime by manipulation of the inlet nozzle velocities since the reactor tube would have to be excessively long. Kodas et al. (1987) describes the proper equations to model lamellae mixing using either the diffusion flame (h) or multiple nozzles (g).

Experimental data on the EP process cannot be directly applied to the diffusion flame case, but a 3D simulation would work well based on the thesis of Nikolic (in progress). The multiple inlet scenario (g) would almost certainly cause more problems than the dual inlets (f) since more inlets allow more chance for plugging.

Mixing: Reactant mixing will dictate the final yield and reactor performance based on powder deposition patterns. Several concepts were considered to increase mixing, but the danger of plugging excluded many of them. For a turbulent reactor, an upstream object (i) can be inserted to induce vortex mixing in its wake. This type of orientation is described in the patent of König (1995). Also, radial injections of inert gas (j) can be used to induce mixing, but this can effectively dilute the reactants enough to hinder conversion. EP used baffles (k) inserted into the reactor with limited success. The introduction of baffles would not only increase mixing by creating back mixing but also act as barriers to collect powder. But on the negative side, introduction of baffles creates higher maintenance with higher possibility of contamination for the system. For low Re number laminar reactors, diffusion-controlled mixing (m) can produce high conversions. For example, the current reactor has achieved yields as high as 88%. The ideal mixing scenario for high yield in diffusion-controlled reactors can be obtained by using pre-mixed feed (l), but this is currently not feasible for a new reactor since reaction and subsequent plugging appear to happen so quickly. A novel approach could involve pre-mixing the feeds in a small diameter high flow upstream reactor section and utilize a large diameter downstream chamber for collection.

Anti-Plugging: Plugging is a major concern for any new reactor design. The current system can be plugged or partially plugged easily. This phenomenon appears to

be strictly flow based, but other factors may also apply. The current system relies solely on the inlet flow rate (n), and has been shown to operate without plugging. Plugging occurs because product is allowed to form on the surface of the nozzle. If a small inert gas flow was used to blanket the nozzles (o), reactants should be hindered from reaching their surfaces. Some experimental work would be required to set the levels of this flow. This technique was demonstrated in the patent of König (1995). A less elegant approach would be to incorporate some sort of “rapper” (p) or physical device to mechanically knock product formations off the nozzle. This alternative has several consequences. At the high temperature of the reactor, moving parts within the reactor would not survive long. Also, some sort of monitoring mechanism is required. The physical intervention into the reactor might also contaminate product. Another idea, which was demonstrated in the patent of König (1995) and Wu et al. (1987), involved a fluid wall reactor (q). Ideally a vertical reactor could be outfitted with a perforated wall. Through an annular region, the inert gas could be supplied at a sufficient flow rate to keep reactant and product particles from impacting the wall. This could eliminate wall adhesion in a large diameter reactor tube and plugging in a small diameter reactor. In principle, wall interactions would be eliminated and any number of materials would be suitable to construct the reactor. A high  $Re$ , continuous flow reactor could thus be utilized with a downstream collection system.

Reactor Orientation: A horizontal flow reactor (r) allows temperature-induced buoyancy effects for gases when operated at low  $Re$  numbers in the diffusion-controlled regime. Since all available data is based on these conditions, the horizontal flow orientation is desirable for a new reactor. A horizontal flow reactor cannot be operated at

low flow continuously without some external mechanism to remove product powder. Also, the length of the reactor tube dictates the maximum allowable flow rate if product powders are to be collected within the tube. Too high of a flow rate and powders will be blown out of the reactor. Therefore, short tubes cannot be effectively used to both produce and collect powder in the turbulent flow region. On the other hand, a vertical downer flow reactor (s) can be used successfully at high  $Re$  to produce powders. From the presentation of Jin (1998), two phase reacting flow within downer reactors produces a flat velocity profile, conversion is a function of length, and low residence times ( $\sim 1$  sec) are required for high conversion. At the bottom of the reactor, some sort of a powder collector must be used though. A downer reactor of this sort would best be applied to continuous operation.

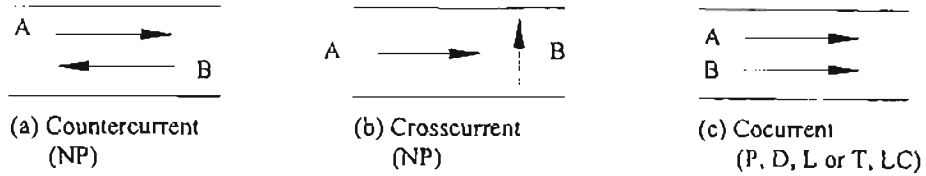
Novel Concepts: A novel approach is to design a “barrel” type reactor (t) which would involve smashing the streams into each other in a counter current fashion. This type of reactor would require high exit velocities on the nozzles into a large stagnant reservoir for settling of powders. Another concept to both reduce installation time and add a mechanical seal to eliminate welding, incorporates a segmented or modular reactor (u) enclosed within a sealed chamber. A positive pressure of inert gas can be supplied to the chamber so that the reactant stream cannot escape the modular reactor. The design benefits would include the allowance for a wide range of materials for the outer shell since it will not contact the reactants or products. Also, set-up and maintenance would be much simpler without welding the pieces together. For a continuous horizontal flow reactor, an extruder (v) can be added to the center to both act as a mixing inducer and transfer product powders out of the heated reactor. Again, at high temperatures within

the reactor lifetime and performance are uncertain. The most novel reactor concept considered involved using a cyclone reactor (w) to continuously produce product powders. This reactor idea is unlikely to yield high conversions due to the low residence time within the reactor, but its real utility would be as a powder collector for a continuous, high Re reactor.

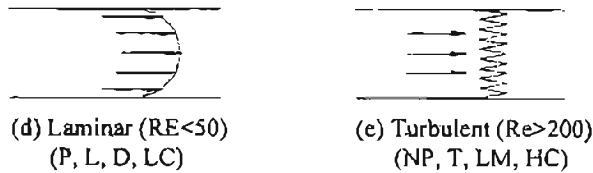
**ABBREVIATIONS**

P - Practical	LM - Low Maintenance	I - Inert Gas
NP - Not Practical	HM - High Maintenance	D - Depends
N - Novel	LC - Low Cost Research	
L - Laminar	HC - High Cost Research	
T - Turbulent	A, B - Reactant Streams	

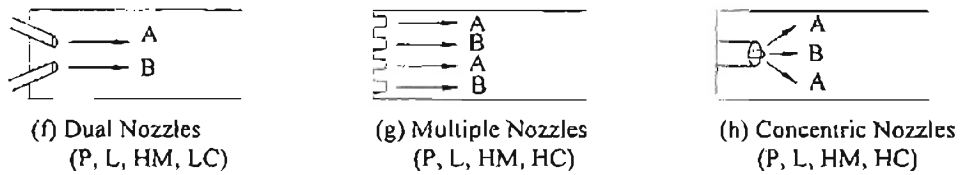
**FLOW SCHEMES**



**FLOW TYPE**



**NOZZLE SCHEMES**



**MIXING SCHEMES**

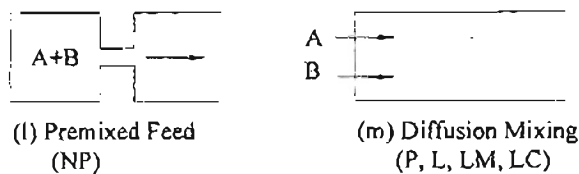
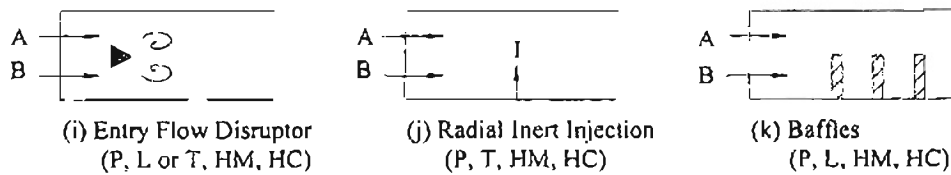
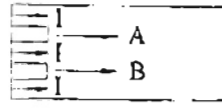


Figure III-12. Possible Schemes for Redesign of EP System.

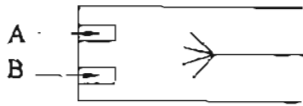
ANTI-PLUGGING SCHEMES



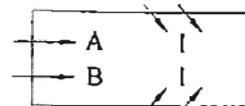
(n) Flow Controlled  
(P, L of T, HM, LC)



(o) Inert blanker for Nozzles  
(P, L or T, HM, HC)

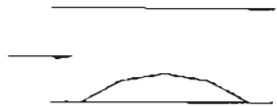


(p) "Rapper" or "Scraper"  
(N, L, HM, HC)



(q) Fluid Wall (Ideally Vertical)  
(N, T, HM, HC)

REACTOR ORIENTATION

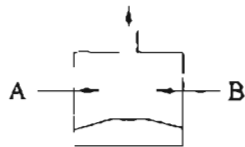


(r) Horizontal Flow  
(P, L or T, LM, LC)



(s) Vertical Flow (Downer)  
(P, T, HM, HC)

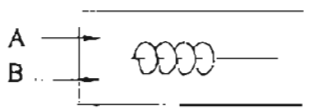
NOVEL REACTOR CONCEPTS



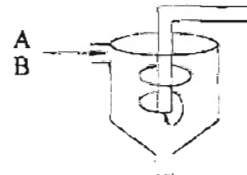
(t) Barrel-Type  
(N, T, HM, HC)



(u) Modular Reactor  
(N, L or T, LM, HC)



(v) Extruder  
(N, T, HM, LC)



(w) Cyclone Reactor  
(N, T, LM, HC)

Figure III-12, continued. Possible Schemes for Redesign of EP System.



## Design Basis

After a review of the process analysis, goals for redesign, and the potential schemes for reactor design, a prudent design basis was chosen for the new reactor design. The design basis sets specific guidelines to which the design proposal will adhere yet still remain general enough to allow more than one suitable design. The design basis is divided into five main requirements ranked below in order of importance.

- 1) 2 kg capacity
- 2) Horizontal modified batch reactor
- 3) Laminar flow (diffusion-controlled mixing)
- 4) Ability to monitor/control mass transfer
- 5) Multiple runs between system maintenance

The relevance of each requirement can be discussed below in summation of this chapter.

The magnitude of increased capacity was established by weighing the immediate production needs of EP with the amount of labor required to operate the reactor. The best estimate for a production run utilizing the new system should be no longer than the 24 to 36 hours required on the old system, but the output should be increased. Two kilograms of product rendered at an appropriate percent yield was a prudent requirement for the new system. Since scale-up was in fact only a matter of doubling the current reactor output, design became much simpler. Modifications could be made to the existing horizontal modified batch reactor design to increase capacity. The current reactor tube appeared to be operating significantly below its maximum capacity. This surplus allowed room for expanding production capacity within the same restriction of furnace diameter. Free

volume and space-time comparisons are performed within the reactor body design section in Chapter IV. Since the new reactor body will have approximately the same dimensions as the old reactor, flow levels cannot be changed. From both the CFD study performed within this thesis and the study performed by Shay (1998), increasing flow beyond the diffusion-controlled regime will lead to lower production yields. Only for the more radical schemes posited earlier can a change in flow level to fully turbulent be considered.

From the process analysis section it is obvious that reactant mass transfer control is of the utmost importance in controlling powder deposition patterns, reactant utilization, and thus yield. Also, the main component in both the steep learning curve and unpredictable performance lies within reactor maintenance. It appears that decreased maintenance, or mechanical intervention, on the boiler-reactor system would reduce uncontrolled variation. This set of guidelines does not allow sweeping interpretation as to the final nature of the system. The intention of these guidelines is to produce a much more efficient and predictable process to synthesis high purity ZnSe powders with possible expansion to other II-VI compounds.

## CHAPTER IV

### NEW REACTOR DESIGN

The prototype design for a new synthesis reactor must meet all the requirements set forth in Chapter III and also meet the goals of the design basis. Such a design is proposed in this chapter. First a brief overview of the salient features of this design concept will be discussed. Then the following sections will detail the design criteria and methods for the reactor. The design is broken into four major components: the boilers – control of mass transfer, the nozzles – control of reactant mixing, the reactor body – powder collection and removal, and the condenser – waste collection. This thesis directly addresses the boiler design and reactor body design. Production time comparisons, waste cost comparisons, and a general reactor operation protocol are located in Appendix E. The initial steps in nozzle design using a FLUENT/UNS CFD model are discussed in Appendix D. The final analysis and design recommendations for prototype nozzles and condenser design were performed by Shay (1998) and will only be summarized within this thesis.

#### Overview

Due to the current low demand for ZnSe, design of a new reactor system was based on scaling up the old system. To aid in this effort, several of the current horizontal LFAR concepts were incorporated into the new design. The prototype reactor was

designed to use the existing reactor furnace and enclosure to ease implementation costs. Modifications were made to the current design to increase both the controllability and predictability of the process.

The prototype design concept centers around a stationary reactor system that is emptied and reloaded for successive runs. A schematic diagram of the prototype system is displayed in Figure IV-1. As discussed in Chapter III, much of the inconsistency involved in the current EP reactor is cultured by the mechanically destructive nature of run set-up and breakdown. Before initial set-up, the reactor will be composed of modular pieces much like the current reactor. But unlike the current reactor, reactant addition spouts will be added to the boilers to facilitate multiple runs between maintenance. The reactor therefore can be loaded several times before it needs to be cut apart for maintenance. These new boilers are also equipped with differential pressure meters to noninvasively monitor liquid metal levels and the subsequent mass transfer in the boilers without contamination. At run completion, the product powder can be removed along with the entire inner collection tube, which will slide out of the reactor tube. This tube can be removed as soon as the reactor is cool enough to handle facilitating quick turnaround. With careful mass flow management, the condenser should mainly be a safety precaution. Controlling mass flow rates will effectively increase yield and decrease waste.

The prototype reactor is slightly more complex than the current design, but since it will be maintained for several runs, this complexity can be neglected as an economic factor. The schematic displayed in Figure IV-1 shows the proposed process layout. The major removable piece (highest breakage) of this reactor is a simple off-the-shelf section

of quartz tubing. Several of these pieces can be fabricated with the only cost being materials. The new lower maintenance design will have the capability of controllably increasing yield and capacity while decreasing waste and breakage.

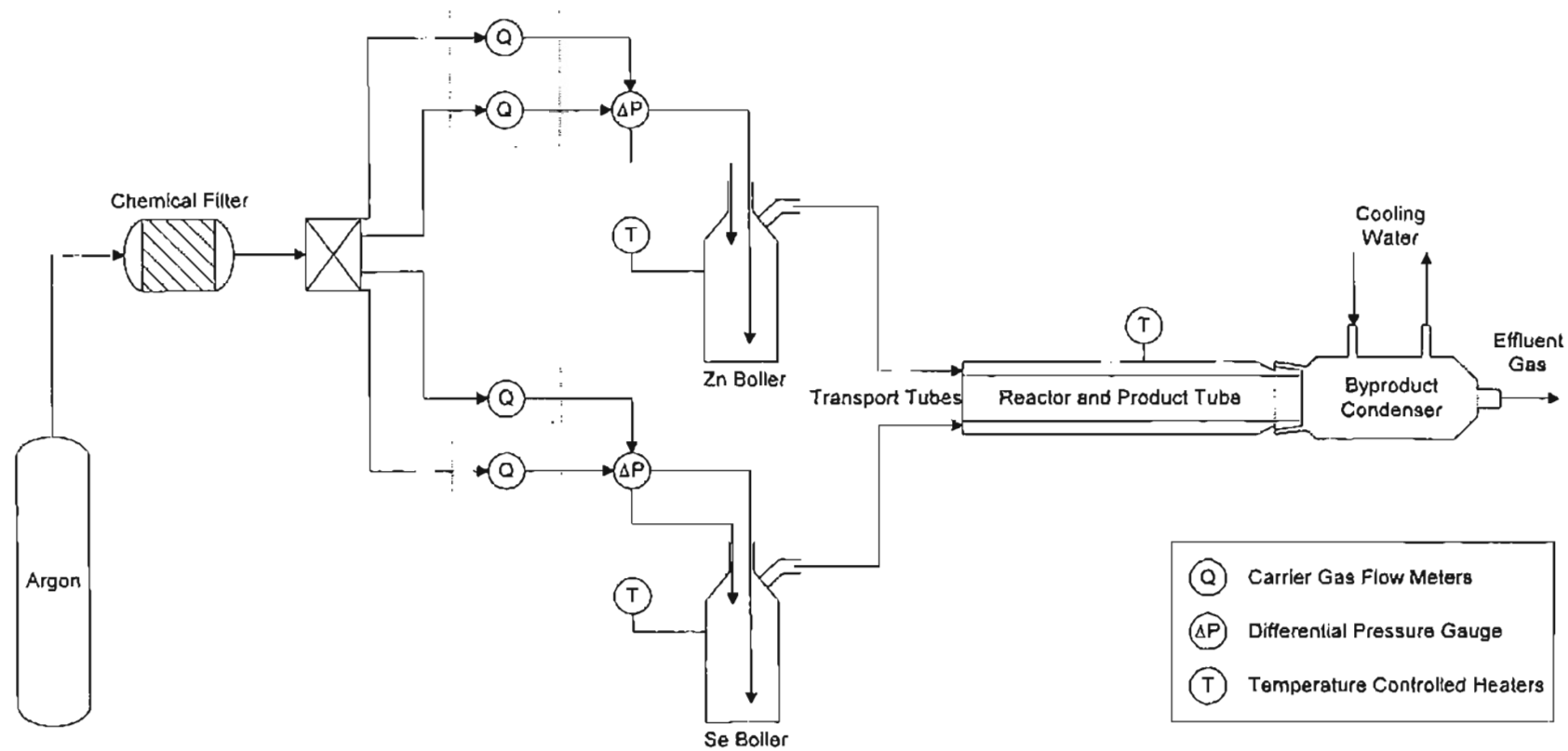


Figure IV-1. Schematic of prototype LFAR system.

## Boilers

The basic goals of boiler redesign are to scale up the size of the boilers to handle higher capacity runs, use the same design for each boiler, create a reproducible heating environment, monitor and control mass transfer, and maintain high purity. The earlier analysis of boiling heat and mass transfer illuminates the difficulties in controlling mass transfer, therefore some sort of control and monitoring system is necessary. In this light, the use of dimensionless numbers such as the Pr, Gr, and Nu for scaling is not warranted until further studies linking the mass transfer characteristics to these parameters can be performed. At this time, scale-up can be performed by geometric means only. To aid in creating a reproducible heating environment for the boilers, a new design is described for the boiler heaters with the addition of heaters for the transport tubes. Major new additions to this design over what currently is used at EP are the monitoring and control capabilities, addition spouts, and transport tube heating. A scaled cross section of the boiler prototype is displayed in Figure IV-2.

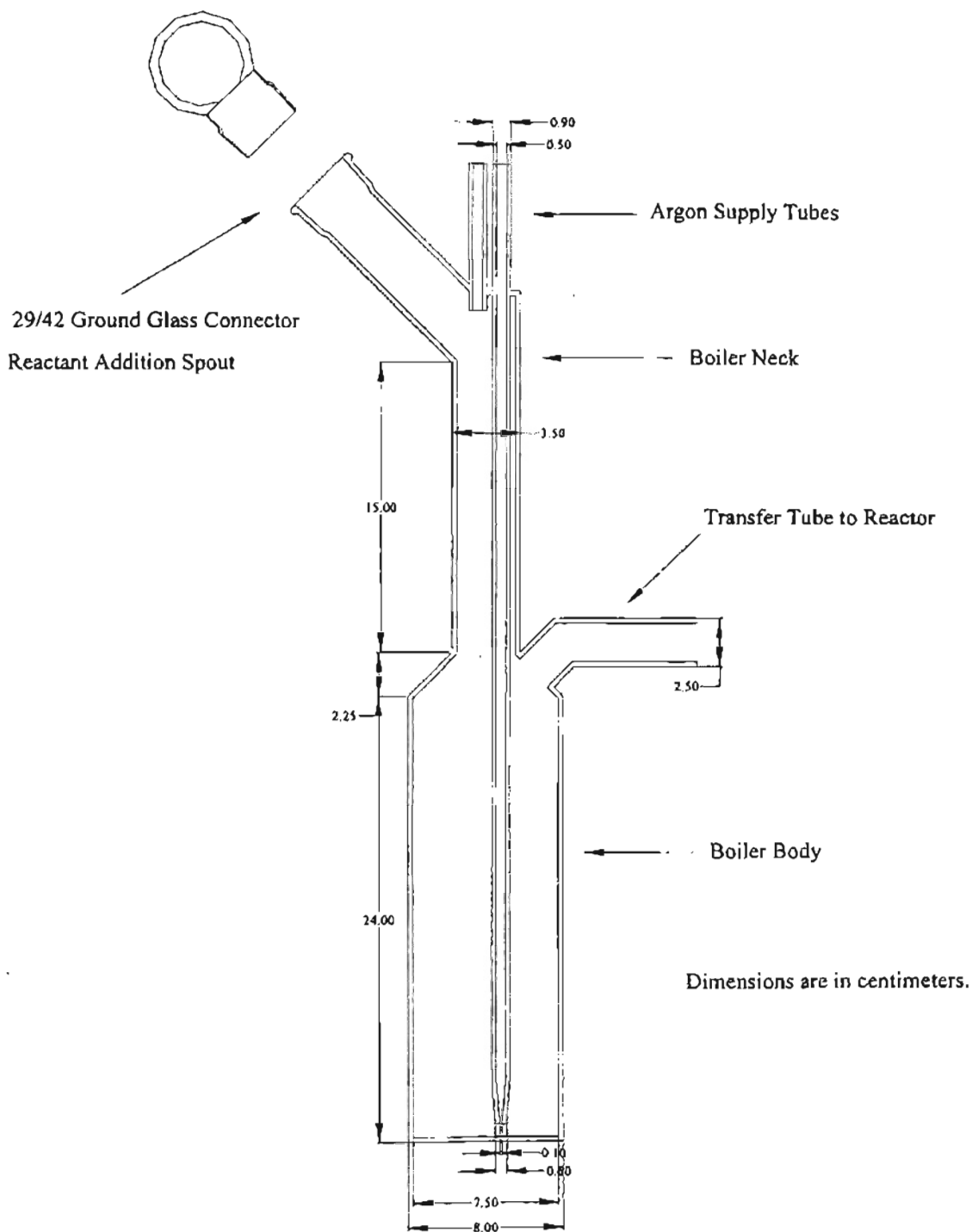


Figure IV-2. Cross-section of prototype boiler.



## Body

The design basis reactor capacity was established to be 2 kg of ZnSe. An appropriate percent yield to work with for design purposes will be set at 75% yield of reactants based on zinc for that 2 kg capacity. This requires an initial stoichiometric loading of 1.208 kg zinc and 1.459 kg selenium. To decide on an appropriate scale factor, the boiler specific weight (b.s.w. = volume of boiler/mass of reactant) of reactant in the overall boilers was calculated for both zinc and selenium with the largest b.s.w. being used as a scale factor for new boilers. For EP's larger capacity runs, 0.7 kg of zinc was loaded into a 283 cm<sup>3</sup> boiler yielding a reactant b.s.w. factor of 0.40 cm<sup>3</sup>/g, and 1 kg of selenium was loaded into a 755 cm<sup>3</sup> boiler yielding a reactant b.s.w. factor of 0.75 cm<sup>3</sup>/g. To maintain a conservative boiler size for the larger capacity boilers, the larger scale factor of 0.75 was multiplied by the larger reactant capacity of 1.459 kg to yield a boiler volume of 1094 cm<sup>3</sup>. Identical boilers for both reactants are recommended to simplify fabrication and maintenance. Using the previous selenium boiler diameter as a guideline, the new boiler bodies should be 7.5 cm ID (8.0 cm OD) by 25.0 cm tall. The prototype boiler will be oriented vertically for reasons which will be expanded upon later, namely to aid in heat and mass transfer. Also, the boilers should be fabricated so that no joints exist since they supply failure opportunity during the heating cycles.

## Neck

The neck is the second design component for the new boilers. The dual purpose neck will serve both to introduce reactants prior to the run and supply the carrier gas during the run. Based on a subjective estimate of the difficulties associated with pouring

the solid shot reactants into funnels performed at EP, the neck should be 3.0 cm ID (3.5 cm OD). The neck will consist of two main sections – a straight section coming out of the top of the boiler body and a section angled out at the top of this. The angled section will have a 29/42 quartz ground glass female taper joint. After reactant addition through this spout, it will be sealed using a 29/42 quartz stopper. No grease should be used, but a taper clip should be applied to hold the stopper in place. Heat conduction upwards through the neck was estimated by assuming that it behaved like a vertical flat plate since the wall thickness (2.5 mm) is much less than the tube circumference (251 mm). Based on this estimate, the straight neck should extend at least 8 cm from the heated section in order to maintain a temperature less than 300 K. Also, the top of the boiler should be insulated with approximately 5 cm of fiberfrax insulation thereby capping the tube furnace. Insulation placement can be seen in Figure IV-3. These two precautions should be taken to minimize the amount of heat that reaches the plastic fittings at the top of the argon supply tubes to the boiler.

#### Argon Supply Tubes

Through the angled section, two 9 mm OD (5 mm ID) quartz argon supply tubes should protrude. The tubes should roughly align with the plane of the angled section of the addition neck. The tube closest to the stopper should not protrude into the neck far enough to interfere with reactant addition. This tube will serve to introduce the main supply of argon carrier gas. The other tube should be long enough to reach within 5 mm of the bottom of the boiler. This tube will supply a slow trickle of argon to be used in measuring the height of the column of liquid metal. Argon carrier gas supply tubes will

be attached using plastic compression fittings such as those used on the original EP system. Currently the argon supply is split using a distribution head with two outlets. This piece of hardware should be duplicated so that each boiler will have two independent argon supplies. Also a chemical trap should be used to remove oxygen, water, and other impurities from the argon supply before introduction to the boilers since current observations link these impurities to the downstream product powders.

### Monitoring and Control

The boilers should be oriented vertically to maintain a linear relation between liquid height, heat, and mass transfer. To deduce the liquid height, the two argon supply tubes for each boiler should be routed through a differential pressure gauge. The differential pressure reading can directly be converted to the height of the liquid metal within the boiler. This pressure can be used to calculate the liquid metal height within the boilers by using the relation  $P = \rho gh$ . Temperature functions for liquid metal densities are located in Appendix A, and the liquid metal temperature can be estimated either by comparison to the values in Chapter III or by performing the convection heat transfer calculations using an estimated heat transfer coefficient. Alternate methods of monitoring the liquid height include using an optical measurement device or including a window in the heater. Standard optical measurement devices were not considered due to their incompatibility with the high temperatures involved within the boilers. Windows were also disregarded due to the possible adverse effects upon heating consistency.

It is recommended that the same temperature controlled boiler system be used for the new boilers with one modification. The exterior boiler thermocouple should contact

the boiler near the bottom, i.e. so it will reflect the heat transfer into the liquid metal for as long as possible during the run. It is also not advisable to utilize heat flux control for the new boilers due the possibility of burnout if the critical heat flux described in Chapter III is approached. In the initial runs the temperatures developed by Shay (1998) should be used. But successive run temperatures should be adjusted according to the recorded mass flow characteristics since the flow of selenium without reflux is almost sure to be too high at the old temperatures.

If a digital differential pressure gauge is used, the possibility exists for future automation through implementation of a neural network or other control system (Shay, 1998). The operator can take frequent readings to determine the mass transfer of reactants based on this differential pressure. Stoichiometric flows, as concluded in Chapter III, should be maintained at the low rates of  $7.28 \times 10^{-4}$  mol/sec of  $Zn_{(g)}$  and  $3.64 \times 10^{-4}$  mol/sec of  $Se_{2(g)}$  which were established by Shay (1998) through CFD experimentation. Also since the liquid metals have high surface tensions, the end of the immersion tube should be drawn down to  $\sim 1$  mm to minimize pressure fluctuation due to uneven bubble departure. Once the liquid level drops below this tube outlet, the immersion argon supply may be discontinued since a mass transfer rate trend has been established. It is advisable that the operator make mass flow (pressure) versus boiler temperature to ease future adjustments. This added level of flow control will help maintain the low, stoichiometric flow required to obtain high yields.

## Heaters

To maintain consistent heating during runs, a three zone furnace should be assembled around the boilers after final welding. Typical ceramic-mounted heating elements like the current EP heaters can be used. A cross section of one boiler, boiler heater, and transport tube heater is displayed in Figure IV-3. One zone should surround each of the boilers, and the third should surround the transport tubes to the reactor. The third, transport tube, zone should be heated to reactor temperature to also act as a feed stream preheater. The zinc boiler in the current system is consistently heated in this way, and mass transfer was shown to be a strict function of heat input in Chapter III. With this three zone heater, reflux will not be allowed within the boilers since the entire body and transport tubes will be heated. Initial experimental runs should be performed with the boiler exterior temperatures set at the midrange values from the experimental study of 1226 K for zinc and 994 K for selenium. Without reflux, the final selenium operating temperature will probably be much lower than this. Optimum temperatures can be determined by calibrating the mass flow versus temperature using the pressure reading method.

This prototype boiler system can be implemented to maintain consistent heating and add control capabilities to the reactor system. After further experimentation, some parameters both physical and operational may be reconfigured to allow better operation.

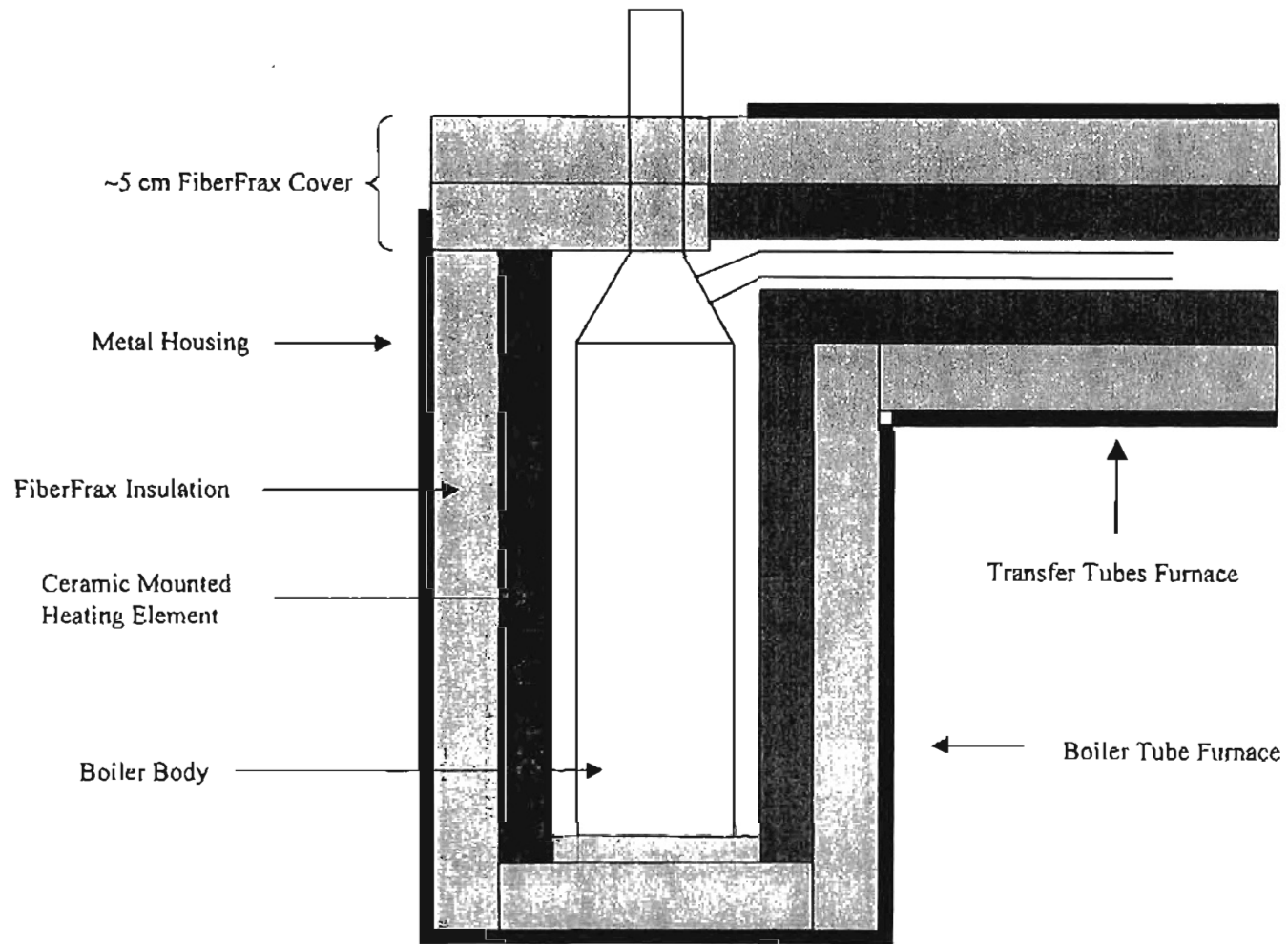
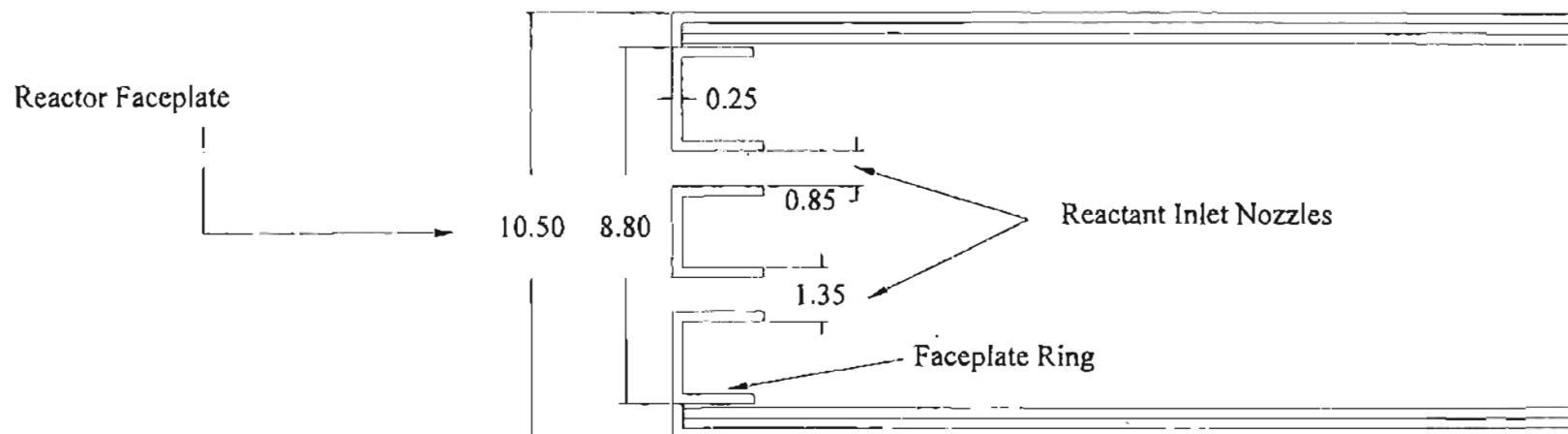


Figure IV-3. Cross-section of boiler and transfer tube furnace.

## Nozzles

Shay (1998) describes a designed experimental study performed on a FLUENT/UNS CFD 2D model to optimize both inlet nozzles and inlet reactant flows. The study is described elsewhere in detail while only the results will be presented within this thesis. The goal of the study was to use the CFD tool to model the impact of nozzle characteristics and flow levels on the reactant mixing. Since reactant mixing occurs mainly due to diffusion between reactant stream lamellae, the optimization preferred low Reynolds number therefore lower flow rates. To arrive at these conclusions, the flow rate, nozzle diameter, nozzle angle, and nozzle position were varied in a three level design matrix.

The range of flows that was used varied from  $3 \times 10^{-4}$  to  $9 \times 10^{-4}$  mol/sec of zinc with stoichiometric selenium. The nozzle diameter was varied from 2 mm to 12 mm through two rounds of study. The initial conditions for the study are developed in Appendix D with further steps discussed in the thesis of Shay (1998). Dual nozzles were used as proposed in the design basis. For larger reactors, it might be more advisable to incorporate multiple nozzles (see possible concepts in Chapter III). For the study, the position of the nozzles was varied from 1 to 3 cm off centerline axisymmetrically. Nozzle angle was also varied between  $-45^\circ$  and  $45^\circ$  with  $0^\circ$  being in the axial direction. The optimum design proposed by Shay (1998) locates the 8.5 mm diameter nozzles oriented at  $0^\circ$  1.425 cm from the reactor axis. This arrangement can be seen in Figure IV-4 which is an enlarged view of the reactor faceplate. The optimum calculated yield based on these flows and nozzles is 90 % from the thesis of Shay (1998).



Dimensions are in centimeters.

Figure IV-4. Enlarged view of prototype reactor faceplate.



## Reactor Body

For the LFAR currently employed by EP and the prototype proposed within this thesis, the reactor body serves dual purposes. The reactor acts not only as a mixing and particle formation chamber but also as a particle collection chamber. For a 1 m reactor space utilization is key. The goal was to produce an effective first generation prototype reactor based on the existing LFAR technology that EP employs. To minimize capital requirements, the prototype reactor developed within this thesis will fit within the existing reactor furnace. The great utility of the prototype design is its ability to be “turned around” easier and quicker than the current EP reactor. This fast turnaround is a direct result of lowering the maintenance required between runs. As mentioned earlier, one of the major goals of this system, in addition to increasing capacity, is to better the performance of the reactor. The key elements to the prototype reactor body are the outer reactor tube that remains static while the inner product collection tube is removable.

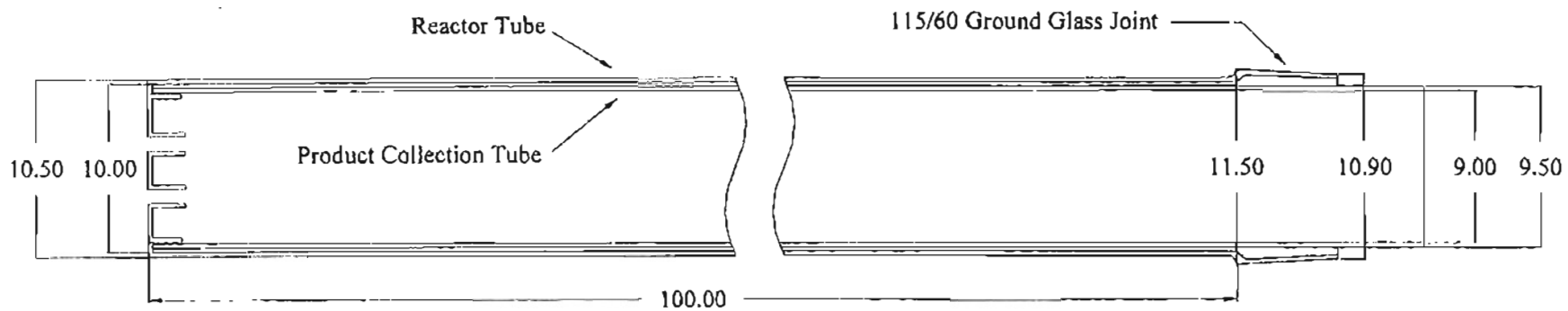
### Product Collection Tube

The product collection tube is actually just a straight section of tubing that has been annealed to seal any pores. This tube has the corresponding functions of the current EP reactor tube, but is much easier to replace, clean, and fabricate. EP uses two sizes of reactor tubes, 105 mm OD and 95 mm OD. The smaller of the two was used during the earlier experimental study described in Chapter III with an approximate capacity of 0.8 kg of powder. From engineering estimates, this appeared to be a much lower capacity than maximum allowable. Collected product powder yielded a conservatively estimated

density of 845 g/L when loosely packed. Based on this estimate, 2 kg of powder would maintain 70% of the void volume of the 0.8 kg capacity yield. Estimates are detailed in Appendix D. An axial cross section of the product tube in position within the reactor tube is shown in Figure IV-5.

To insure that the flow and mixing characteristics do not change significantly with the change in capacity, a Pe and Re comparison was performed in Appendix D. The average Pe and Re for the best actual run (88% yield) were calculated to be 0.3 and 3, respectively. When the capacity was increased to 2 kg of powder within the same tube size, the Pe and Re were 0.4 and 4, respectively. Since transition from diffusion-controlled mixing occurs at Pe greater than 300, the difference in Pe number estimates was negligible. Also since the transition from laminar to turbulent flow occurs at Re greater than 2000, the Re difference was negligible. Little change in performance should be expected with the increase in capacity, which means that the current reactor tube is quite oversized for its current capacity of less than 1 kg.

The product tube can therefore be effectively designed as the same 90 mm ID as the experimental reactor tubes. The product tube should be long enough that approximately 5 cm extends beyond the exit of the reactor tube. This extra length will allow sufficient area to be grasped during product tube removal. It is expected that product powders may prove cohesive enough to hamper removal of the product tube. To aid in removal of the product tube, it should be twisted to break any deposits loose for removal.



Dimensions are in centimeters.

Figure IV-5. Cross-section of reactor tube with product tube inserted.

## Product Tube Insertion/Removal

In addition to the minor procedural suggestion of twisting the tube to break loose any deposits, other means have been devised to aid in the usage of the product tube. To insure proper and reproducible alignment of the product tube from run to run, quartz rod rails should be attached to the floor of the reactor tube. These rails will allow the easy insertion and removal of the product tube while decreasing the amount of impact the product and reactor tubes will engage in. Also, a ring will be affixed to the faceplate to act as a passive seal and guide for the front of the product tube. The rails should be at least a pair of 2.5 mm quartz rods which run the length of the reactor. Approximate position can be seen in the radial cross section in Figure IV-6. The face plate ring will be 85 mm OD and should be approximately 2 cm long. The ring is shown at the reactor face plate in Figure IV-4. After the run has been completed, the product tube removal offers the dual hazard of breaking either the reactor tube or product tube. Either case would lead to a failed run and extra maintenance. As one last aid in the removal and insertion of the product tube, a PVC rack or guide should be fabricated which will line up the product tube for smooth removal and insertion into the reactor.

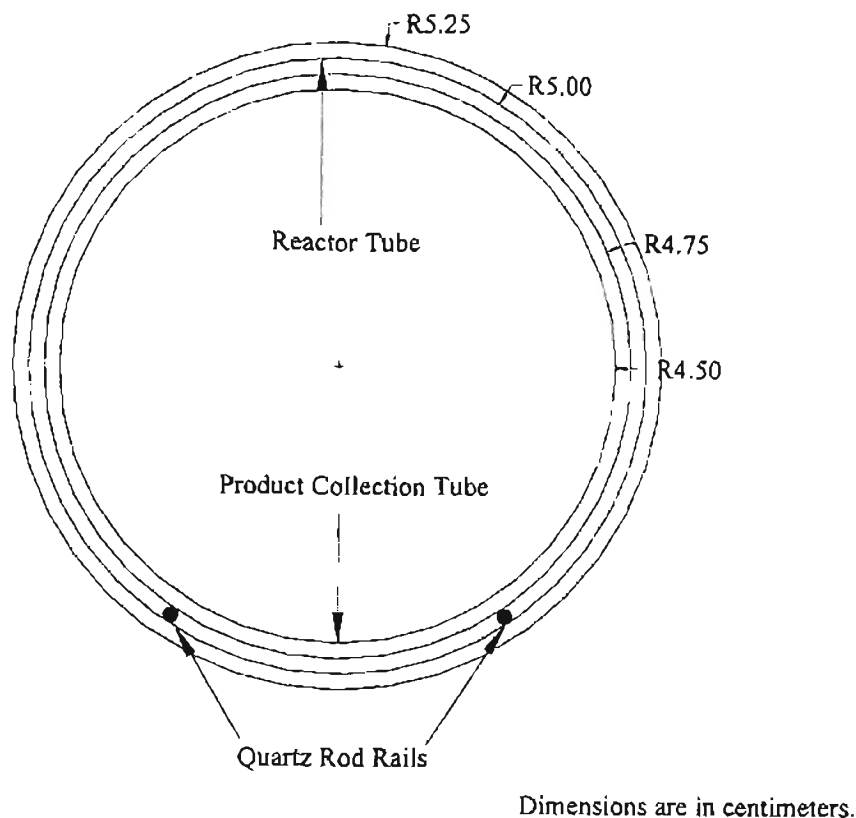


Figure IV-6. Radial cross-section of reactor tube.

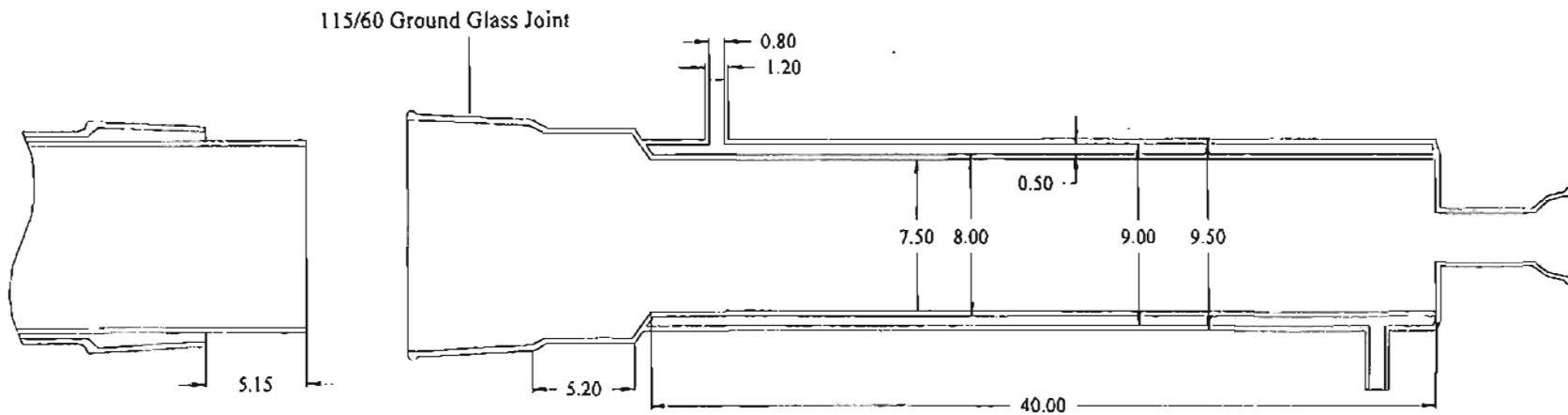
### Reactor Tube

The reactor tube was sized to allow suitable clearance both for its insertion into the furnace and the interior product tube. Since the furnace inner diameter was approximately 120 mm and the product tube dimensions were ideally 95 mm OD, the reactor tube must fit within the remaining annular region. Therefore, the tube diameter was chosen to be 105 mm OD (100 mm ID). The tube is sealed from the ambient environment by welding at the front end and a ground glass joint at the rear. The quartz ground glass joint must also fit within the same annular region; therefore, a 115/60 standard male quartz taper joint (115 mm OD) was selected. To minimize stresses upon

the reactor tube, great care should be taken to support the boilers within the heater units and the condenser at the rear. The reactor should be the same length as the furnace (~ 1 m) to minimize the amount of condensibles that need to be scraped off after a run. A cross section of the reactor tube with the product tube inserted is shown in Figure IV-5. The effect of the annular gas region between the tubes on the overall heat transfer will be addressed through the theses of Foster (in progress) and Nikolic (in progress).

### Condenser

An evaluation of the current condenser design including capacity was undertaken by Shay (1998) with the goals of both optimizing the current condenser and providing a uniform procedure for future capacity increases. An axial cross section of the proposed condenser design is displayed in Figure IV-7. Detailed heat exchanger correlations were used to determine that the 2 kg capacity reactor would require a condenser 40 cm in length and 4.5 cm ID. Water as a heat transfer medium should be pumped at a rate determined by Shay (1998) through 0.8 mm ID inlets into the 5 mm annular region of the jacket. The front end connector will feature a 1 1/2" female ground glass joint to mate tightly with the reactor tube. Also, the connector section on the condenser will extend approximately 5 cm before the jacketed section in order to contain the product tube protrusion from the reactor. This extension should be approximately 10.2 cm diameter to allow enough space for condensate deposition without bonding the product tube and condenser together. Based on on-site observations, it is advisable that the rear of the condenser be connected to a point source scrubber. The excessive selenium appeared to foul the scrubber attached to the vent hood typically used for effluent gas removal.



Dimensions are in centimeters.

Figure IV-7. Axial cross-section of prototype condenser.

## Production Comparison

The prototype reactor aims to eliminate the current inefficiencies within the EP LFAR operations and technology through both procedural and mechanical alterations. The goal of the prototype more specifically is to increase capacity, decrease labor, and increase predictable performance. To get a good estimate of the increase in performance, a labor and materials comparison is performed in Appendix E. A better estimate can only be obtained through actual experimentation on a physical prototype.

Due to the fast turnaround nature of the prototype, an 18 hour savings over the current production run is estimated. This includes a 24 hour allowance for run and cool down in both systems. The current system runs for approximately 6 hours while the new system will run approximately 12 hours. An average unadjusted run time comparison then lies at 60 hours for the current system and 42 hours for the prototype. But these production time estimates do not account for the probability of aborted or failed runs due to inconsistent mass flow. Based on the twenty-percent failure rate of the current system, an adjustment factor is defined in Appendix E of 1.25 for the production time on the current system. The prototype will have a much higher level of control and therefore much lower incidence of run failure. A conservative estimate of one out of ten runs failing yields an adjustment factor of 1.11 for the prototype. The adjusted production times become 76 hours for the current system and 47 hours for the prototype. After data can be gathered on a physical prototype, an actual adjustment factor can be applied. The example performed in Appendix E compares the production time for 10 kg of ZnSe in the old system and prototype estimate based on a yield of 0.8 kg for the old system and 2 kg



for the new. The comparison is very favorable for the prototype by requiring about 10 days as opposed to 40 days for the current system.

As far as reactor capital costs, no significant amount of difference should be seen between the old system and the new. The amount of quartz used will not vary greatly between the two reactor designs. The raw materials cost is the most variable between the two reactor designs. In the introduction to Chapter III, it was estimated that raw materials waste and disposal accounted for about \$100,000 in loss during the year prior to the study. This was a 60% raw material loss and disposal cost estimate. For the prototype to attempt the same amount of production, not only would production time be about 75% less, but also the material loss and disposal costs would be much less. A conservative estimate of loss would be 20% (the study of Shay (1998) suggests that this number would better approach 10%). At a 20% raw material loss, the raw material costs and waste disposal for the prototype would be around \$35,000. This is a cost savings of almost 1/3. In Appendix E, a direct per kilogram comparison is made between the old EP system and the estimated prototype's performance. A labor cost of \$20/hr is assumed for EP technicians, and the unsupervised purge and cool down segments for the run are neglected. A typical 0.8 kg ZnSe run with 40% molar yield is compared to a prototype expectation of 2.0 kg ZnSe with an 80% molar yield. The estimated cost savings for the prototype compared to the current EP reactor system is \$5400/kg. But again, this is only an estimate. It needs to be supported through prototype fabrication and testing.

## CHAPTER V

### CONCLUSIONS AND RECOMMENDATIONS

Engineering analysis of the EP LFAR technology consisted of three main sections: engineering observations, mathematical models, and possible design concepts. Based on engineering observations, system performance was concluded to be a strong function of product powder deposition patterns. Four “regions of deposition” were assigned.

- I. Zinc inlet plug – yield ~ 0%
- II. Extensive structural formation – yield ~ 0-45%
- III. Transition (minor structures) – yield ~ 45-69%
- IV. Loose powder bed – yield ~ 69-100%

First of their kind mass flow estimates based on steady state power input to the boilers were used to deduce that stoichiometric, low flows of reactants produced higher yields. The concept of a minimum nucleation velocity was defined to address this yield dependence on the flow levels. Specifically, it is recommended that flow levels exceed this minimum nucleation velocity to eliminate plugging and structural formation.

Mass flow estimates were also used as the basis to evaluate heat transfer and the boiling process within the boilers. Due to the smooth nature of the quartz walls and the low Pr of the boiling liquid metals, the boiling process was deduced to be strained. In explanation, the boiling occurred at much too high liquid temperatures. For such high

temperatures to be used without the possibility of the quartz boilers failing, temperature-controlled heaters must be used. As a check of these boiling conclusions, a run should be attempted with the boilers set at temperatures that provide heat flux below the critical value. The resulting magnitude of mass flow rates will confirm or refute the postulate. Also, mass flow rates within the boilers were shown to be functions of heat flux and argon flow rate for zinc and selenium, respectively. Ideally, the mass transfer rate should be a sole function of heat transfer, but since a variable reflux occurs in the selenium boiler mass flow is unpredictable. At the least, the present system selenium heater should be enlarged to eliminate the reflux possibility.

Standard dimensional analysis techniques were applied to the EP technology to confirm that it was indeed an LFAR. The reactor produced  $Pe$  less than 1 and  $Re$  less than 20 confirming the laminar flow/diffusion-controlled nature of the system. A FLUENT/UNS isothermal CFD model was developed to estimate an empirical rate constant for the assumed first order reaction. This technique and that of Shay (1998) are the first estimates of reaction kinetics for the ZnSe formation. Further work is suggested to incorporate a statistical particle formation model into the CFD code to produce a more comprehensive model. A study done on the model further supported observations by concluding that low, stoichiometric flow rates are optimum for producing a high yield in the LFAR. In addition to accounting for particle formation, a future model should be 3D and nonisothermal to more closely model the system.

Finally, a comprehensive first generation prototype design was proposed. Implementation of this design should increase not only the capacity but also the predictability of the LFAR. Significant cost savings were estimated to be of 75% on

labor and 66% on raw materials over the current system. Incorporation of at least some of the concepts with the current technology is highly suggested. Based on the comparison of performance estimates for the prototype and historical trends for the current system, significant cost savings of \$5400/kg of ZnSe produced should be expected after the initial prototype reactor startup.

## REFERENCES

- Abramovich, G. N., The Theory of Turbulent Jets, Scripta Technica, trans., M. I. T. Press, Cambridge, Massachusetts (1963).
- Alavi, K., "MBE," Handbook of Compound Semiconductors – Growth, Processing, Characterization, and Devices, P. H. Holloway and G. E. McGuire, eds., Noyes Publications, Park Ridge, New Jersey (1995).
- Bailar, J. C. and A. F. Trotman-Dickenson, Comprehensive Inorganic Chemistry, Pergamon Press, Oxford (1973).
- Bardi, G., and G. Trionfetti, "Vapour Pressure and Sublimation Enthalpy of Zinc Selenide and Zinc Telluride by Thermogravimetric Knudsen-Effusion Method," *Thermochimica Acta*, 157, 287-294 (1990).
- Barin, I., O. Knacke, and O. Kubaschewski, Thermochemical Properties of Inorganic Substances, Supplement, Springer-Verlag, New York (1977).
- Bird, R. B., W. E. Stewart, and E. N. Lightfoot, Transport Phenomena, John Wiley & Sons, New York (1960).
- Boev, E. I., L. A. Benderskii, and G. A. Milkov, *Zhur. Fiz. Khim.* 43, 1393 (1969).
- Brebrick, R. F., and H. Liu, "Partial Pressures of Zn and Se<sub>2</sub> over ZnSe(c) from Optical Density Measurements," *High Temperature and Materials Science* 35, 215-237 (1996).
- Brooks, L. S., *Journal of the American Chemical Society* 74, 227 (1952).
- Cox, J. D., D. D. Wagman, and V. A. Medvedev, eds., CODATA Key Values for Thermodynamics, Hemisphere Publishing Corporation, New York (1989).
- Cooper, C. D. and F. C. Alley, Air Pollution Control. A Design Approach, Waveland Press, Inc., Prospect Heights, Illinois (1994).
- Divis, R., "CdSe Synthesis," Procedure PS# 00171, Eagle-Picher, Inc., Miami, Oklahoma (1997).

- Durst, F., L. Kadinski, and M. Schafer, "A Multigrid Solver for Fluid Flow and Mass Transfer Coupled with Grey-Body Surface Radiation for the Numerical Simulation of Chemical Vapor Deposition Process," *Journal of Crystal Growth* 146, 202-208 (1995).
- Flogel, P. *Z. Anorg. Chem.* 370, 16 (1969).
- Fluent, "User's Guide for FLUENT/UNS & RAMPANT, Release 4.0," Vol. 2, Fluent Incorporated, Lebanon, New Hampshire (1996).
- Foster, B., "CFD Analysis of High Temperature Zinc Selenide Aerosol Reactor," M.S. Thesis, Department of Mechanical Engineering, Oklahoma State University, Stillwater, Oklahoma (in progress circa 1998-1999).
- Goldfinger, P., and M. Jeunehomme, "Mass Spectroscopic and Knudsen-Cell Vaporization Studies of Group 2B-6B Compounds," *Trans. Far. Soc.* 59, 2851-2867 (1963).
- Ghajar, A., G. Foutch, and A. Johannes, OSU-Eagle-Picher, Inc. OCAST Funding Proposal (1996).
- Grein, C. H., J. P. Faurie, V. Bousquet, E. Tournie, R. Benedek, and T. de la Rubia, "Simulations of ZnSe/GaAs Heteroepitaxial Growth," *Journal of Crystal Growth* 178, 258-267 (1997).
- Hahn, B., Preis, H., Schindler, M., Reisinger, T., and Gebhart, W., "Role of Nitrogen Precursors in MOVPE Growth of ZnSe," *Journal of Crystal Growth* 179, 415-422 (1997).
- Heraeus, "Price List – Fused Silica, Fused Quartz," Heraeus Amersil Inc., Sayreville, New Jersey (April 7, 1986).
- Hidy, G. M., Aerosols: An Industrial and Environmental Science, Academic Press, Inc., New York (1984).
- Ho, C. Y., R. W. Powell, and P. E. Liley, "Thermal Conductivity of the Elements: A Comprehensive Review," *Journal of Physical and Chemical Reference Data* 3 (Suppl. 1), I575-578 and I736-739 (1974).
- Hsu, Y.-Y. and R. W. Graham, Transport Processes in Boiling and Two-Phase Systems. Including Near-Critical Fluids, McGraw-Hill, Inc., New York (1976).
- Hultgren, R., R. L. Orr, P. O. Anderson, and K. K. Kelley, Selected Thermodynamic Properties of Metals and Alloys, John Wiley & Sons, New York (1963).

- Hultgren, R., P. D. Desai, D. T. Hawkins, M. Gleiser, K. K. Kelley, and D. D. Wagman, Selected Values of the Thermodynamic Properties of the Elements, American Society for Metals, Metals Park, Ohio (1973).
- Incropera, F. P. and D. P. DeWitt, Introduction to Heat Transfer, 3<sup>rd</sup> ed., John Wiley & Sons, New York (1996).
- Irvine, S. J. and J. Bajaj, "A Study of the Growth Kinetics of II-VI Metalorganic Vapour Phase Epitaxy Using in Situ Laser Reflectometry," *Journal of Crystal Growth* 145, 74-81 (1994).
- Jin, Y., "Fundamental Study of Hydrodynamics and Modeling of Downer Reactors," Presented at the Oklahoma State University School of Chemical Engineering Seminar Series, Stillwater, Oklahoma (September 24, 1998).
- Kays, W. M. and M. E. Crawford, Convective Heat and Mass Transfer, 3<sup>rd</sup> ed., McGraw-Hill, Inc., New York (1993).
- Kleinstreuer, C., Engineering Fluid Dynamics: An Interdisciplinary Systems Approach, Cambridge University Press, New York (1997).
- Kodas, T. T., S. K. Freidlander, and S. Pratsinis, "Effect of Reactant Mixing on Fine Particle Production in a Tubular Flow Reactor," *Industrial & Engineering Chemistry Research* 26, 1999-2007 (1987).
- König, T., "Process for the Preparation of Finely Divided Metal and Ceramic Powders," U. S. Patent 5,472,477 (1995).
- Komeeva, I. V., V. V. Sokolov, and A. V. Novoselova, *Zhur. Neorg. Khim.* 5, 241 (1960).
- Kudryavtsev, A. A., The Chemistry & Technology of Selenium and Tellurium, translated from 2<sup>nd</sup> Russian ed. by E. M. Elkin, Collet's Publishers Ltd., London (1974).
- Levenspiel, O., Chemical Reaction Engineering, John Wiley & Sons, New York (1972).
- Libicky, A., "Synthesis and Crystal Growth of CdSe, ZnTe, and ZnSe," II-VI Semiconducting Compounds, 1967 International Conference, New York (1967).
- Lide, D. R., editor, CRC Handbook of Chemistry and Physics, Vol. 79, CRC Press, Cleveland, Ohio (1998).
- Lucovsky, G., "Selenium, the Amorphous and Liquid States," The Physics of Selenium and Tellurium: Proceedings of the International Conference on the Physics of Selenium and Tellurium, Springer-Verlag, New York (1979).

- Mills, K. C., Thermodynamic Data for Inorganic Sulfides, Selenides, and Tellurides, Butterworth, London (1974).
- Morgan, S. W. K., Zinc and its Alloys and Compounds, John Wiley & Sons, New York (1985).
- Morton, "CVD Zinc Selenide," Morton Advanced Materials Website, [www.mortoncvd.com](http://www.mortoncvd.com) (1998).
- Nasar, A. and M. Shamsuddin, *Z. Metallkunde* 81, 244 (1990).
- Nauman, E. B., Chemical Reactor Design, John Wiley & Sons, pub., Krieger Pub. Co, Malabar, Florida, reprinted (1987).
- Nayar, A., The Metals Databook, McGraw-Hill, New York, (1997).
- Nikolic, J., "CFD Simulation and Analysis of High Temperature ZnSe Aerosol Reactor," M.S. Thesis, Department of Mechanical Engineering, Oklahoma State University, Stillwater, Oklahoma (in progress).
- Pratsinis, S., "Simultaneous Nucleation, Condensation, and Coagulation in Aerosol Reactors," *Journal of Colloid and Interface Science* 124 (2), 416-427 (1988).
- Pratsinis, S., and Vemury, S., "Particle Formation in Gases: A Review," *Powder Technology* 88, 267-273 (1996).
- Ranade, V. V., "Improve Reactors Via CFD," *Chemical Engineering* 104 (5), 96-102 (1997).
- Reid, R. C., J. M. Prausnitz, and B. E. Poling, The Properties of Gases & Liquids, 4<sup>th</sup> ed., McGraw-Hill, Dubuque, Iowa (1987).
- Rossini, Wagman, Evans, Levine, and Jaffe, N. B. S., circa 500 (1952).
- Rushton, J. H., "The Axial Velocity of a Submerged Axially Symmetrical Fluid Jet," *AIChE Journal* 26 (6), 1038-1041 (1980).
- Sadakata, M., Xu, Y. B., and Harano, A., "A Systematic Approach for the Design of Aerosol Reactors," *Powder Technology* 88, 261-266 (1996).
- Schönherr, E., M. Freiberg, D. Siche, and H. Hartmann, "The Vapour Composition and Vapor Pressure of ZnSe from a Modified Knudsen Technique Between 1190 and 1310 K," *Berichte der Bunsen-Gesellschaft fuer Physikalische Chemie* 100 (11), 1766-1771 (1996).



- Schönherr, E., M. Freiberg, D. Siche, and H. Hartmann, "Correction on the Vapor Composition of ZnSe Determined with a Modified Knudsen Technique," *Berichte der Bunsen-Gesellschaft für Physikalische Chemie* 102 (4), 704 (1998).
- Secco, E. A. and C. H. Su, "Gas-Solid Exchange Reactions: Zinc Vapor and Polycrystalline Zinc Selenide," *Canadian Journal of Chemistry* 46 (10), 1621-1624 (1968).
- Sha, Y-G., C-H. Su, W. Palosz, M.P. Volz, D.C. Gillies, F.R. Szofran, S.L. Lehoczky, H-C. Liu, and R.F. Brebick. "Mass Flux of ZnSe by Physical Vapor Transport," *Journal of Crystal Growth* 146, 42-48 (1995).
- Shay, C. D., "Design and Optimization of a High Temperature Reactor for the Production of Group II-VI Compounds Via Computer Models and Statistical Experimentation," M.S. Thesis, Department of Chemical Engineering, Oklahoma State University, Stillwater, Oklahoma (December 1998).
- Sigma, "Aldrich Catalog Handbook of Fine Chemicals," Sigma-Aldrich Co., USA (1998).
- Stewart, R. B. and R. T. Jacobsen, "Thermodynamic Properties of Argon from the Triple Point to 1200 K with Pressures to 1000 MPa," *Journal of Physical and Chemical Reference Data* 18 (2), 639-677 (1989).
- Su, C.-H., P.-K. Liao, Y. Huang, S.-S. Liou, and R. F. Brebrick, *Journal of Chemical Physics* 81, 11 (1984).
- Tilton, J. N., "Fluid and Particle Dynamics," Perry's Chemical Engineers' Handbook, 7<sup>th</sup> ed., D. W. Green ed., McGraw-Hill, New York (1997).
- Tong, L. S., and Y. S. Tang, Boiling Heat Transfer and Two-Phase Flow, 2<sup>nd</sup> ed., Taylor & Francis, Washington, D. C. (1997).
- Veuhoff, E., "MOCVD," Handbook of Compound Semiconductors – Growth, Processing, Characterization, and Devices, P. H. Holloway and G. E. McGuire, eds., Noyes Publications, Park Ridge, New Jersey (1995).
- Viswanath, D. S. and G. Natarajan, Data Book on the Viscosity of Liquids, Hemisphere Publishing Corporation, New York (1989).
- Wankat, P. C., and K. S. Knabel, "Mass Transfer," Perry's Chemical Engineers' Handbook, 7<sup>th</sup> ed., D. W. Green ed., McGraw-Hill, New York (1997).

- Wahlbeck, P. G., D. L. Myers, and V. V. Truong, "Validity of the Ruff-MKW Boiling Point Method: Vapor Pressures, Diffusion Coefficients in Argon and Helium, and Viscosity Coefficients for Gaseous Cadmium and Zinc," *Journal of Chemical Physics* 83 (5), 2447-56 (1985).
- Wösten, W. J. and M. G. Geers, *Journal of Physical Chemistry* 25, 1252 (1962).
- Wu, J. J., H. V. Nguyen, and R. C. Flagan, "A Method for the Synthesis of Submicron Particles," *Langmuir* 3, 266-271 (1987).
- Wu, M. K., R. S. Windeler, C. K. R. Steiner, T. Börs, and S. K. Friedlander, "Controlled Synthesis of Nanosized Particles by Aerosol Processes," *Aerosol Science and Technology* 19, 527-548 (1993).
- Yao, T., Y. Miyoshi, Y. Makita, and S. Maekawa, "Growth Rate and Sticking Coefficient of ZnSe and ZnTe Grown by Molecular Beam Epitaxy," *Japanese Journal of Applied Physics*, 16 (2), 369-370 (1977).
- Yao, T. and M. Shigeru, "Molecular Beam Epitaxy of Zinc Chalcogenides," *Journal of Crystal Growth* 53, 423-431 (1981).
- Yoshikawa, Akihiko, Hideyuki Oniyama, Hiroyasu Yasuda, and Shigeki Yamaga. "Growth Kinetics in MOMBE of ZnSe Using Dimethylzinc and Hydrogen Selenide as Reactants," *Journal of Crystal Growth* 94, 69-74 (1989).
- Young, D. F., B. R. Munson, and T. H. Okiishi, A Brief Introduction to Fluid Mechanics, John Wiley & Sons, Inc., New York (1997).
- Xiong, Y., and Pratsinis, S., "Gas Phase Production of Particles in Reactive Turbulent Flows," *Journal of Aerosol Science* 22 (5), 637-655 (1991).

## APPENDICIES

## APPENDIX A

### THERMODYNAMIC, TRANSPORT, AND PHYSICAL PROPERTIES

A prerequisite for the data analysis and subsequent model development for this thesis was the compilation of a list of physical, thermodynamic, and transport properties for the species zinc, selenium, zinc selenide, and argon in all their applicable phases. Just like all first-level investigations of chemical reactors, few sources existed which contained any significant amount of property data or correlations. As a result, several properties had to be estimated using theoretical correlations. The following appendix both describes the methods of property estimation where applicable and compiles the properties with references. Compilation tables list the literature source where the specific value was obtained, the experimental source, and experimental or theoretical techniques used to develop either the value or the correlation if available. When possible, both the literature and empirical sources for the compiled data are listed. For ease of use, these references are included in the Reference section of this thesis.

Within each section of this appendix, the technique for property estimation is described and the gathered properties are tabulated. Physical properties are considered to be molecular weight, phase transition temperature, phase density, liquid surface tension, and vapor pressure. Thermodynamic properties are considered to be equilibrium constant, heat capacity, enthalpy, entropy, and Gibb's free energy. Transport properties are considered to be thermal conductivity, viscosity, and diffusivity (or diffusion

coefficient). No attempt has been made to gauge the reliability of the various sources or empirical techniques for determination of these properties. Property tables are listed in reverse chronological order of publishing.

### Physical Properties

Physical properties have been gathered and tabulated below. For liquid density and surface tension, an Andrade-type extrapolation was used. This type of extrapolation is performed by fitting a linear equation to the logarithmic plot. Linear extrapolation of this sort is not recommended, but due to both the shortage of liquid data and the lack of adequate theoretical methods this can be the only recourse (Reid et al., 1987).

TABLE A-1

#### Species Molecular Weights

Species	$M_i$
ZnSe	144.33
Se	78.96
Se <sub>2</sub>	157.92
Zn	65.39

TABLE A-2

#### Physical Properties – Miscellaneous

Property	Species	Value	Source
$E_f$ Lattice Energy (kJ/mol)	ZnSe <sub>(s)</sub>	3610	Bailar et al., 1973
Particle Diameter, $D_p$ (cm)	ZnSe <sub>(s)</sub>	~17.4e-04	Secco, 1967
		50-70e-04	Morton, 1998

TABLE A-4

## Physical Properties – Phase Transition Temperatures

Property	Species	Appl. Range	Value	Empirical Source	Source
Melting Point, $T_m$ (K)	ZnSe <sub>(s)</sub>	1 atm	1799	Mills, 1974	Brebrick and Liu, 1996
			1576		Libicky, 1967
			>1373		Bailar et al., 1973
	Se <sub>(s)</sub>		490		Nayar, 1997
			493		Brebrick and Liu, 1996
			493		Bailar et al., 1973
	Zn <sub>(s)</sub>		693		Nayar, 1997
			692.7		Morgan, 1985
			965.7		Hultgren et al., 1973
			692.6		Brebrick and Liu, 1996
Boiling Point, $T_b$ (K)	ZnSe <sub>(s)</sub>	~2273	Bailar et al., 1973		
	Se <sub>(l)</sub>	958	Nayar, 1997		
		958	Bailar et al., 1973		
	Zn <sub>(l)</sub>	1179	Nayar, 1997		
		1180	Morgan, 1985		
		1179	Bailar et al., 1973		

TABLE A-5

Physical Properties – Density ( $\rho$  in  $\text{kg/m}^3$ )

Species	Appl. Range	Value	Empirical Source	Source
ZnSe <sub>(s)</sub>		5300		Bailar et al., 1973
		5270		Morton, 1998
Se <sub>(s)</sub>	298 K	4809		Nayar, 1997
		4820		Bailar et al., 1973
Se <sub>(l)</sub>	623 - 873 K	3750 - 0.75*(T-493 K)	1970	Lide, 1998
Zn <sub>(s)</sub>	297 K	7133		Nayar, 1997
	298 K	7140		Morgan, 1985
	692.5 K	6830		Morgan, 1985
	299 K	7140		Bailar et al., 1973
	693 K	6920		Bailar et al., 1973
Zn <sub>(l)</sub>		6576 - 0.980*(T-692 K)	1972, 1973	Lide, 1998
	692.5	6620		Morgan, 1985
	1073	6250		Morgan, 1985

TABLE A-6

Physical Properties – Surface Tension ( $\sigma$  in kg/m)

Species	Appl. Range	Value	Source
Se <sub>(l)</sub>	493 K	10.53	Kudryavtsev, 1974
	503 K	10.33	Kudryavtsev, 1974
	513 K	10.22	Kudryavtsev, 1974
	523 K	10.05	Kudryavtsev, 1974
	533 K	9.85	Kudryavtsev, 1974
	543 K	9.83	Kudryavtsev, 1974
	553 K	9.80	Kudryavtsev, 1974
	563 K	9.61	Kudryavtsev, 1974
	573 K	9.61	Kudryavtsev, 1974
	583 K	9.57	Kudryavtsev, 1974
	T > 583 K	-0.0045 T + 12.145	Data Extrapolation in this Thesis
Zn <sub>(l)</sub>	692.7 K	9.52	Morgan, 1985
	713 K	81.6	Bailar et al., 1973
	T > 692.7 K	Exp(6.1322 Exp(-236.38/T))	Data Extrapolation in this Thesis



TABLE A-7

## Physical Properties – Vapor Pressure

Units	Species	Appl. Range	Values or Functions			Empirical Source	Literature Source
			$\log P = A - B/T + \log T$				
			A	B	C		
P (kPa)	ZnSe	1180 - 1405 K	$8.99 \pm 0.06$	$12,641 \pm 70$		Schönherr et al., 1998	Schönherr et al., 1998
P (kPa)		1190 - 1310 K	$9.19 \pm 0.08$	$12,896 \pm 96$		Schönherr et al., 1996	Schönherr et al., 1996
P (kPa)		1025 - 1288 K	$9.15 \pm 0.06$	$12,798 \pm 73$		Average	Bardi and Tronfetti, 1990
P (kPa)		1147-1288 K	$9.15 \pm 0.08$	$12,770 \pm 100$		Bardi and Tronfetti, 1990	Bardi and Tronfetti, 1990
P (kPa)		1025-1136 K	$9.15 \pm 0.04$	$12,825 \pm 46$		Bardi and Tronfetti, 1990	Bardi and Tronfetti, 1990
P (kPa)		1173-1413 K	9.733	13,326		Flogel, 1969	Bardi and Tronfetti, 1990
P (kPa)		1123-1473 K	$9.306 \pm 0.067$	$13,199 \pm 86$		Boev et al., 1969	Bardi and Tronfetti, 1990
P (kPa)		1060-1393 K	$9.528 \pm 0.170$	$13,492 \pm 204$		Wösten and Geers, 1962	Bardi and Tronfetti, 1990
P (kPa)		980-1190 K	8.715	14,320		Goldfinger and Jeunehomme, 1963	Bardi and Tronfetti, 1990
P (kPa)		916-1095 K	10.63	14,202		Korneeva et al., 1960	Bardi and Tronfetti, 1990
P (kPa)	Se		5.2078	4989.5		Brooks, 1952	Brebrick and Liu, 1996
P (atm)	Se <sub>2</sub>	1000 - 1400 K	6.580917	12,760.80			Brebrick and Liu, 1996
P (atm)	Zn	600 - 692.6 K	5.9839	6714.7			Brebrick and Liu, 1996
P (atm)		T > 692.6 K	9.874	6742	-1.3555		Brebrick and Liu, 1996
P (mm Hg)		764 - 1254 K	12.448	6674.4	-1.2742		Bailar et al., 1973
P (mm Hg)		300 - 700 K	9.664	7198			Bailar et al., 1973
P <sub>in</sub>	ZnSe		0.5 atm				Libicky, 1967

## Thermodynamic Properties

Vaporization studies done on ZnSe and other II-VI compounds yield raw data in the form of system pressure and mass loss rates versus temperature data for the subliming system. An empirical equation then is fit to these P-T data to determine a total pressure equation such as the latest update by Schönherr et al. (1998) for subliming ZnSe:

$$\log_{10}(P_1/\text{kPa}) = -(12641 \pm 70)/T/\text{K} + (8.99 \pm 0.06) \quad \text{for } 1180 \text{ K} < T < 1405 \text{ K}$$

After obtaining these empirical correlations, 2<sup>nd</sup> law and 3<sup>rd</sup> law analysis were typically used by the references to determine equilibrium constants, standard enthalpy, standard entropy, and standard free energy of formation and reaction.

A heat of reaction for the single-phase formation of ZnSe was estimated from the compiled heats of formation and reaction. The relation can best be described graphically below in Figure A-1. The standard reference state enthalpy value is shown as point A. The transition from A to B corresponds to the sums of the heats of formation for one mole of Zn(g) and ½ Se<sub>2</sub>(g). From B to C corresponds to the heat required to raise the vapors to 1000 °C. From D to E corresponds to the heat of sublimation and from A to E corresponds to the heat of reaction. The only unknown value is the heat of reaction for the single phase reaction which can be deduced from the relations shown in Figure A-1. The values for each of these states are therefore shown in Table A-8.

TABLE A-8

Enthalpy Values for ZnSe Formation

Path	State Value	$\Delta H$ (kJ/mol)
A	Reference Value	0
A $\rightarrow$ B	$\Delta H^\circ_f(\text{Zn}_{(g)} + 1/2\text{Se}_{2(g)})$	243.5
B $\rightarrow$ C	$\Delta H^\circ_f + C_p\Delta T$	263.8
C $\rightarrow$ D	$\Delta H_{\text{rxn}(g)}$	113.2
E $\rightarrow$ D	$\Delta H_{\text{sub}}$	377
A $\rightarrow$ E	$\Delta H^\circ_{\text{rxn}(s)}$	-178

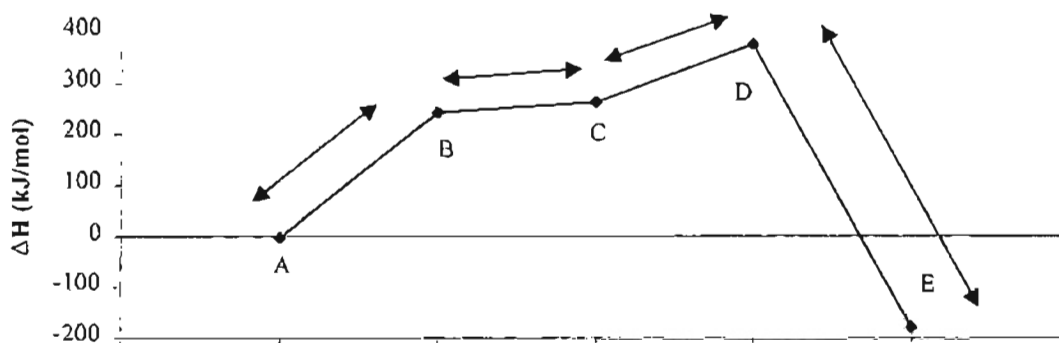


Figure A-1. Enthalpy diagram for the ZnSe formation process.

TABLE A-9

## Thermodynamic Properties – Equilibrium Constants

Property	Species	Appl. Range	Values and Functions			Empirical Source	Source
			log P = A - B/T + log T				
			A	B	C		
$K_{p(atm)}$		$Se_{(g)} = 0.5 Se_{2(g)}$	-2.585	-8655.0	-0.101	Mills, 1974	Brebrick and Liu, 1996
		$Se_{3(g)} = 1.5 Se_{2(g)}$	1.428	1716.0	0.454		
		$Se_{4(g)} = 2 Se_{2(g)}$	5.336	4984.0	-0.119		
		$Se_{5(g)} = 2.5 Se_{2(g)}$	12.06	10984.0	-0.1291		
		$Se_{6(g)} = 3 Se_{2(g)}$	16.83	14775.0	-0.478		
		$Se_{7(g)} = 3.5 Se_{2(g)}$	20.95	17956.0	-0.675		
		$Se_{8(g)} = 4 Se_{2(g)}$	25.877	21027.0	-1.015		
$K_p (kPa^{3/2})$	ZnSe	1147-1288 K	13.30 ± 0.08	19,155 ± 100		Bardi and Trionfetti, 1990	Bardi and Trionfetti, 1990
		1025-1136 K	13.30 ± 0.04	19,238 ± 46		Bardi and Trionfetti, 1990	Bardi and Trionfetti, 1990
		1173-1413 K	14.19	19,989		Flogel, 1969	Bardi and Trionfetti, 1990
		1123-1473 K	13.54 ± 0.07	19,799 ± 86		Boev et al., 1969	Bardi and Trionfetti, 1990
		1060-1393 K	13.88 ± 0.17	20,238 ± 204		Wösten and Geers, 1962	Bardi and Trionfetti, 1990
		980-1190 K	12.66	18,510		Goldfinger and Jeunehomme, 1963	Bardi and Trionfetti, 1990
		916-1095 K	15.53	21,303		Korneeva et al., 1960	Bardi and Trionfetti, 1990
$K_p (kPa^{3/2})$	ZnSe	298 K	$2(P/3)^{3/2}$		Schönherr et al., 1996	Schönherr et al., 1996	

General Decomposition Reaction:  $ZnSe_{(s)} = Zn_{(g)} + 1/2 Se_{2(g)}$

TABLE A-10

## Thermodynamic Properties – Heat Capacity

Property	Species	Appl. Range	Values and Functions	Theoretical Method	Empirical Source	Source	
$C_p$ (J/mol-K)	ZnSe <sub>(s)</sub>		29.835 + 0.028187*T + 2850.65/T		Brebrick and Liu, 1996		
			50.17 + 5.77e-3*T		Goldfinger and Jeunehomme, 1963		
	Zn <sub>(s)</sub>	298-692.7 K	22.40 + 10.05e-3*T			Morgan, 1985	
			24.60 + 0.003401*T + 7.146e-6*T <sup>2</sup>		Hultgren et al., 1973	Brebrick and Liu, 1996	
	Zn <sub>(l)</sub>		25.4			Bailar et al., 1973	
			31.40			Morgan, 1985	
			32.05		Hultgren et al., 1973	Brebrick and Liu, 1996	
	Zn <sub>(g)</sub>		31.38			Bailar et al., 1973	
			20.80			Morgan, 1985	
	Se <sub>2(g)</sub>	298-2000 K	20.79			Bailar et al., 1973	
44.559-2.654e-3*T -2.479e5/T <sup>2</sup>					Goldfinger and Jeunehomme, 1963	Barin et al., 1977	
Se <sub>(s)</sub>	298 K	17.89 + 0.0251*T		Hultgren et al., 1973	Brebrick and Liu, 1996		
		25			Nayar, 1997		
Se <sub>(l)</sub>		35.14		Hultgren et al., 1973	Brebrick and Liu, 1996		
$\Delta C_p$ (J/mol-K)	ZnSe <sub>(s)</sub>	298 K	47.80	Third law	Brebrick and Liu, 1996	Brebrick and Liu, 1996	

TABLE A-11

## Thermodynamic Properties – Enthalpy

Property	Species	Appl. Range	Values and Functions	Empirical Method	Theoretical Method	Empirical Source	Source
$\Delta H_f$ (kJ/mol)	ZnSe <sub>(s)</sub>	298 K	-177.8				
		298 K	-177.6			Nasar and Shamsuddin, 1990	Brebrick and Liu, 1996
		298 K	-164	Knudsen	Second law	Goldfinger and Jeunehomme, 1963	Goldfinger and Jeunehomme, 1963
		298 K	-200		Second law	Wösten and Geers, 1962	Goldfinger and Jeunehomme, 1963
		298 K	-220		Second law	Korneeva et al., 1960	Goldfinger and Jeunehomme, 1963
		298 K	-156		Third law	Korneeva et al., 1960	Goldfinger and Jeunehomme, 1963
		298 K	-140			Rossini et al., 1952	Goldfinger and Jeunehomme, 1963
	Zn <sub>(g)</sub>	298 K	130.5				Cox et al., 1989
		298 K	130.7				Bailar et al., 1973
$\Delta H_{vap}$ (kJ/mol)	Zn	1180 K	114.7				Morgan, 1985
			136.867				Brebrick and Liu, 1996
			115.31				Bailar et al., 1973
	Se(2)	958 K	121.75				Kudryavtsev, 1974
			143.9-0.032*T				Kudryavtsev, 1974
$\Delta H_{fus}$ (kJ/mol)	Zn		7.3220			Hultgren et al., 1973	Brebrick and Liu, 1996
			6.598				Nayar, 1997
			7.38				Bailar et al., 1973
			7.28				Morgan, 1985
			692.7 K	7.28			
	Se		6.706				Nayar, 1997
			5.8580			Mills, 1974	Brebrick and Liu, 1996

TABLE A-11, continued

## Thermodynamic Properties – Enthalpy

Property	Species	Appl. Range	Values and Functions	Empirical Method	Theoretical Method	Empirical Source	Source
$\Delta H_{\text{sub}}$ (kJ/mol)	ZnSe <sub>(s)</sub>	298 K	377 ± 4	Knudsen-effusion	Third law	Bardi and Trionfetti, 1990	Bardi and Trionfetti, 1990
		298 K	382 ± 3		Second law		
		298 K	369.4 ± 0.5	Knudsen-effusion	Third law	Schönherr et al., 1996	Schönherr et al., 1996
		298 K	376.9 ± 1.9		Second law		
		298 K	377.9 ± 0.9		Second law	Bardi and Trionfetti, 1990	Bardi and Trionfetti, 1990
		298 K	376.0 ± 0.3		Third law	Bardi and Trionfetti, 1990	Bardi and Trionfetti, 1990
		298 K	378.0 ± 0.2		Third law	Bardi and Trionfetti, 1990	Bardi and Trionfetti, 1990
		298 K	395.7		Second law	Flogel, 1969	Bardi and Trionfetti, 1990
		298 K	392.1 ± 1.6		Second law	Boev et al., 1969	Bardi and Trionfetti, 1990
		298 K	399.4 ± 3.9		Second law	Wösten and Geers, 1962	Bardi and Trionfetti, 1990
		298 K	364.1		Second law	Goldfinger and Jeunehomme, 1963	Bardi and Trionfetti, 1990
		298 K	416.4		Second law	Komeeva et al., 1960	Bardi and Trionfetti, 1990

TABLE A-12

Thermodynamic Properties -- Gibbs Free Energy of Formation ( $\Delta G_f$  in kJ/mol)

Species	Appl. Range	Values and Functions					Theoretical Method	Empirical Source	Source
ZnSe <sub>(s)</sub>		$\Delta G_f^\circ = A + B T + C T^2 + D T \ln T + E \ln T$ (J/mol)							
		A	B	C	D	E			
	1260-1410	-361,807 ± 7979	191.485 ± 5.883				Data correlation	Brebrick and Liu, 1996 (Optical density)	
	298-493	-187,769	-69.8741	0.00347845	10.4399	2850.65	Third law	Brebrick and Liu, 1996	
	493-692.5	-188,171	-169.863	-0.00907355	27.6951	2850.65		Brebrick and Liu, 1996	
	T ≥ 692.5	-191,732	-220.082	-0.0140936	36.6911	2850.65		Brebrick and Liu, 1996	
		-164,404	-154.656	62,550.50	6.64200E-04	24.1144	Second Law	Brebrick and Liu, 1996	
			$\Delta G_f^\circ = RT \ln ((2 \cdot 3^{1/2}/9) P_{\text{tot}}^{1.5})$					Brebrick and Liu, 1996	
			$\Delta G_f^\circ = RT \ln (P_{\text{Zn}} P_{\text{Se}_2}^{1.5})$					Brebrick and Liu, 1996	
	1350-1410 K	-341.088	0.1759					Y.-G. Sha et al., 1995 (PVT-Optical density)	
	1350-1410		$\Delta G_f^\circ = RT \ln (P_{\text{Zn}} P_{\text{Se}_2}^{1.5})$						
Zn <sub>(g)</sub>	298 K	95.178						Bailar et al., 1973	
	298 K	-163,000						Bailar et al., 1973	



TABLE A-13

## Thermodynamic Properties – Entropy

Property	Species	Appl. Range	Values	Theoretical Method	Empirical Source	Source
$\Delta S_f$ (J/mol-K)	ZnSe <sub>(s)</sub>	298 K	-11.683			Brebrick and Liu, 1996
$\Delta S_{vap}$ (J/mol-°C)	Zn		97.24			Bailar et al., 1973
$\Delta S_{fus}$ (J/mol-°C)	Zn		9.636			Bailar et al., 1973
S (J/mol-K)	ZnSe <sub>(s)</sub>	298 K	72.216			Brebrick and Liu, 1996
		298 K	82.8	Second law	Goldfinger and Jeunehomme, 1963	Goldfinger and Jeunehomme, 1963
		298 K	69.5	Second law	Wösten and Geers, 1962	Goldfinger and Jeunehomme, 1963
		298 K	30	Second law	Korneeva et al., 1960	Goldfinger and Jeunehomme, 1963
		298 K	84	Third law	Korneeva et al., 1960	Goldfinger and Jeunehomme, 1963
	Zn <sub>(s)</sub>	298	41.6			Bailar et al., 1973
	Zn <sub>(s)</sub>	298	41.63		Hultgren et al., 1973	Brebrick and Liu, 1996
	Zn <sub>(g)</sub>	298	160.87			Bailar et al., 1973
	Se <sub>(s)</sub>	298	41.97		Hultgren et al., 1973	Brebrick and Liu, 1996

## Transport Properties

The various transport properties viscosity ( $\mu$ ), thermal conductivity ( $k$ ), and mass diffusivity (or mass diffusion coefficient,  $D_{AB}$ ) of the gaseous species Zn, Se<sub>2</sub>, Ar, and ZnSe were estimated for use in the FLUENT CFD chemical reaction model according to Chapman-Enskog kinetic theory. Bird et al. (1960) describes the Chapman-Enskog theory of the potential energies of interaction method using the Lennard-Jones parameters,  $\sigma$  and  $\epsilon$ , to estimate the viscosity of a gas at low density. The characteristic diameter,  $\sigma$ , and the characteristic energy of interaction,  $\epsilon$ , are empirical parameters estimated from either critical point, melting point, or normal boiling point temperature and density. In Table A-14  $\sigma$  and  $\epsilon/\kappa$  are listed for each of the species along with the bases for their calculation. Critical properties were not available for ZnSe so its transport properties were estimated as analogous to the other three species where necessary.

TABLE A-14

Lennard-Jones Parameters for Gaseous Species

	Zn	Se <sub>2</sub>	Ar
$\sigma$ , Å	2.594	3.576	3.418
$\epsilon/\kappa$ , K	1330	1130	124
Source	Normal melting point	Sha et al., 1995	Bird et al., 1960

The viscosity of the pure gaseous species can then be estimated from these empirical parameters according to Chapman-Enskog theory:

$$\mu = 2.6693 \times 10^{-6} \frac{\sqrt{MT}}{\sigma^2 \Omega_\mu} \quad (\text{A-1})$$

where

$\mu$  = viscosity in kg/m-sec

$T$  = temperature in K

$\sigma$  = characteristic diameter in Å

$\Omega_\mu = \Omega_k =$  function of  $\kappa T/\epsilon$

$\kappa$  = Boltzmann's constant,  $1.380 \times 10^{-16}$  erg/molecule-K

$M$  = molar mass in kg/kgmol.

Viscosity estimates for the pure gaseous species as a function of temperature are tabulated in Table A-15. Bird et al. use the Wilke formula to estimate the viscosity of mixtures of these gas species:

$$\mu_{\text{mix}} = \frac{\sum_{i=1}^n x_i \mu_i}{\sum_{j=1}^n x_j \Phi_{ij}} \quad (\text{A-2})$$

where

$$\Phi_{ij} = \frac{1}{\sqrt{8}} \left( 1 + \frac{M_i}{M_j} \right)^{-1/2} \left[ 1 + \left( \frac{\mu_i}{\mu_j} \right)^{1/2} \left( \frac{M_j}{M_i} \right)^{1/4} \right]^2 \quad (\text{A-3})$$

$n$  = number of components in the mixture

$\mu_i$  = viscosity of component  $i$  in kg/m-sec

$x_i$  = mole fraction of component  $i$  and

$M_i$  = molar mass of component  $i$  in kg/kgmol.

Thermal conductivities for Zn and Ar were estimated using the Chapman-Enskog theory for monatomic gas at low density as presented by Bird et al. (1960):

$$k = 0.08322 \frac{\sqrt{T/M}}{\sigma^2 \Omega_k} \quad (\text{A-4})$$

and for Se<sub>2</sub> using the Eucken method for polyatomic gases at low density:

$$k = \left( \hat{C}_p + \frac{5}{4} \frac{R}{M} \right) \mu \quad (\text{A-5})$$

where

$\hat{C}_p$  = heat capacity per kilogram at constant pressure

R = ideal gas constant,  $8.314 \frac{\text{kg m}^2}{\text{kmol K}}$ .

Thermal conductivity estimates for the pure gaseous species are tabulated in Table A-15 below.

TABLE A-15

Gas Viscosity and Thermal Conductivity Estimates at Selected Temperatures.

Temp., K	$\mu$ , kg/m-sec			k, J/m-sec-K		
	Zn	Se <sub>2</sub>	Ar	Zn	Se <sub>2</sub>	Ar
400	2.30e-5	2.00e-5	2.82e-5	1.10e-2	6.62e-3	2.20e-2
600	3.32e-5	2.93e-5	3.79e-5	1.58e-2	9.76e-3	2.96e-2
800	4.39e-5	3.92e-5	4.63e-5	2.09e-2	1.30e-2	3.61e-2
1000	5.51e-5	4.89e-5	5.36e-5	2.63e-2	1.61e-2	4.18e-2
1200	6.63e-5	5.89e-5	6.04e-5	3.16e-2	1.93e-2	4.71e-2
1400	7.75e-5	6.87e-5	6.64e-5	3.69e-2	2.22e-2	5.18e-2
1600	8.84e-5	7.80e-5	7.28e-5	4.21e-2	2.50e-2	5.68e-2

Wahlbeck et al. (1985) empirically determined diffusion coefficients for Zn in Ar using the Ruff-MKW boiling point method. This yielded an average empirical diffusion

coefficient of  $1.13 \times 10^{-3} \text{ m}^2/\text{sec}$  at 1000 K. Chapman-Enskog kinetic theory, which was used to calculate the viscosity and thermal conductivity above, yielded a values of the order  $1 \times 10^{-4} \text{ m}^2/\text{sec}$  at 1000 K for the binary combinations of Zn, Se<sub>2</sub>, and Ar. Without empirical data for all the combinations, the use of the single empirical coefficient was not prudent. Therefore all diffusion coefficient values were estimated using kinetic theory. This method provides good estimates for low density monatomic and polyatomic gases and mixtures up to 1000 K and 70 atm (Wankat and Knabel 1997) so in future, if possible, empirical values should be utilized.

From Bird et al. (1960), the following mixing rules were used to estimate  $\sigma_{AB}$  and  $\epsilon_{AB}/K$ . These values are located in Table A-16.

$$\sigma_{AB} = 0.5(\sigma_A + \sigma_B) \quad (\text{A-6})$$

$$\epsilon_{AB}/K = \sqrt{\epsilon_A \epsilon_B} \quad (\text{A-7})$$

The Chapman-Enskog kinetic theory formula for the diffusion coefficients was subsequently for estimations. Some selected values are tabulated in Table A-17.

$$\mathcal{D}_{AB} = 0.0018583 \frac{\sqrt{T^3 \left( \frac{1}{M_A} + \frac{1}{M_B} \right)}}{p \sigma_{AB}^2 \Omega_{D,AB}} \quad (\text{A-8})$$

where  $p$  was assumed to be 1 atmosphere and  $\Omega_{D,AB}$  was interpolated from Appendix B (Bird et al., 1960).

TABLE A-16

## Lennard-Jones Parameters for Binary Gas Mixtures

	Zn-Ar	Zn-Se <sub>2</sub>	Se <sub>2</sub> -Ar
$\sigma_{AB}$ , Å	3.006	3.085	3.497
$\epsilon_{AB}/K$ , K	406.1	1225.9	374.3

TABLE A-17

## Gas Diffusion Coefficient Estimates at Selected Temperatures.

Temp (K)	$\Omega_{D,AB}$			$\mathcal{D}_{AB}$ (m <sup>2</sup> /sec)		
	Zn-Ar	Zn-Se <sub>2</sub>	Se <sub>2</sub> -Ar	Zn-Ar	Zn-Se <sub>2</sub>	Se <sub>2</sub> -Ar
298	1.710	-	1.612	1.24E-05	-	8.59E-06
400	1.454	2.550	1.394	2.27E-05	9.01E-06	1.54E-05
600	1.205	2.090	1.167	5.04E-05	2.02E-05	3.39E-05
800	1.080	1.798	1.051	8.65E-05	3.61E-05	5.80E-05
1000	1.005	1.592	0.980	1.30E-04	5.70E-05	8.68E-05
1200	0.953	1.454	0.932	1.80E-04	8.21E-05	1.20E-04
1400	0.915	1.352	0.898	2.36E-04	1.11E-04	1.57E-04
1600	0.887	1.269	0.871	2.98E-04	1.45E-04	1.98E-04

Values for the liquid phase transport properties, thermal conductivity and viscosity were also needed for the heat transfer analysis performed on the boilers. Below, the available empirical data is tabulated. Most data values did not approach 1000 °C therefore extrapolation was needed to obtain useful correlations. A similar Andrade type logarithmic extrapolation to that used on the liquid surface tension data was used.

TABLE A-18

Liquid Thermal Conductivity (Ho et al., 1974)

	Temp (K)	k (W/m-K)	1/T (K <sup>-1</sup> )	ln k (ln sec <sup>-1</sup> )
Zn <sub>(l)</sub>	692.73	49.5	0.001444	3.901973
	700	49.9	0.001429	3.910021
	773.2	54.2	0.001293	3.992681
	800	55.7	0.001250	4.019980
	873.2	59.9	0.001145	4.092677
	900	61.5	0.001111	4.119037
	973.2	65.7	0.001028	4.185099
	1000	67.3	0.001000	4.209160
	1073.2	71.5	0.000932	4.269697
	1100	73.0	0.000909	4.290459
	Extrapolated from the data			
Function	ln k = 5.024exp(-1.768E2/T)			
1150	74.3	0.000870	4.308	
1200	76.4	0.000833	4.336	
1250	78.4	0.000800	4.362	
1300	80.3	0.000769	4.385	
-----				
Se <sub>(l)</sub>	490	1.97		
	490	0.285		
	Average	1.13		

TABLE A-19.

Liquid Viscosity Data for Zinc (Viswanath and Natarajan, 1989)

Temp (K)	$\mu_{zn}$ (kg/m-sec)
690	4.136E-05
700	3.929E-05
720	3.579E-05
740	3.298E-05
760	3.066E-05
780	2.873E-05
800	2.710E-05
830	2.509E-05
860	2.346E-05
890	2.212E-05
920	2.101E-05
950	2.006E-05
980	1.925E-05
1010	1.854E-05
1040	1.793E-05
1070	1.739E-05
1100	1.691E-05
Extrapolated using this data	
Function	$\ln \mu$ (cPoise) = 0.1009exp(1829.4/T(K))
1150	1.641E-05
1200	1.589E-05
1250	1.547E-05
1300	1.510E-05



TABLE A-20

Liquid Viscosity Data for Selenium (Lucovsky, 1979)

Temp (K)	$\mu_{Se}$ (kg/m-sec)
513	2E-03
595	2E-04
Extrapolated Data:	
Function	$\ln \mu(\text{Poise}) = 7.3108E-5 \exp(544.85/T(K))$
493	4.609E-04
500	3.948E-04
550	1.466E-04
600	6.422E-05
650	3.194E-05
700	1.755E-05
750	1.045E-05
800	6.634E-06
850	4.444E-06
900	3.113E-06
950	2.263E-06
1000	1.699E-06

## APPENDIX B

### MASS FLOW ESTIMATES AND OTHER DERIVED VALUES

TABLE B-1

## Mass Transfer Estimates

Run Classification	Run Identification							Average Values			All A,B,C		
	BA97155 <sup>1</sup>	BA97161	BA97142	BA98009	BA97209	BA97217	BA97204	A	B	C			
Powder Deposition Pattern	A	A	A	B	B	B	C	A	B	C			
	Loose	Loose	Short tube	Loose	Tubes	Tubes	Tubes						
Molar Yield (Zinc Basis)	87.6%	73.7%	58.7%	69.9%	41.4%	34.8%	45.5%	73.3%	48.7%	45.5%	58.8%		
Reactant	Zinc	Mass (g)	500.0	501.4	514.5	500.0	500.0	500.0	505.3	500.0	500.0	502.3	
		Moles (mol)	7.646	7.668	7.868	7.646	7.646	7.646	7.646	7.727	7.646	7.646	7.681
Loading	Selenium	Mass (g)	667.4	700.3	700.9	685.2	762.0	644.0	683.5	689.5	697.1	683.5	691.9
		Moles (mol)	8.452	8.869	8.877	8.678	9.650	8.156	8.656	8.733	8.828	8.656	8.763
Initial Liquid Contact	Zinc	Length, L (m)	0.178	0.178	0.178	0.178	0.178	0.178	0.178	0.178	0.178	0.178	
		Area, A <sub>c</sub> (m <sup>2</sup> )	0.00986	0.00986	0.00997	0.00986	0.00986	0.00986	0.00986	0.00990	0.00986	0.00986	0.00988
Dimensions (Excluding Ends)	Selenium	Length, L (m)	0.0448	0.0470	0.0470	0.0459	0.0511	0.0432	0.0459	0.0462	0.0467	0.0459	0.0464
		Area, A <sub>c</sub> (m <sup>2</sup> )	0.0105	0.0111	0.0111	0.0108	0.0120	0.0102	0.0108	0.0109	0.0110	0.0108	0.0109
Estimated Time, t, for Complete Transfer (hours)	Zinc	Low t Est.	3.50	3.00	3.33	3.00	3.83	-	-	3.28	3.42	-	3.33
		Time Avg.	3.88	3.25	3.72	3.38	4.08	4.42	5.75	3.61	3.96	5.75	4.07
		High t Est.	4.25	3.50	4.10	3.75	4.33	-	-	3.95	4.04	-	3.99
		Δt	0.75	0.50	0.77	0.75	0.50	-	-	0.67	0.63	-	0.47
	Selenium	Low t Est.	-	2.75	3.33	-	2.33	1.92	3.0	3.04	2.12	3.00	2.67
		Time Avg.	4.25	3.00	3.72	3.00	2.71	2.29	4.38	3.66	2.67	4.38	3.33
		High t Est.	-	3.25	4.10	-	3.08	2.67	5.75	3.68	2.88	5.75	3.77
		Δt	-	0.50	0.77	-	0.75	0.75	2.75	0.64	0.75	2.75	0.79
Mole Flow Rate (mol/sec)	Zinc	Low t Est.	6.07E-04	7.10E-04	6.56E-04	7.08E-04	5.55E-04	-	-	6.58E-04	6.31E-04	-	6.47E-04
		Time Avg.	5.48E-04	6.55E-04	5.88E-04	6.29E-04	5.21E-04	4.81E-04	3.69E-04	5.97E-04	5.43E-04	3.69E-04	5.42E-04
		High t Est.	5.00E-04	6.09E-04	5.33E-04	5.66E-04	4.91E-04	-	-	5.47E-04	5.28E-04	-	5.40E-04
	Selenium	Low t Est.	-	8.96E-04	7.40E-04	-	1.15E-03	1.18E-03	8.02E-04	8.18E-04	1.17E-03	8.02E-04	9.54E-04
		Time Avg.	5.52E-04	8.21E-04	6.64E-04	8.04E-04	9.90E-04	9.89E-04	5.50E-04	6.79E-04	9.28E-04	5.50E-04	7.67E-04
		High t Est.	-	7.58E-04	6.01E-04	-	8.69E-04	8.50E-04	4.18E-04	6.80E-04	8.59E-04	4.18E-04	6.99E-04
Argon	Zinc	1.78E-04	1.78E-04	1.78E-04	2.03E-04	2.03E-04	2.03E-04	1.34E-04	1.78E-04	2.03E-04	1.34E-04	1.82E-04	
	Selenium	1.81E-04	1.81E-04	1.81E-04	2.04E-04	2.06E-04	2.06E-04	1.42E-04	1.81E-04	2.05E-04	1.42E-04	1.86E-04	

TABLE B-1, CONTINUED

## Mass Transfer Estimates

Run Classification			Run Identification							Average Values			All A,B,C
			BA97155 <sup>1</sup>	BA97161	BA97142	BA98009	BA97209	BA97217	BA97204	A	B	C	
Powder Deposition Pattern			Loose	Loose	Short tube	Loose	Tubes	Tubes	Tubes				
Molar Yield (Zinc Basis)			87.6%	73.7%	58.7%	69.9%	41.4%	34.8%	45.5%	73.3%	48.7%	45.5%	58.8%
Nozzle Exit Velocity, $u_0$ (m/sec) for 18 mm $D_0$	Zinc	Low t Est.	0.322	0.364	0.342	0.366	0.305	-	-	0.343	0.336	-	0.340
		Time Avg.	0.298	0.342	0.314	0.335	0.291	0.275	0.202	0.318	0.300	0.202	0.294
		High t Est.	0.278	0.323	0.292	0.309	0.279	-	-	0.297	0.294	-	0.296
	Selenium	Low t Est.	-	0.442	0.378	-	0.546	0.558	0.380	0.410	0.552	0.380	0.461
		Time Avg.	0.301	0.411	0.347	0.405	0.481	0.480	0.278	0.353	0.456	0.278	0.386
		High t Est.	-	0.385	0.321	-	0.433	0.425	0.225	0.353	0.429	0.225	0.358

<sup>1</sup> This run had approximately 5% of selenium left over which is reflected in mass above.

TABLE B-2

## Boiler And Vaporization Duties

Run Classification			Run Identification							Average Values			
			BA97155	BA97161	BA97142	BA98009	BA97209	BA97217	BA97204	A	B	C	A,B,C
Molar Yield (Zinc Basis)			87.6%	73.7%	58.7%	69.9%	41.4%	34.8%	45.5%	73.3%	48.7%	45.5%	55.8%
Average Boiler Duty, $Q_{\text{Boiler}}$ (W)	Zinc	Low t Est.	516	532	-	575	515	-	-	524	545	-	535
		Time Avg.	514	528	553	570	513	498	480	532	527	480	513
		High t Est.	512	524	-	564	511	-	-	518	538	-	528
	Selenium	Low t Est.	-	685	-	613	625	630	616	685	623	616	641
		Time Avg.	739	676	696	623	615	610	588	704	616	588	636
		High t Est.	-	666	-	633	604	590	560	666	609	560	612
Boiling Duty <sup>1</sup> , $\dot{N} \cdot \Delta H_{\text{vap}}$ (W)	Zinc	Low t Est.	69.6	81.4	75.3	81.2	63.6	-	-	75.4	72.4	-	73.9
		Time Avg.	62.9	75.2	67.5	72.2	59.7	55.1	42.4	68.5	62.3	42.4	57.7
		High t Est.	57.3	69.8	61.1	65.0	56.3	-	-	62.8	60.6	-	61.7
	Selenium	Low t Est.	-	109.2	90.3	-	140.2	144.1	97.7	99.7	142.2	97.7	113.2
		Time Avg.	67.3	100.1	80.9	97.9	120.7	120.5	67.0	82.8	113.1	67.0	87.6
		High t Est.	-	92.4	73.3	-	106.0	103.6	51.0	82.9	104.8	51.0	79.5
Argon Vapor Duty, $Q_{\text{Ar}}$ (W)	Zinc	Inflow	1.11	1.11	1.11	1.26	1.27	1.27	0.83	1.11	1.26	0.83	1.07
		Outflow	4.50	4.50	4.50	5.13	5.14	5.14	3.41	4.50	5.14	3.41	4.35
	Selenium	Inflow	1.13	1.13	1.13	1.27	1.28	1.28	0.88	1.13	1.28	0.88	1.10
		Outflow	3.68	3.65	3.67	4.11	4.13	4.11	2.89	3.66	4.12	2.89	3.56
Boiler Efficiency (W)	Zinc	Low t Est.	14%	16%	14%	14%	13%	-	-	14%	13%	-	14%
		Time Avg.	12%	14%	12%	13%	12%	11%	9%	13%	12%	9%	11%
		High t Est.	11%	14%	11%	12%	11%	-	-	12%	11%	-	12%
	Selenium	Low t Est.	-	16%	13%	-	23%	24%	16%	15%	23%	16%	18%
		Time Avg.	10%	15%	12%	16%	20%	20%	12%	12%	19%	12%	14%
		High t Est.	-	14%	11%	-	18%	18%	10%	13%	18%	10%	14%

<sup>1</sup> Heat of vaporization is calculated at boiling point:  $\Delta H_{\text{Zn}} = 114.7$  kJ/mol and  $\Delta H_{\text{Se}} = 121.9$  kJ/mol.

TABLE B-3

## System Temperatures

Run Classification		Run Identification						Average Values					
		BA97155	BA97161	BA97142	BA98009	BA97209	BA97217	BA97204	A	B	C	A,B,C	
Molar Yield (Zinc Basis)		87.6%	73.7%	58.7%	69.9%	41.4%	34.8%	45.5%	73.3%	48.7%	45.5%	55.8%	
Run Temperature Settings (K)	Zinc	1226	1226	1226	1223	1223	1223	1229	1226	1223	1229	1226	
	Selenium	994	994	994	991	991	991	997	994	991	997	994	
	Reactor	1273	1273	1273	1248	1248	1248	1248	1273	1248	1248	1256	
Bulk Liquid Temperature, $T_L$ (K)	Zinc	Low t Est.	1220	1218	1219	1215	1217	-	-	1219	1216	-	1218
		Time Avg.	1220	1219	1220	1216	1217	1218	1225	1220	1217	1225	1221
		High t Est.	1221	1219	1220	1217	1218	-	-	1220	1217	-	1219
	Selenium	Low t Est.	-	970	973	-	962	957	973	971	960	973	968
		Time Avg.	978	972	975	968	966	963	981	975	966	981	974
		High t Est.	-	973	977	-	969	967	985	975	968	985	976
Inner Wall Temperature, $T_{iw}$ (K)	Zinc	Low t Est.	1220	1219	1219	1216	1217	-	-	1219	1217	-	1218
		Time Avg.	1220	1219	1220	1217	1218	1218	1225	1220	1217	1225	1221
		High t Est.	1221	1220	1221	1217	1218	-	-	1220	1218	-	1219
	Selenium	Low t Est.	-	984	985	-	979	976	987	985	977	987	983
		Time Avg.	988	984	986	981	980	979	990	986	980	990	986
		High t Est.	-	985	987	-	982	980	992	986	981	992	986
Inner Wall Excess Temperature $T_c = T_{iw} - T_{sat}$	Zinc	Low t Est.	39.8	38.7	39.4	35.8	37.3	-	-	39.3	36.6	-	37.9
		Time Avg.	40.4	39.3	40.1	36.6	37.7	38.1	45.2	39.9	37.4	45.2	40.9
		High t Est.	40.9	39.8	40.6	37.2	38.0	-	-	40.4	37.6	-	39.0
Selenium	Low t Est.	-	25.6	27.4	-	20.7	18.1	29.5	26.5	19.4	29.5	25.1	
	Time Avg.	30.3	26.5	28.3	23.5	22.4	20.5	32.5	28.4	22.2	32.5	27.7	
	High t Est.	-	27.22	29.04	-	23.73	22.29	34.04	28.13	23.01	34.04	28.39	

TABLE B-4

## Dimensionless Numbers and Heat Transfer Coefficients

Run Classification		Run Identification						Average Values				
		BA97155	BA97161	BA97142	BA98009	BA97209	BA97217	BA97204	A	B	C	A, B, C
Molar Yield (Zinc Basis)		87.6%	73.7%	58.7%	69.9%	41.4%	34.8%	45.5%	73.3%	48.7%	45.5%	55.8%
Prandtl Number, Pr	Zinc	1.08E-04	1.08E-04	1.08E-04	1.08E-04	1.08E-04	1.08E-04	1.07E-04	1.08E-04	1.08E-04	1.07E-04	1.08E-04
	Selenium	3.99E-02	4.00E-02	3.99E-02	4.00E-02	4.00E-02	4.00E-02	3.99E-02	3.99E-02	4.00E-02	3.99E-02	3.99E-02
Grashof Number, Gr	Zinc	2.77E+10	6.06E+09	2.09E+10	1.13E+10	1.35E+10	1.82E+09	4.52E+09	1.82E+10	8.87E+09	4.52E+09	1.05E+10
	Selenium	2.00E+09	3.03E+09	2.55E+09	2.62E+09	4.18E+09	2.89E+09	1.98E+09	2.52E+09	3.23E+09	1.98E+09	2.58E+09
Nusselt Number, Nu	Zinc	15.4	9.6	14.1	11.7	12.3	6.8	8.8	13.0	10.2	8.8	10.7
	Selenium	25.5	29.2	27.6	27.9	32.4	28.8	25.5	27.5	29.7	25.5	27.6
Heat Transfer Coefficient, $h_L$ (W/m <sup>2</sup> -K)	Zinc	26366	16525	24154	19953	21076	11579	15151	22348	17536	15151	18345
	Selenium	645	703	664	686	717	754	627	671	719	627	672

TABLE B-5

## Critical Heat Flux

Zinc:

RUN	$Q_{VAP}$ (W)	$A_c$ (m <sup>2</sup> )	$q_{VAP}$ (W/m <sup>2</sup> )	$q_{CRIT}$ (W/m <sup>2</sup> )	$T_c$ ( $T_{iw} - T_{sat}$ )	$T_{iw}$	P (Pa)	$\rho_G$ (kg/m <sup>3</sup> )	$\rho_L$ (kg/m <sup>3</sup> )	$\sigma$ (kg/m)
BA98009	72.2	0.00986	7323	4.2E+06	37	1221	17048	0.110	6058	156
BA97209	59.7	0.00986	6055	4.1E+06	38	1220	16639	0.107	6059	156
BA97217	55.1	0.00986	5588	4.1E+06	38	1220	16639	0.107	6059	156
BA97161	75.2	0.00986	7627	4.0E+06	39	1217	15405	0.100	6062	156
BA97142	67.5	0.00997	6770	4.0E+06	40	1218	15817	0.102	6061	156
BA97155	62.9	0.00986	6379	4.0E+06	40	1218	15817	0.102	6061	156
BA97204	42.4	0.00986	4300	4.4E+06	45	1225	18680	0.120	6054	157

Selenium:

RUN	$Q_{VAP}$ (W)	$A_c$ (m <sup>2</sup> )	$q_{VAP}$ (W/m <sup>2</sup> )	$q_{CRIT}$ (W/m <sup>2</sup> )	$T_c$ ( $T_{iw} - T_{sat}$ )	$T_{iw}$	P (Pa)	$\rho_G$ (kg/m <sup>3</sup> )	$\rho_L$ (kg/m <sup>3</sup> )	$\sigma$ (kg/m)
BA97217	120.5	0.0102	11814	1.5E+06	20.5	988	15979	0.154	3379	8
BA97209	120.7	0.0120	10058	1.4E+06	22.4	984	13899	0.134	3382	8
BA98009	97.9	0.0108	9065	1.5E+06	23.5	986	14941	0.144	3380	8
BA97161	100.1	0.0111	9018	1.3E+06	26.5	981	12328	0.119	3384	8
BA97142	80.9	0.0111	7288	1.3E+06	28.3	980	11802	0.114	3385	8
BA97155	67.3	0.0105	6410	1.3E+06	30.3	979	11275	0.109	3386	8
BA97204	67.0	0.0108	6198	1.6E+06	32.5	990	17013	0.163	3377	8



## APPENDIX C

### DESCRIPTION OF FLUENT/UNS MODEL

FLUENT/UNS is a very powerful finite element/volume CFD modeling package. It combines several built in models to handle flow, heat transfer, and chemical reaction with the capabilities to complex system complex geometries. The goal of this thesis was to analyze experimental data and observations to first optimize the current EP ZnSe synthesis reactor and secondly to produce a new reactor design. A FLUENT/UNS model was used as a tool in this analysis and design. A 2D cross section of the current EP reactor drawn and meshed by Foster (in progress) as the geometry for the model. The Foster geometry is displayed in Figure C-1. Reactant streams were introduced using 12.7 mm I. D. velocity inlets at the left of the boilers. Reactant streams were supplied at 300 K while boilers were walls were heated to the observed temperatures for each run. To mimic the heat loss in the neck of the selenium boiler, the temperature was arbitrarily set to 600 K for each run. The face-plate on the reactor was set at zero flux boundary condition. The reactor was split into the three heating zones which were present on the EP furnace, a six inch, two feet, and six inch sections, followed by a zero heat flux boundary for the final few inches of the reactor. The reactor outlet was modeled as an outflow boundary condition.

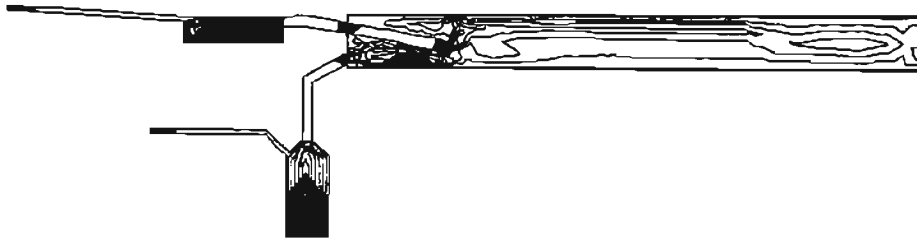


Figure C-1. Foster (in progress) geometry for EP reactor.

One of the main reasons for performing the modeling effort was to reproduce the complex flow mixing phenomena at the entrance of the reactor. In this respect, the built-in turbulent RNG  $k$ - $\epsilon$  model was used in the solver. The flow in the tube away from the entrance is otherwise laminar, but this model can be applied to such mixed conditions effectively (Fluent, 1996). The blunt fully developed velocity profile is evident in Figure C-2 which is a general graphic output of the steady-state velocity profile within the model.

For the kinetic study performed in this thesis, the energy equation was turned off making the reactor model isothermal. This assumption was made to simplify rate constant estimation. In the thesis of Shay (1998), a second order rate constant obtained from a plug flow assumption and trial and error fit of diffusion coefficients were used for optimization of nozzles in a nonisothermal reactor. Both models produced the similar results that the reactor prefers low, stoichiometric flows of reactants. Mole fractions were computed at the model outlet by using the average surface integral calculations built into UNS.

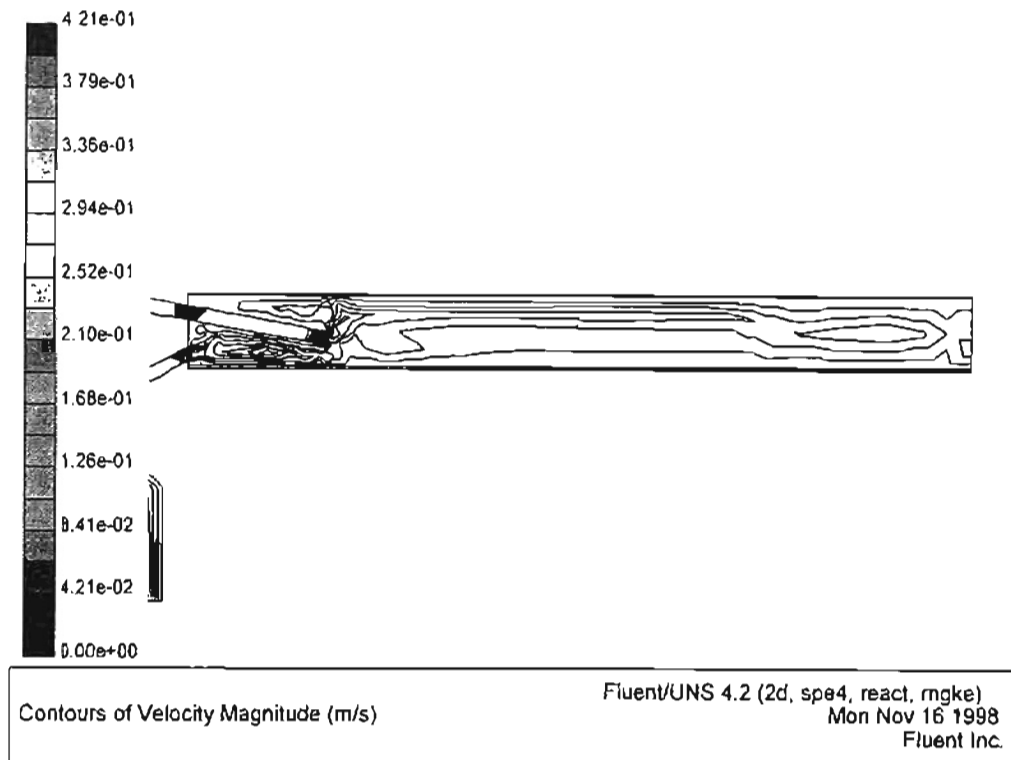


Figure C-2. Laminar velocity profile in FLUENT/UNS output.

The latter two FLUENT/UNS models do not address the unsteady nature of the EP reactor, the observed temperature profiles within the reactor, radiation heat transfer, 3D flow patterns, changing density of the vapor stream (gas-to-particle conversion), or the resulting alteration of reactor wall profile due to deposition. The thesis of Foster (in progress) aims at modeling the complex heat transfer effects of the entire reactor system, furnace, air gaps, and reactor with both mixed convection and radiation heat transfer. Foster's thesis also further addresses the kinetics of the ZnSe synthesis reaction. The thesis of Nikolic (in progress) addresses the 3D flow characteristics of both the current EP reactor and the optimized reactor design of this thesis and Shay (1998).

The inputs to reproduce the chemical model of this thesis are described in the following section. The next section lists mass fractions and stream velocity components

that were entered for the kinetic estimation. The last section lists the mass fractions, velocity components, and output yield values from the parametric flow study described in Chapter III.

### General Set-up

**\*\*Load the property data base which is needed to enter new species physical properties.\*\***

File → Read → Scheme → “propdb.scm”

**\*\*Load the previously drawn mesh file.\*\***

File → Read → Case → “mesh\_file.msh”

**\*\*Set the scale type for the CFD model.\*\***

Grid → Scale... → Scale Factors → x = 1 and y = 1  
 → Units → Grid created in mm  
 → Conversion →  
 → Change Length Units  
 → Okay

**\*\*Define models and species properties.\*\***

Define → Models → Domain → Space = 2D  
 → Time = Steady/unsteady  
 → Okay

**\*\*Set flow model type.\*\***

→ Viscous → Models → Turbulent: RNG k-epsilon  
 → Rest of settings are defaults  
 → Okay

**\*\*Enable heat transfer.\*\***

→ Heat Transfer → Heat transfer on  
 → Viscous heating

→ Species diffusion source

→ Okay

**\*\*Enable Arrhenius reaction rate model.\*\***

→ Species → Model → Finite rate reaction  
→ Transport

→ Okay

**\*\*Define gravity forces.\*\***

→ Body Forces →  $y = -9.81 \text{ m/sec}^2$

→ Okay

**\*\*Now define all species properties and chemical reaction using the Materials panel.\*\***

**\*\*Begin mixture-materials creation, define reaction name under mixture properties.\*\***

Define →

Materials → Material Type → Mixture

→ Mixture Name → "ZnSe\_formation"

→ Chemical → "ZnSe\_for"  
→ Formula

→ Change/Create

**\*\*Responds "Overwrite mixture-template?" Select "Yes."\*\***

→ Properties → Mixture → Skip for now.  
→ Species

→ Reaction → Skip for now.  
→ Model

→ Density → Volume-weighted-  
mixing-law

→ Heat Capacity → Mixing-law

→ Thermal → Mixing-law  
→ Conductivity

→ Viscosity → Mixing-law

→ Mass → Skip for now  
→ Diffusivity

**\*\*IMPORTANT: SAVE**

→ Change/Create **CHANGES WHEN EXITING  
ALL FIELDS\*\***

**\*\*Enter fluid species properties for the model.\*\***

→ Material Type → Fluid  
→ Database → Argon  
→ Copy  
→ Close

**\*\*The following section describes the procedure to modify default species to represent gas phase reaction. The species data is tabulated after input explanations.\*\***

→ Select an  
→ existing species  
→ Type over  
→ name  
→ Type over chemical formula  
→ Density → Piecewise linear  
→ Heat Capacity → Constant or Polynomial  
→ Molecular  
→ Weight  
→ Heat of  
→ Formation  
→ Reference Temperature  
→ Change/Create

**\*\*Responds “overwrite species?” Select “Yes.”\*\***

**\*\*Repeat for all species (Zn-g, Se<sub>2</sub>-g, ZnSe-g).\*\***

**\*\*Now change default solid to quartz.\*\***

→ Material Type → Solid  
→ Follow same procedure as above for “Fluids”

**\*\*Now finish creating mixture-materials model for chemical reaction and diffusion.\*\***

→ Material Type → Mixture

→ Properties → Mixture → Edit...  
 → Species

**\*\*To “Selected Species” list add Zn-g, Se<sub>2</sub>-g, ZnSe-g, and Ar in that order. Last species is considered bulk (inert) species. Remove any default species.\*\***

→ Okay

→ Reaction → Finite rate/eddy  
 → Model → dissipation  
 → Edit...

**\*\*Enter stoichiometric coefficients for reaction, concentration exponents, pre-exponential, activation energy, and set temperature exponent = 0. Kinetics are detailed in Chapter III.**

→ Okay

→ Mass → Multicomponent  
 → Diffusivity

**\*\*Now values can be entered based on Chapman-Enskog estimation method. Values for isothermal runs are located following species properties tables in this section.\*\***

**\*\*Now the procedure for entering boundary conditions is described. But for the kinetic analysis in this thesis, all walls are isothermal.\*\***

**\*\*Set inlet stream velocities and mass fractions.\*\***

Define	→	Boundary	→	Velocity-	→	Enter linear velocity
		Conditions		inlet-1		
					→	Enter stream temperature
					→	Enter component mass fractions
					→	Okay

→ Velocity- inlet-2 → Repeat procedure

**\*\*Set wall boundary conditions.\*\***

→ Wall-1 to 16 → Material = quartz  
→ Set wall heat b.c.

**\*\*Walls typically either had constant temperature, constant heat flux, or inner wall were coupled.\*\***

→ Close

**\*\*Save the newly created case file before running.\*\***

File → Write → Case → "filename.cas"

### Input Species Properties

**\*\*For this thesis, data values for  $k$ ,  $\mu$ ,  $\rho$ , and  $D$  were entered as piecewise linear functions. But in future CFD models, it is recommended to use the built in kinetic theory model for ideal gases.\*\***

TABLE C-1  
FLUENT/UNS Species Properties

Species	MW	$C_p$ (J/kg-K)	$\Delta H_f$ (J/kg)	$T_{ref}$ (K)
Zn-g	65.37	317.68	1.3e+08	298.15
Se <sub>2</sub> -g	157.92	282.16-0.016806*T	2.271e+08	298.15
ZnSe-g	144.33	259.41+1.1571e-04*T	1.92e+08	298.15
Argon	default	default	default	298.15



TABLE C-2

FLUENT/UNS Input Ideal Gas Density ( $\text{kg/m}^3$ )

Temperature (K)	Zn-g	Se <sub>2</sub> -g	ZnSe-g	Ar
400	1.9923	4.8115	4.3975	1.2172
600	1.3282	3.2077	2.9316	0.8115
800	0.9962	2.4058	2.1987	0.6086
1000	0.7969	1.9246	1.7590	0.4869
1200	0.6641	1.6038	1.4658	0.4057
1400	0.5692	1.3747	1.2564	0.3478
1600	0.4981	1.2029	1.0994	0.3043
1800	0.4427	1.0692	0.9772	0.2705
2000	0.3985	0.9623	0.8795	0.2434

TABLE C-3

FLUENT/UNS Input Gas Viscosity ( $\text{kg/m-sec}$ )

Temperature (K)	Zn-g	Se <sub>2</sub> -g	ZnSe-g	Ar
400	2.30E-05	2.00E-05	2.15E-05	2.82E-05
600	3.32E-05	2.93E-05	3.13E-05	3.79E-05
800	4.39E-05	3.92E-05	4.16E-05	4.63E-05
1000	5.51E-05	4.89E-05	5.20E-05	5.36E-05
1200	6.63E-05	5.89E-05	6.26E-05	6.04E-05
1400	7.75E-05	6.13E-05	7.31E-05	6.64E-05
1600	8.84E-05	6.87E-05	8.32E-05	7.28E-05
1800	9.90E-05	7.80E-05	9.29E-05	7.89E-05
2000	10.9E-05	8.68E-05	10.2E-05	8.50E-05

TABLE C-4

FLUENT/UNS Input Gas Thermal Conductivity (J/m-sec-K)

Temperature (K)	Zn-g	Se <sub>2</sub> -g	ZnSe-g	Ar
400	1.10E-02	0.662E-02	0.881E-02	2.20E-02
600	1.58E-02	0.976E-02	1.28E-02	2.96E-02
800	2.09E-02	1.30E-02	1.70E-02	3.61E-02
1000	2.63E-02	1.61E-02	2.12E-02	4.18E-02
1200	3.16E-02	1.93E-02	2.55E-02	4.71E-02
1400	3.69E-02	2.00E-02	2.96E-02	5.18E-02
1600	4.21E-02	2.22E-02	3.36E-02	5.68E-02
1800	4.72E-02	2.76E-02	3.74E-02	6.16E-02
2000	5.21E-02	3.00E-02	4.11E-02	6.63E-02

TABLE C-5

FLUENT/UNS Input Mass Diffusivity (m<sup>2</sup>/sec)

Temperature (K)	Zn-Ar	Zn-Se <sub>2</sub>	Se <sub>2</sub> -Ar	ZnSe-Ar	Zn-ZnSe	Se <sub>2</sub> -ZnSe
400	2.27E-05	9.01E-06	1.54E-05	Same as	Same as	Se <sub>2</sub> -Zn
600	5.04E-05	2.02E-05	3.39E-05	Se <sub>2</sub> -Ar		
800	8.65E-05	3.61E-05	5.80E-05			
1000	1.30E-04	5.70E-05	8.68E-05			
1200	1.80E-04	8.21E-05	1.20E-04			
1400	2.36E-04	1.11E-04	1.57E-04			
1600	2.98E-04	1.45E-04	1.98E-04			
1800	3.65E-04	1.81E-04	2.42E-04			
2000	4.37E-04	2.22E-04	2.89E-04			

FLUENT/UNS Kinetic Study Data

TABLE C-6

Reactant Stream Inputs for Kinetic Estimates and k Values ( $E_A = 1.92$  kJ/mol)

Exp. Run	Mass Fraction Reactants		Boiler Inlet Velocity, m/sec		Empirical k (sec <sup>-1</sup> )
	Zn	Se	Zn	Se	-
BA97155 6/5/97	0.848		0.152		0.0463
	0.835	0.833	0.141	0.0888	0.0447
	0.822		0.132		0.0336
BA98009 E13C3	0.851		0.177		0.0270
	0.835	0.866	0.162	0.113	0.0279
	0.820		0.149		0.0262
BA97161 6/10/97	0.867	0.890	0.172	0.122	0.0336
	0.858	0.881	0.162	0.115	0.0320
	0.849	0.873	0.153	0.109	0.0304

TABLE C-7

FLUENT/UNS Inputs for Reactant Streams in Parametric Study of Flow Effects on ZnSe Yield

Test	Mole Flow Rate (mol/sec)				Inlet Mass Fraction		Inlet Velocity (m/sec)		Outlet Mole Fraction		Molar Yield % Based on Zn	
	Zn	Ar(Zn)	Se <sub>2</sub>	Ar(Se <sub>2</sub> )	Zn	Se <sub>2</sub>	Zn	Se <sub>2</sub>	Zn	ZnSe	Stoichiometric	Kinetic
Kinetic Yield at overall average flows	5.42E-04	2.00E-04	3.84E-04	2.00E-04	0.816	0.883	0.144	0.113	0.1384	0.3406	70.7%	71.1%
Stoichiometric Flows- What level performs better?	3.00E-04	2.00E-04	1.50E-04	2.00E-04	0.711	0.748	0.0971	0.0680	0.07068	0.343	100.0%	82.9%
	6.00E-04	2.00E-04	3.00E-04	2.00E-04	0.831	0.856	0.155	0.0971	0.1579	0.3945	100.0%	71.4%
	9.00E-04	2.00E-04	4.50E-04	2.00E-04	0.880	0.899	0.214	0.126	0.2317	0.3810	100.0%	62.2%
Vary Reactant Ratio												
Zinc -50%	3.00E-04	2.00E-04	3.00E-04	2.00E-04	0.711	0.856	0.0971	0.0971	0.06943	0.2717	50.0%	79.6%
Zinc -25%	4.50E-04	2.00E-04	3.00E-04	2.00E-04	0.786	0.856	0.126	0.0971	0.1137	0.3443	75.0%	75.2%
Zinc +25%	9.00E-04	2.00E-04	3.00E-04	2.00E-04	0.880	0.856	0.214	0.0971	0.2434	0.4437	66.7%	64.6%
Zinc +50%	7.50E-04	2.00E-04	3.00E-04	2.00E-04	0.860	0.856	0.185	0.0971	0.2021	0.4261	80.0%	67.8%
Selenium -50%	6.00E-04	2.00E-04	1.50E-04	2.00E-04	0.831	0.748	0.155	0.0680	0.2991	0.3008	50.0%	50.1%
Selenium -25%	6.00E-04	2.00E-04	2.25E-04	2.00E-04	0.831	0.816	0.155	0.0826	0.1616	0.4340	75.0%	72.9%
Selenium +25%	6.00E-04	2.00E-04	4.50E-04	2.00E-04	0.831	0.899	0.155	0.126	0.1521	0.3302	66.7%	68.5%
Selenium +50%	6.00E-04	2.00E-04	3.75E-04	2.00E-04	0.831	0.881	0.155	0.112	0.1546	0.3593	80.0%	69.9%

## APPENDIX D

### NOZZLE DESIGN THROUGH CFD SIMULATION

What are the goals in nozzle design?

1. Want each reactant molecule of A to hit each of B enough times that AB is formed in 100% yield within the length of the reactor.
2. Want these AB's to form soon enough that they will settle within the reactor chamber.
3. Want sufficient nozzle velocity that AB doesn't use nozzle as nucleation site.

What factors govern these concerns?

Factor 1. Controlled by relative mole flow rates, reaction kinetics, geometry of nozzles and nozzle Reynolds number.

Factor 2. Controlled by reactor space time/ linear velocity of reactor contents

Factor 3. Controlled by nozzle exit velocity.

Factors 1-3. Controlled by mole flows of reactants and carrier.

Accurate mole flow rate estimates are therefore needed to design the nozzles correctly, but we only have rough estimates. The first task is to ascertain from these estimates what the magnitude of the minimum flow rate should be and then use ideal gas law to establish levels for maximum and minimum mole flow rates, nozzle diameters, nozzle positions, and nozzle orientations. Secondly, these nozzle designs are inserted into an experimental matrix for a designed experimental (DOE) study using a CFD

simulation model on FLUENT. From this model, a set of theoretically optimum parameters can be established for direct implementation into a physical prototype for the II-VI synthesis process. Keeping in mind for the first task of setting levels that the CFD model only predicts gaseous product formation, suitable lower levels must be estimated. These parameters such as reactant flow must safely lie above the threshold for structure formation and plugging since the CFD model does directly predict this phenomenon. Therefore, these threshold levels must be set first according to data and observations gained from the current process. Also, knowledge of nozzle performance characteristics must be utilized to establish the higher levels to ensure that the nozzles will operate as intended.

#### Minimum Mole Flow/Max Nozzle Throat

Of the accumulated data, 7 runs, 3 production (BA97155, BA97161, and BA97142) and 4 experimental (BA98009, BA97217, BA97209, and BA97204), provide reasonable estimates of mass transfer rates. One production run had a slight structure while 3 experimental runs had significant structures. To estimate the minimum allowable nozzle velocity to avoid structures, these last 3 runs were examined. Since the structures formed at the zinc inlet, zinc nozzle throat velocity ( $u_0$ ) will serve as the design variable. At the boiler temperature (1223-1229 K),  $u_0$  varies from ~0.2-0.3 m/sec. This flow in itself does not signal that the nozzle will form complex structure since the remainder of the non-structure forming runs had  $u_0$  which varied from 0.3-0.4. Therefore the actual minimum velocity for nucleation to occur on the nozzle lies within the 0.2 to 0.4 m/sec

range. To negate this uncertainty, the minimum  $u_{o,min}$  will be set at  $5 u_{o,WH} = 1.5$  m/sec. This is sufficiently high to offset the uncertainty in flow rates.

From inspection of these 3 structure forming runs, the maximum mole flow rate for zinc ( $6.2 \times 10^{-4}$  mol/sec) is chosen to be the minimum reactant mole flow design value for the experimental study. Since the previous experimental study points to a one to one mole ratio for optimum yield the corresponding selenium ( $Se_2$ ) minimum design mole flow rate is set at  $3.1 \times 10^{-4}$  mol/sec. Without a better understanding of particle formation rates and settling velocities the earlier experimental values for argon flow are maintained at 300 mL/min or  $2.0 \times 10^{-4}$  mol/sec per nozzle. To achieve  $u_{o,min}$ , the zinc nozzle throat must be 8mm inside diameter while the  $Se_2$  nozzle throat must be 6 mm inside diameter. The minimum design nozzle diameter ( $D_{o,min}$ ) is therefore set at 6 mm. Equal mole flow rates are thus achieved while at least maintaining  $u_{o,min}$ .

#### Maximum Mole Flow/Min Nozzle Throat

The maximum mole flow rate for reactants is established by first estimating the increase in mass flow rate that can be expected by using the combined immersion and superficial argon flows. Using the best estimate for mole flow obtained from the selenium boiler ( $2.9 \times 10^{-4}$  mol/sec) the diffusion mole flux of  $Se_2$  gas is estimated to be  $0.182$  mol/m<sup>2</sup>-sec. In addition to being the single best estimate of mass flow rate from the data, the selenium value is chosen since the liquid has a constant cross sectional area in the vertical boiler. This yields a more steady approximation of mole flux. An equation describing the overall mole flux takes the form of Fick's Law (Bird et al. 1960):

$$N_{Se_2,z} = -D_{Se_2-Ar} \frac{\partial c_{Se_2}}{\partial z} + x_{Se_2} (N_{Se_2,y} + N_{Ar,z}) \quad (D-1)$$

where

$N_{Se_2,z}$  = molar flux of selenium gas in the z-direction

$N_{Ar,z}$  = molar flux of argon gas in the z-direction

$\mathcal{D}_{Se_2-Ar}$  = diffusivity or diffusion coefficient for selenium gas in argon

$\frac{\partial c_{Se_2}}{\partial z}$  = concentration gradient for selenium gas in the z-direction

$x_{Se_2}$  = mole fraction of selenium gas.

The first term on the right side represents transport by diffusion while the second term represents convective transport. The estimated flow rate comes from a boiler in which argon is superficially blown across the surface of the boiling metal. For this case, the molar flux term for argon on the right hand side is zero; therefore the convective term is based solely on mole flux of  $Se_2$ . To estimate the maximum possible mole flux of  $Se_2$  gas, the molar flux is assumed to remain constant when the convective term becomes nonzero. It is noted that the actual mass transfer of selenium will probably occur faster than the estimate, but the estimate serves to set some reasonable levels for CFD experimentation since the boiling process is not part of the reactor model. For this initial estimate, 2/3 of the argon flow is diverted into the immersion tube to bubble through the boiling metal. It is estimated that 20 bubbles per second are produced from the 200 mL/min @300 K ( $1.35 \times 10^{-4}$  mol/sec) argon. These bubbles are assumed to be hemispherical. The volume of a single bubble is calculated at the pressure halfway up the column of molten metal. The sum of the resulting surface area and the liquid surface area are used to estimate the mole flow rate from the constant molar flux estimation. The calculations follow.



Constant molar flux estimate:

$$N_{Se_1} = 0.182 \text{ mol/m}^2\text{-sec}$$

Assume that overall mole flow rate of selenium is equal to the product of the molar flux and the sum of the surface area of the liquid plus the total surface area of the bubbles:

$$\dot{N}_{Se_1, \text{Tot}} = N_{Se_1} (A_s + A_{\text{Bub}}) \quad (\text{D-2})$$

$$A_s = (0.0225 \text{ m})^2 \pi = 1.59 \times 10^{-3} \text{ m}^2$$

$A_{\text{Bub}}$  is estimated below.

Pressure exerted by metal halfway up the column:

Assume 1094 g molten Se (amount to produce 2 kg of ZnSe at 100% yield)

Volume of liquid metal:

$$V_{Se-L} = \frac{1.094 \text{ kg}}{3990 \frac{\text{kg}}{\text{m}^3}} = 2.74 \times 10^{-4} \text{ m}^3$$

Half height of column of liquid metal:

$$\frac{h}{2} = \frac{2.74 \times 10^{-4} \text{ m}^3}{(2)(0.0225 \text{ m})^2 \pi} = 0.086 \text{ m}$$

Pressure exerted by liquid metal at half height:

$$P_L = (0.086 \text{ m})(3990 \frac{\text{kg}}{\text{m}^3})(9.81 \frac{\text{m}}{\text{sec}^2}) = 3375 \text{ Pa}$$

Use the ideal gas law to estimate the volume of a single bubble:

$$V_{\text{Bub}} = \left( \frac{\dot{N}_{Se_1} + \dot{N}_{Ar}}{\text{No. Bub/sec}} \right) \frac{(RT)}{(P_L + P_{Ar})} \quad (\text{D-3})$$

Assume that  $\dot{N}_{Se_1} = 0.5(\dot{N}_{Ar})$ ,  $T = 994 \text{ K}$ , and  $P_{Ar} = 101,325 \text{ Pa}$

$$V_{\text{Bub}} = \left( \frac{(1.5)(1.35 \times 10^{-4} \frac{\text{mol}}{\text{sec}})}{20 \frac{\text{Bub}}{\text{sec}}} \right) \frac{(8.314 \frac{\text{m}^3 \cdot \text{Pa}}{\text{mol} \cdot \text{K}})(994 \text{ K})}{(3375 \text{ Pa} + 101,325 \text{ Pa})}$$

$$V_{\text{Bub}} = 7.99 \times 10^{-7} \text{ m}^3$$

Assume the bubbles are hemispherical:

$$V_{\text{Bub}} = \frac{2}{3} \pi r^3 \text{ and } A_{\text{Bub}} = 2\pi r^2$$

therefore,

$$A_{\text{Bub}} = 2.62 \pi^{1/3} V_{\text{Bub}}^{2/3} = 2.62 \pi^{1/3} (7.99 \times 10^{-7} \text{ m}^3)^{2/3}$$

$$A_{\text{Bub}} = 3.30 \times 10^{-4} \text{ m}^2$$

Now the molar flow rate can be estimated:

$$\dot{N}_{\text{Se}, \text{Tot}} = (0.182 \text{ mol/m}^2 \cdot \text{sec})(1.59 \times 10^{-3} + 20 \cdot 3.30 \times 10^{-4} \text{ m}^2)$$

$$\dot{N}_{\text{Se}, \text{Tot}} = 1.67 \times 10^{-3} \text{ mol/sec}$$

This mole flow rate estimate is 5 times as large as the minimum mole flow estimate so it will be acceptable. The mole flow rate for zinc will be set to twice the value for that of selenium to maintain the correct stoichiometry. In practice, the relative level of argon aeration for the zinc boiler may change, but for the simulation mole flow rates will be set stoichiometrically equal.

To set the  $D_o$  for the high velocity nozzle, the maximum exit velocity obtained should be as high as possible to offer significant variation from the low levels in the experimental design. Maintaining simplicity of design is of the utmost importance in the new reactor so the nozzles are designed as converging nozzles. The exit velocity for compressible fluids such as the reactant gas streams from a converging nozzle is limited by the speed of sound in that fluid (Kleinstreuer, 1997). As the velocity approaches the

speed of sound, the flow becomes choked and a maximum is reached. From the earlier reference the speed of sound is calculated as

$$a = \sqrt{\gamma RT} \quad (D-4)$$

where

$$\gamma = \frac{C_p}{C_v} = \frac{C_p}{C_p - R} \quad (D-5)$$

R = Ideal gas constant, 8.314 J/mol-K

T = Temperature, K

C<sub>p</sub>, C<sub>v</sub> = Constant pressure and constant volume heat capacity, J/mol-K

The speed of sound is estimated below in Table D-1 for the pure species components at 1000 K.

TABLE D-1

Speed of sound in pure species gases at 1000 K

Species	$\gamma$	a, m/sec
Zn	1.67	118
Se <sub>2</sub>	1.25	102
Ar	1.67	118

The potential for flow choking would be detrimental to the future design for the reactor system since pressure would increase in the boiler sections of the apparatus. This increase in boiler pressure could lead to unwanted breakage and control problems.

Therefore, the maximum  $u_0$  for the high velocity nozzle with the maximum mole flow rate is set at 85% the speed of sound in the pure Se<sub>2</sub> reactant gas or 85 m/sec. The high

velocity nozzle  $D_0$  is set to be 2.5 mm to safely maintain subsonic flow in the system but achieve the highest linear velocities out of the nozzle throat.

### Nozzle Position/Orientation

For product formation to occur within the reactor, two rates come into play: the chemical reaction rate and the rate of transport of reactant molecules. The transport rate is limiting and controls the extent of product formation within the reactor. For the CFD model, it is assumed that the chemical reaction rate is sufficiently fast enough for the transport rate to maintain its dominance across the range of process parameter levels. Fick's Law can again be used to describe the transport processes within the reactor. When the diffusion of reactant molecules controls the overall transport rate, uncertain reactor performance has been shown from experimental data. Therefore, the convective mixing must be maintained at a sufficient level to negate the reliance on diffusion for bulk reaction. The position and orientation of the nozzles directly impacts the convective mixing of the two fluid jets. In order to achieve a level of maximum intermingling of the two jets, the two nozzles should be aimed cross-currently,  $90^\circ$  from the reactor axis, at a suitable range for fluid elements to intermingle sufficiently. In application, this would cause the system to plug. The maximum angle for nozzle orientation is therefore set at a conservative value of  $-90^\circ/2$  or  $-45^\circ$  from the reactor axis. The minimum angle is set at  $0^\circ$  from the reactor axis corresponding to cocurrent flow. The cocurrent flow orientation by nature will place the burden of mixing more upon diffusive transport of reactants across the jet boundary layers. The position of the nozzles,  $r_0$ , is set for the minimum level to be  $\approx 1 D_0^+$  (1 cm) and the maximum level to be  $5 D_0^+$  (3 cm) from the center of the nozzle

throat to the axis of the reactor. The initial experimental levels for the CFD simulation are tabulated in Table D-2 below.

TABLE D-2

Initial Experimental Levels for CFD Model

Level	$\dot{N}_{\text{Tot}}$ (mol/sec)		$D_o$ (mm)	$r_o$ (cm)	$\alpha$
	Zn, Ar	Se <sub>2</sub> , Ar			
+	$3.5 \times 10^{-3}$	$1.9 \times 10^{-3}$	6	1	45°
-	$8.2 \times 10^{-4}$	$5.1 \times 10^{-4}$	2.5	3	0°

### Discussion

In subsonic nozzles, the driving force is a pressure gradient formed by a higher pressure region upstream from the nozzle forcing a fluid into a low pressure reservoir below the nozzle. The limit of the nozzle exit velocity is the speed of sound in that fluid as mentioned earlier. As the upstream pressure approaches the downstream pressure, the linear velocity of the flow increases. From the linear flow rates for these nozzles, the nozzle Reynolds number ( $Re_o$ ) can be calculated. The Reynolds number,  $Re = uD/v$  is a common measure of the turbulence in a system, where  $v = \mu/\rho =$  kinematic viscosity. The jets emitted by the two nozzles in the system can be termed properly as free shear flows since their velocity gradients are caused by the upstream mechanism of exiting the nozzle walls. Kleinstreuer (1997) defines a free shear flow as the latter with  $Re \gg 1$  and  $\partial p/\partial x \approx 0$ . Further, Kleinstreuer (1997) defines a range for turbulent behavior of free shear flows in terms of the nozzle Reynolds number,  $Re_o$ . For  $Re > 30$ , round jets are

considered turbulent. Tilton (1997) describes a free turbulent fluid jet as composed of 4 regions:

1. Region of flow establishment which has a length of about  $6 D_o$ .
2. Transition region which has a length of about  $8 D_o$ .
3. Established flow region which can have a length up to  $100 D_o$  depending on initial velocity and Reynolds number.
4. Terminal region where the centerline velocity quickly approaches the ambient fluid velocity.

Rushton (1980) refined an earlier correlation to predict the angle of spread for a turbulent fluid jet,

$$\tan \Theta/2 = 0.238 v^{0.135} \quad (D-6)$$

where kinematic viscosity is in Stokes. From the regions of Tilton (1997) and the correlation of Rushton (1980), a mixing pattern for two fluid jets can be approximated without the aid of complicated computer models. The angles of the turbulent jets for the pure species gases are tabulated in Table D-3 below.

TABLE D-3  
Turbulent Jet Angles

Species	$\nu$ (Stokes)	$\Theta$
Zn	1.081	27.0°
Se <sub>2</sub>	0.3972	23.7°
Ar	1.585	28.4°

Using the ideal gas densities, Lennard-Jones viscosities, and mole flow rates for Zn, Se<sub>2</sub>, and Ar at the reactor temperature (1248 K), the respective nozzle Reynolds

numbers are estimated in Table D-4. Nozzle kinematic viscosity for the mixture of reactant and carrier gas is found using the Wilke formula from Bird et al. (1960) which is annotated in Appendix A. The density of the nozzle mixture is calculated on a mass-weighted basis:

$$\rho_{mix} = X_i \rho_i + X_j \rho_j \quad (D-7)$$

where

$X_i$  = mass fraction of component  $i$  in the mixture and

$\rho_i$  = mass density of species  $i$  in  $\text{kg/m}^3$ .

TABLE D-4

Estimated Mixture Viscosities and Densities at 1248 K and 1 atm.

Nozzle	Level	$\dot{N}_{Tot}$ (mol/sec)	$\mu$ (kg/m-sec)	$\rho$ (kg/m <sup>3</sup> )
Zinc	+	$3.5 \times 10^{-3}$	$6.89 \times 10^{-5}$	0.6286
	-	$8.2 \times 10^{-4}$	$6.79 \times 10^{-5}$	0.5966
Selenium	+	$1.9 \times 10^{-3}$	$6.18 \times 10^{-5}$	1.506
	-	$5.1 \times 10^{-4}$	$6.33 \times 10^{-5}$	1.379

TABLE D-5

Estimated Nozzle Reynolds Number for Experimental CFD at 1248 K and 1 atm.

Nozzle	$D_o$ (mm)	$\dot{N}_{Tot}$ Level	$u_o$ (m/sec)	$Re_o$
Zinc	2.5	+	73.0	1665
		-	17.1	376
	6	+	12.7	695
		-	2.97	157
Selenium	2.5	+	39.6	2412
		-	10.6	577
	6	+	6.88	1006
		-	1.85	242

The proposed settings within this appendix were used as a starting point for the FLUENT/CFD optimization of nozzles performed in the thesis of Shay (1998).



## APPENDIX E

### PROTOTYPE REACTOR CALCULATIONS

This appendix describes the reactor scaling calculations, an estimated production time comparison between the current EP technology and the prototype, and the general protocol for the prototype reactor operation.

#### Prototype Design Calculations

This section details the calculations and estimates used to produce a Pe and Re comparison between the old capacity reactor and the new capacity prototype reactor for proper reactor sizing.

- a. Estimate the density of loosely-packed product powder from observation that 800 g of ZnSe powder fills a 1 quart collection vessel with some extra room.

$$\rho_{\text{pow}} = \frac{800\text{g}}{0.9463\text{L}} = 845 \frac{\text{g}}{\text{L}}$$

- b. Calculate the volume of the 90 mm I. D. reactor tube.

$$V_{\text{reactor}} = \pi r^2 L = \pi(4.5\text{cm})^2 (100\text{cm})$$

$$V_{\text{reactor}} = 6.36\text{L}$$

- c. Estimate the “free volume” or vapor volume of the reactor tube when full at 0.8 kg and 2 kg capacity.

$$0.8 \text{ kg} \rightarrow \phi(0.8) = 6.36\text{L} - \frac{800\text{g}}{845\text{g/L}} = 5.41\text{L}$$

$$2\text{kg} \rightarrow \phi(2) = 6.36L - \frac{2000g}{845g/L} = 3.99L$$

$$\text{Ratio} \rightarrow \frac{\phi(2)}{\phi(0.8)} = 0.74$$

- d. Now estimate an average residence time,  $\tau$ , for each of the two capacities based on typical molar flow estimates and 88% conversion of reactant streams.

Estimated component flow rates:

$$N_{Ar} = 4 \cdot 10^{-4} \text{ mol/sec}$$

$$N_{Se_2} = 3 \cdot 10^{-4} \text{ mol/sec}$$

$$N_{Zn} = 6 \cdot 10^{-4} \text{ mol/sec}$$

$$\text{Average molar flow rate, } \bar{N} = \frac{N_{In} + N_{Out}}{2}$$

$$N_{in} = (4 + 3 + 6) \cdot 10^{-4} \text{ mol/sec} = 13 \cdot 10^{-4} \text{ mol/sec}$$

$$N_{out} = (4 + (1 - 0.88)(6 + 3)) \cdot 10^{-4} \text{ mol/sec} = 5.1 \cdot 10^{-4} \text{ mol/sec}$$

$$\bar{N} = \frac{13 \cdot 10^{-4} + 5.1 \cdot 10^{-4}}{2} = 9.1 \cdot 10^{-4} \text{ mol/sec}$$

- e. Now estimate the volumetric flow rate assuming isothermal at 1000 °C and 1 atm.

$$\bar{Q} = \frac{\bar{N}RT}{P} = \frac{(9.1 \cdot 10^{-4})(8.314)(1273)}{101325} = 9.5 \cdot 10^{-5} \frac{\text{m}^3}{\text{sec}}$$

- f. Assume that this flow rate is representative of both the old and new prototype reactors, and determine  $\tau$ .

$$\tau_{0.8} = \frac{V_{\text{reactor}} + \phi(0.8)}{2\bar{Q}} = 62 \text{ sec}$$

$$\tau_2 = \frac{V_{\text{reactor}} + \phi(2)}{2\bar{Q}} = 55 \text{ sec} \quad (11\% \text{ decrease})$$

- g. Now calculate the Pe. Assume an average diffusion coefficient which is on the order of  $1 \times 10^{-4} \text{ m}^2/\text{sec}$ . Reactor is 0.090 m I. D.  $Pe < 300$  characterize a diffusion-controlled system (Nauman, 1987).

$$Pe = \frac{R^2}{D\tau}$$

$$Pe_{0.8} = \frac{0.045^2}{(1 \cdot 10^{-4})(62)} = \underline{0.33 \ll 300}$$

$$Pe_2 = \frac{0.045^2}{(1 \cdot 10^{-4})(55)} = \underline{0.37 \ll 300}$$

$$Pe_{0.8} \cong Pe_2$$

No significant alteration in mixing can be expected in the scale up based on the Pe number comparison.

- h. Now perform a Re comparison for the original and scale-up systems assuming that the kinematic viscosity,  $\nu$ , is on the order of  $1 \times 10^{-4} \text{ m}^2/\text{sec}$ . Use the hydraulic diameter to calculate  $u$  from  $\bar{Q}$ . Estimate the hydraulic area to be the average of the “full” and “empty” areas.

$$Re = \frac{uD}{\nu}$$

$$A_{0.8} = \frac{V_{\text{reactor}} + \phi(0.8)}{2(1 \text{ m})} = 5.89 \cdot 10^{-3} \text{ m}^2$$

$$A_2 = \frac{V_{\text{reactor}} + \phi(2)}{2(1 \text{ m})} = 5.18 \cdot 10^{-3} \text{ m}^2$$

- i. Assuming that the powder deposits in a flat bed, geometry can be used to determine the perimeter of the open cross sectional area.

$$A = 0.5r^2(\theta - \sin \theta)$$

$$\theta_{0.8} = 4.82 \text{ rad}$$

$$\theta_2 = 4.23 \text{ rad}$$

$$s = r\theta, h = 2r \sin \frac{\theta}{2}$$

$$s_{0.8} = 0.217 \text{ m}, h = 0.0602 \text{ m}$$

$$s_2 = 0.190 \text{ m}, h = 0.0770 \text{ m}$$

$$D = \frac{A}{P}, P = s + h$$

$$D_{0.8} = 0.0212 \text{ m}$$

$$D_2 = 0.0194 \text{ m}$$

$$Re_{0.8} = 3.4 \ll 2100$$

$$Re_2 = 3.6 \ll 2100$$

$$Re_{0.8} \cong Re_2$$

No significant difference in the fully developed laminar flow can be expected between the original and scaled up prototype reactor.

#### Production Comparison

Below, an estimated timeline comparison is described between the current EP process and the estimated prototype process.

TABLE E-1

#### Run Timeline Comparison

TASK	ESTIMATED TIME TO PERFORM TASK	
	OLD DESIGN	NEW DESIGN
Weigh reactants and add to boilers	15 min	15 min
Install reactor tube	5 min	5 min
Install bottom boiler	5 min	5 min
Weld bottom boiler	10 min	10 min
Install top boiler	5 min	5 min
Weld top boiler	10 min	10 min
Install condenser	10 min	10 min

Set argon flows	5 min	10 min
Set temperature controllers	5 min	5 min
Purge reactor overnight	16 hr	16 hr
Run and cool down*	24 hr	24 hr
Remove and empty condenser	10 min	10 min
Disconnect argon and remove heaters	10 min	-
Remove and empty reactor tube	30 min	15 min
Cut off boilers	10 min	-
Clean reactor tube	1.5 hr	30 min
Clean boilers	1 hr	-
Dry quartz pieces overnight**	16 hr	-
Total Run Time	60.5 hr	42 hr
Service Factor	1.25	1.11
Adjusted Total Run Time	76 hr	47 hr
Estimated Capacity	0.8 kg	2.0 kg

\*Longer run time and shorter cooling time will be applied to the New Design.

\*\*The straight tube can dry in the warm reactor during the purge cycle.

It is important to notice the service factors above. To account for run failures, glassware breakage, and unexpected maintenance, an adjustment (service) factor was defined to increase the production time an appropriate amount. A service factor of 1.0 dictates that the run proceeded without mishap. The service factor is defined as perfect service divided by the service level achieved within the design:

$$f = \frac{100\%}{\text{actual \% service}} \quad (\text{E-1})$$

From available process data and experience, the current reactor is in service 80% of the time (one out of five runs results in failure). The service factor for the current reactor is

calculated to be

$$f_{OLD} = \frac{100}{80} = 1.25$$

Due to less maintenance requirements and the flow monitoring system, it was estimated that one out of every ten runs will be aborted in the prototype.

$$f_{NEW} = \frac{100}{90} = 1.11$$

How much can productivity be increased through the new design? Assume that 10 kg of powdered product is desired. How do the old design and new design run timelines compare?

Example: How long will it take to produce 10 kg of powder?

Old Design	950 hrs (about 40 working days)
New Design	235 hrs (about 10 working days)
% Difference	75%

The proposed design would produce the desired 10 kg of powder in 75% less time than the old system. This initial estimate provides a key example of the potential for increased capacity.

Cost savings for the prototype would be significant. As mentioned in the introduction to Chapter III, the current system operates at about a 60% loss rate of raw materials. Based on the costs of \$162/100g for zinc, \$135/100g for selenium, and \$1760/kg waste disposal, EP lost about \$100,000 in the year prior to the study. The prototype reactor should operate around a 10% loss rate based on the experimental study of Shay (1998), but a more conservative estimate would be 20% loss rate. If the same 367 moles of ZnSe were attempted with the prototype system, the losses would amount to

4800 g zinc (\$7776), 5769 g selenium (\$7824), and about \$20,000 in waste disposal charges. This total of \$35,000 in loss is a very conservative estimate but still amounts to a cost savings of almost 2/3 over the current system in material costs. From the above time line comparison, the labor difference should also result in a 75% savings over the current system.

These savings can be quantified if a labor cost is assumed. The labor cost was assumed to be \$20/hr for EP technicians. A direct comparison was performed assuming that the 16 hour purge time for both old and prototype runs, 18 hours cool down for old runs, and 12 hour cool down time for prototype runs did not count against labor costs. The results of this comparison are best summarized in Table E-2.

TABLE E-2

Estimated Cost Savings on Prototype Reactor

	Old Reactor	Prototype Estimate
Capacity	0.8 kg ZnSe	2.0 kg ZnSe
Molar Yield	40%	80%
Run Time	76 hr	47 hr
Labor Free Time	-34 hr	-28 hr
Total Labor	42 hr	19 hr
Labor Cost (@\$20/hr)	\$840/0.8kg ZnSe	\$380/2.0kg ZnSe
Zinc Waste	544 g/0.8kg ZnSe	227 g/2.0kg ZnSe
Zinc Waste Cost	\$881/0.8kg ZnSe	\$368/2.0kg ZnSe
Selenium Waste	785 g/0.8kg ZnSe (~1.2*Zn)	274 g/2.0kg ZnSe
Selenium Waste Cost	\$1059/0.8kg ZnSe	\$370/2.0kg ZnSe
Waste Disposal Cost	\$2339/0.8kg ZnSe	\$882/2.0kg ZnSe
Total Cost	\$5119/0.8kg ZnSe	\$2000/2.0kg ZnSe
Total Cost per kg ZnSe	\$6399/kg ZnSe	\$1000/kg ZnSe
Total Savings		\$5400/kg

## General Protocol

First and foremost, all applicable safety precautions should be taken such as wearing safety goggles, respirators, etc. when dealing with the reactor, chemicals, and maintenance. The procedure should follow the general scheme:

1. Align reactor and boilers then seal the junctions by welding. Solely their respective heaters should support the quartz boilers while the reactor tube should be centered within the reactor furnace therefore supported separately from the boilers.
2. Carefully insert product tube so that it butts against the reactor faceplate.
3. Attach the condenser without the use of grease. Silicon from the grease may contaminate the product powders. Attach point source scrubber to condenser.
4. Carefully add pre-weighed stoichiometric amounts of reactants to boilers.
5. Seal boilers (without grease) using quartz stoppers and clips.
6. Add precut pieces of insulation to top openings in boiler heaters, transport tube heater, and rear of reactor furnace. Be sure to insulate the opening in the furnace not the reactor tube or condenser. Insulating the tube will lower the effectiveness of the condenser.
7. Attach argon carrier supply to all four supply tubes.
8. Purge the system with argon for several hours by flowing argon through all four supply tubes.



9. Reduce argon flow rates through tubes. The flow of the two main streams should be set at run levels, and the two immersion streams should be set to a trickle.
10. Heat the boilers to approximately 10°C below the reactant boiling temperatures. Allow temperature to stabilize.
11. Monitor pressure difference between supply streams for each boiler and calculate the amount of molten reactant using the density functions in Appendix A.
12. To initiate run, set final temperatures for boilers.
13. Monitor mass flow rates using the pressure monitors and adjust boiler temperatures to maintain stoichiometric flows accordingly.
14. Allow run to continue a set amount of time after the pressure monitor fails to work in order to finish mass transfer.
15. At run completion, shut off power and let reactor cool to handling temperatures. Use fans to speed cooling if necessary.
16. Once cool enough, remove scrubber and condenser.
17. Twist product tube and carefully remove from the reactor.
18. Collect product.
19. Examine reactor tube using a flashlight. Carefully brush out or vacuum any fugitive powders.
20. Insert a clean product tube, and start at step 1.

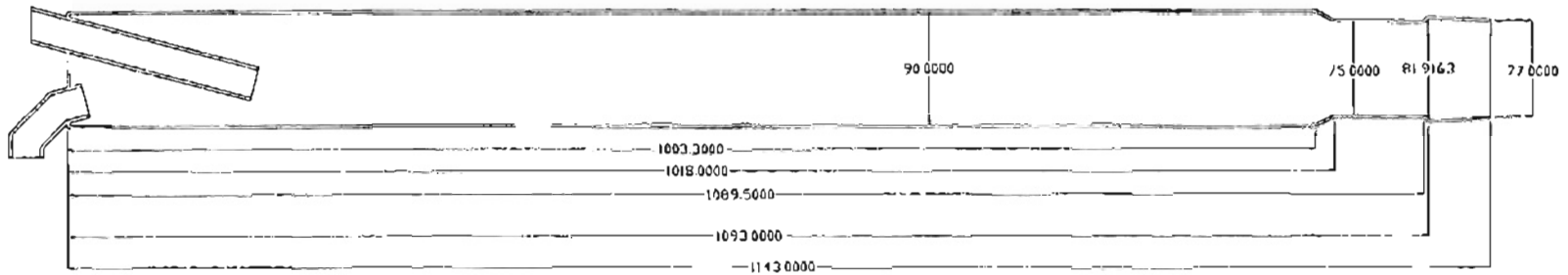
21. Maintain the system by disassembling entirely every X runs. Clean pieces using the usual acid bath techniques. Examine pieces for any flaws or cracks and respond accordingly.

With several runs, the operator can fine tune the boiler temperatures, flow rates, operating curves, and procedures.

## APPENDIX F

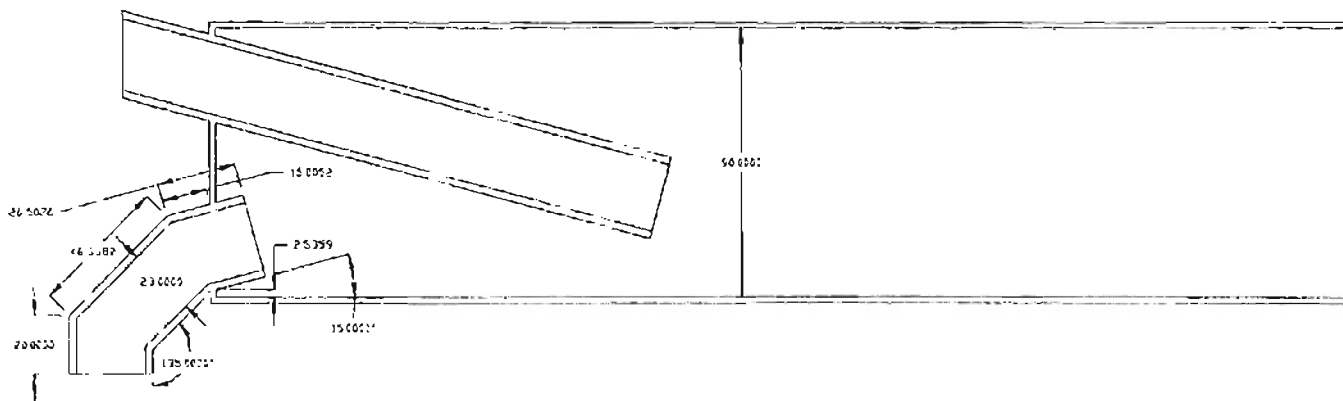
### CURRENT EP PROTOCOL AND REACTOR DIMENSIONS

The protocol for operating the current EP II-VI synthesis reactor is annotated in the EP document PS# 00171 (Divis, 1997) for a CdSe synthesis run. Slight modifications were made to this procedure for ZnSe and were mentioned in detail in Chapter III of this thesis and in the thesis of Shay (1998).



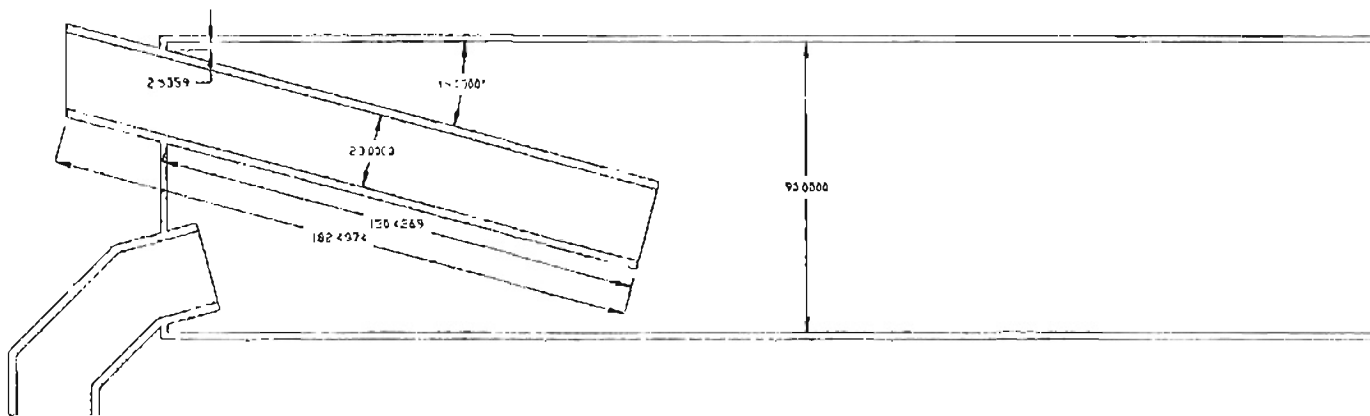
- Notes: (1) All dimensions are in millimeters  
 (2) The zinc and selenium transfer arm wall thicknesses are 2.5 mm  
 (3) All other wall thicknesses are 2.0 mm  
 (4) All tubing entrances and exits are cut parallel to the vertical or horizontal except for the transfer arm exits

Figure F-1. Drawing of EP reactor tube (Foster, in progress).



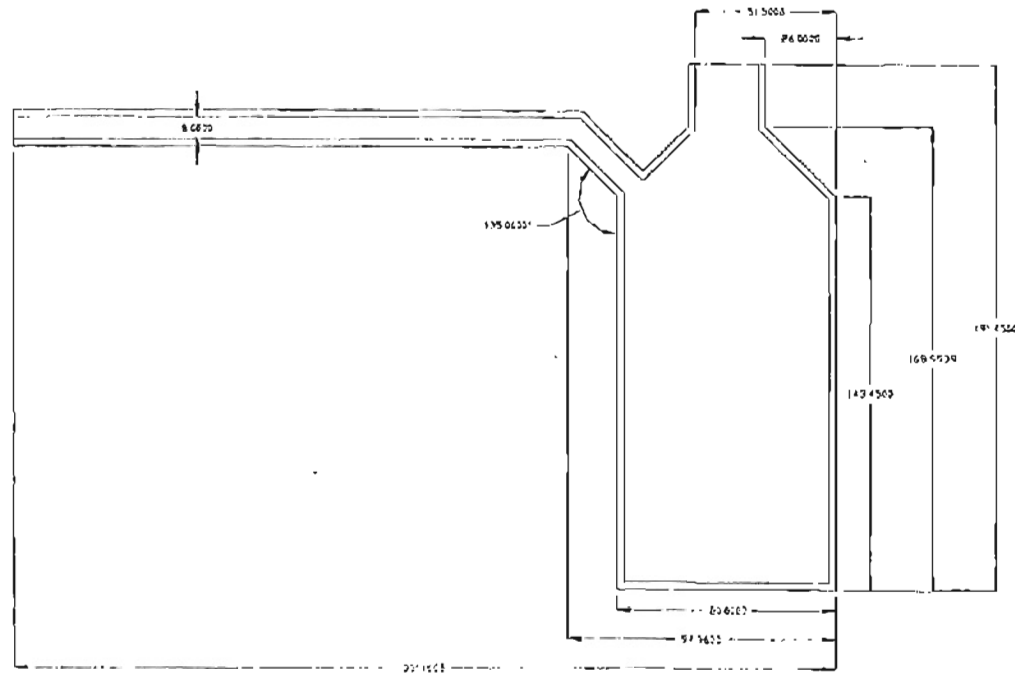
- Notes: (1) All dimensions are in millimeters  
 (2) The zinc and selenium transfer arm wall thicknesses are 2.5 mm  
 (3) All other wall thicknesses are 2.0 mm  
 (4) All tubing entrances and exits are cut parallel to the vertical or horizontal except for the transfer arm exits

Figure F-2. Selenium transfer arm (Foster, in progress).



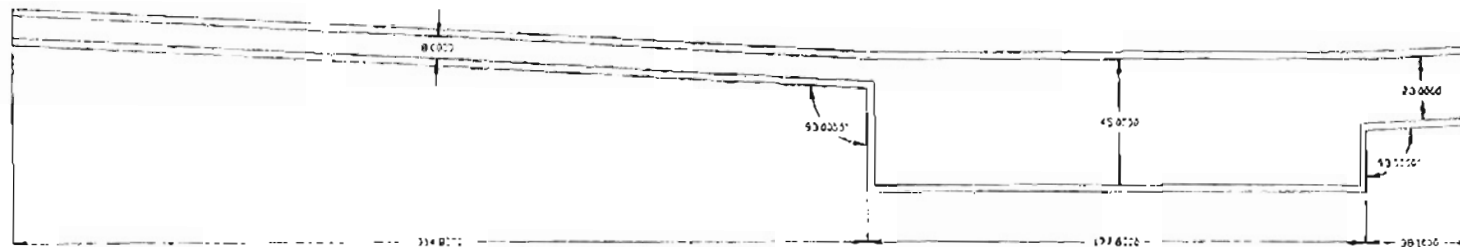
- Notes: (1) All dimensions are in millimeters  
(2) The zinc and selenium transfer arm wall thicknesses are 2.5 mm  
(3) All other wall thicknesses are 2.0 mm  
(4) All tubing entrances and exits are cut parallel to the vertical or horizontal except for the transfer arm exits

Figure F-3. Zinc transfer arm (Foster, in progress).



- Notes: (1) All dimensions are in millimeters  
 (2) All wall thicknesses are 2.5 mm  
 (3) All tubing entrances and exits are cut parallel to the vertical or horizontal

Figure F-4. Selenium boiler (Foster, in progress).



- Notes: (1) All dimensions are in millimeters  
(2) All wall thicknesses are 2.5 mm  
(3) All tubing entrances and exits are cut parallel to the vertical or horizontal

Figure F-5. Zinc boiler (Foster, in progress).



VITA

Delmar Ray Morrison III

Candidate for the Degree of

Master of Science

Thesis: ANALYSIS AND DESIGN OF A LAMINAR FLOW AEROSOL  
REACTOR FOR THE PRODUCTION OF ZnSe POWDER

Major Field: Chemical Engineering

Biographical:

Personal Data: Born in Tulsa, Oklahoma, on March 21, 1974.

Education: Graduate from Union High School, Tulsa, Oklahoma in May 1992, received Bachelor of Arts in Chemistry (Honors) from Knox College, Galesburg, Illinois in January 1997, completed requirements for Master of Science degree in Chemical Engineering at Oklahoma State University in December 1998.

Experience: Independent laboratory research in chemistry at Knox College, 1994 to 1996; Packer Engineering, Engineering summer intern, Naperville, Illinois, May 1996 to August 1996.